UNIVERSITÀ DEGLI STUDI DI PALERMO
Doctorate Degree in Civil, Environmental and Materials Engineering

Dipartimento di Ingegneria (DI)

S.S.D. ICAR/02

River flow monitoring: LS-PIV technique, an image-based method to assess discharge

Ph.D. STUDENT

Francesco ALONGI

TUTOR

Prof. Giuseppe CIRAOLO

COORDINATOR

Prof. Antonina PIRROTTA

Cycle XXXV

2022

Table of contents

Abstract

The measurement of the river discharge within a natural ort artificial channel is still one of the most challenging tasks for hydrologists and the scientific community. Although discharge is a physical quantity that theoretically can be measured with very high accuracy, since the volume of water flows in a well-defined domain, there are numerous critical issues in obtaining a reliable value.

Discharge cannot be measured directly, so its value is obtained by coupling a measurement of a quantity related to the volume of flowing water and the area of a channel cross-section. Direct measurements of current velocity are made, traditionally with instruments such as current meters. Although measurements with current meters are sufficiently accurate and even if there are universally recognized standards for the current application of such instruments, they are often unusable under specific flow conditions. In flood conditions, for example, due to the need for personnel to dive into the watercourse, it is impossible to ensure adequate safety conditions to operators for carrying out flow measures.

Critical issue arising from the use of current meters has been partially addressed thanks to technological development and the adoption of acoustic sensors. In particular, with the advent of Acoustic Doppler Current Profilers (ADCPs), flow measurements can take place without personnel having direct contact with the flow, performing measurements either from the bridge or from the banks. This made it possible to extend the available range of discharge measurements.

However, the flood conditions of a watercourse also limit the technology of ADCPs. The introduction of the instrument into the current with high velocities and turbulence would put the instrument itself at serious risk, making it vulnerable and exposed to damage. In the most critical case, the instrument could be torn away by the turbulent current.

On the other hand, considering smaller discharges, both current meters and ADCPs are technologically limited in their measurement as there are no adequate water levels for the use of the devices.

The difficulty in obtaining information on the lowest and highest values of discharge has important implications on how to define the relationships linking flows to water levels. The stage-discharge relationship is one of the tools through which it is possible to monitor the flow in a specific section of a watercourse. Through this curve, a discharge value can be obtained from knowing the water stage. Curves are site-specific and must be continuously updated to account for changes in geometry that the sections for which they are defined may experience over time. They are determined by making simultaneous discharge and stage measurements. Since instruments such as current meters and ADCPs are traditionally used, stage-discharge curves suffer from instrumental limitations. So, rating curves are usually obtained by interpolation of field-measured data and by extrapolate them for the highest and the lowest discharge values, with a consequent reduction in accuracy.

This thesis aims to identify a valid alternative to traditional flow measurements and to show the advantages of using new methods of monitoring to support traditional techniques, or to replace them. Optical techniques represent the best solution for overcoming the difficulties arising from the adoption of a traditional approach to flow measurement. Among these, the most widely used techniques are the Large-Scale Particle Image Velocimetry (LS-PIV) and the Large-Scale Particle Tracking Velocimetry. They are able to estimate the surface velocity fields by processing images representing a moving tracer, suitably dispersed on the liquid surface. By coupling velocity data obtained from optical techniques with geometry of a cross-section, a discharge value can easily be calculated.

In this thesis, the study of the LS-PIV technique was deepened, analysing the performance of the technique, and studying the physical and environmental parameters and factors on which the optical results depend.

As the LS-PIV technique is relatively new, there are no recognized standards available for the proper application of the technique. A preliminary numerical analysis was conducted to identify the factors on which the technique is significantly dependent. The results of these analyses enabled the development of specific guidelines through which the LS-PIV technique could subsequently be applied in open field during flow measurement campaigns in Sicily. In this way it

was possible to observe experimentally the criticalities involved in applying the technique on real cases. These measurement campaigns provided the opportunity to carry out analyses on field case studies and structure an automatic procedure for optimising the LS-PIV technique. In all case studies it was possible to observe how the turbulence phenomenon is a worsening factor in the output results of the LS-PIV technique. A final numerical analysis was therefore performed to understand the influence of turbulence factor on the performance of the technique. The results obtained represent an important step for future development of the topic.

Introduction

The hydrological cycle (Figure I) plays a crucial role in regulating the climate system of the Earth. Water is necessary for any form of life, making it one of the most significant governing forces in the biosphere. Although the necessity of monitoring the hydrological cycle components is well known, high-level accuracy of monitoring applications is not always feasible, particularly in the discharge monitoring (Shiklomanov et al., 2002; Vörösmarty et al., 2002).

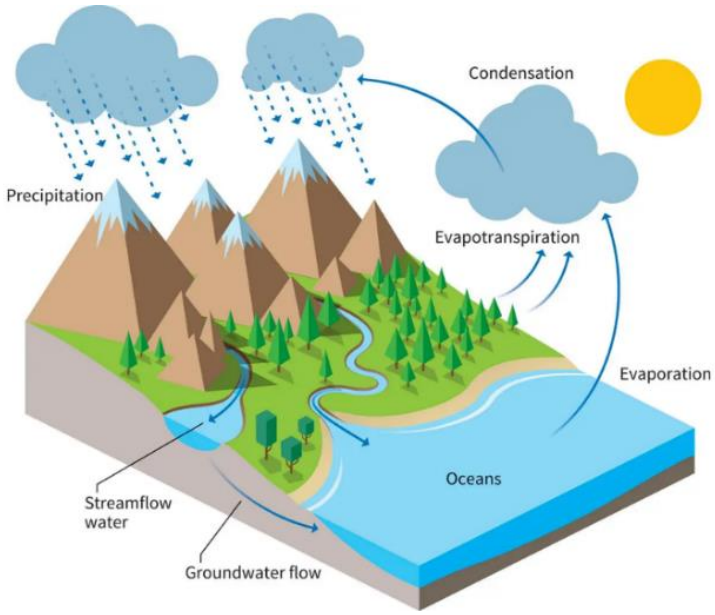

Figure I – Hydrological cycle scheme. (http://lessoplanet.com)

River discharge is one of the most well-defined components of the entire hydrological cycle, but the access to river channels is usually limited (Fekete & Vörösmarty, 2007). The monitoring network is sparse in many parts of the world, and no global mechanism exists to collect and distribute river discharge data in real time. A few hydro-meteorological agencies are distributing river discharge data via web, in various data formats. There is, then, a lack of organicity in data sharing and universally adopted standards.

Streamflow, or discharge, is defined as the volumetric rate of water (volume per unit time) flowing in an open channel, including any sediment or other solids that may be dissolved or mixed with it that adhere to the Newtonian physics of open channel hydraulics. Streamflow is usually expressed in cubic metres per second (m^3/s). It cannot be measured directly but must be calculated from variables that can be measured directly, such as stream width, depth, and velocity. Even though streamflow is calculated indirectly from other variables, the final result of the calculations is commonly referred to as "streamflow measurement" or "discharge measurement".

River discharge monitoring is typically referred as a regional task, with much less information available than for other meteorological variables. Because of the Hydrological Decade (1965-1974), UNESCO published the first compilation of river discharge data in the mid-1980s. (UNESCO IHP, 1984). The UNESCO publications, originally published as a series of printed books, were digitised in the late 1980s and served as the foundation for several global discharge compilations (Vörösmarty et al., 1996a; Bodo, 2001) as well as the Global Runoff Data Centre (GRDC) data archive. GRDC, hosted by the Bundesanstalt für Gewiisserkunde (Federal Institute of Hydrology, Koblenz, Germany), was established in 1988 and operates under the patronage of the World Meteorological Organization. The GRDC is a global archive of data spanning up to 200 years that promotes multinational and global long-term hydrological studies. The GRDC data archive is probably the most comprehensive discharge dataset globally, being commissioned by the WMO to collect, archive and disseminate hydrological data. According to WMO guidelines, data access is restricted. Although access to the actual discharge time series is limited, GRDC makes available a catalogue of their data holdings, which includes numerous attributes about monitoring stations and the quality of the discharge time series (e.g., station name, location, length of records, percentage of missing data, etc.). However, more comprehensive regional data sets exist (e.g., USGS Archive and Realtime discharge data, R-ArcticNet and Arctic-RIMS, LBA-

Hydronet, and so on), but combining these regional archives with global datasets would require significant effort.

Generally, the water in a stream in a specific location knows no local or national jurisdictional boundaries. Through the hydrological cycle, the same water may eventually move to any other part of the planet. Streamflow data from all parts of the globe are thus required to enable hydrologists to discover the quantity of the earth's water resources on a comprehensive and continuous basis. Streamflow data collected using non-standard methods may be suspect. The International Organization for Standardization (ISO) established a technical committee on streamflow measurement in 1956 for this and other reasons. This committee, known as TC113, has produced a number of international streamflow standards that are now used globally. TC113 includes 37 of the 104 ISO member countries. Furthermore, the WMO publishes guides and technical reports on stream gauging and selected ISO standards as technical regulations, which are distributed to the 187 WMO member countries.

Standardization activity at the European level is the responsibility of CEN (European Committee for Standardization) and CENELEC (European Committee for Electrotechnical Standardization). The primary objective of European standardisation is to harmonise standards across Europe to facilitate the exchange of goods and services by removing trade barriers caused by technical requirements. CEN is supported by the national standardisation institutes of 27 countries. Other European countries have affiliate status as well. Streamflow is governed by TC318 "Hydrometry," which was established in 1994.

River discharge monitoring is a really difficult task. While increasing the number of monitoring stations may indicate an improvement in this task, it does not always imply an improvement in the quality of monitoring of the monitored river systems. Remote sensing (particularly satellite-borne sensors) has shown great promise in providing new ways to monitor large river discharge. While remote sensing has the potential to provide consistent information for large areas, its application to discharge monitoring faces several major challenges. First, by definition, remote sensing is a spatial measurement, whereas river discharge is essentially a point measurement. Furthermore, traditional discharge measurement entails intensive field surveys to establish rating curves relating the monitored flow property to actual discharge, rather than simply recording some tracking variable (typically the stage height). Even if remote sensing techniques could replace ground-based monitoring of some river flow characteristics (stage height using an

altimeter or flow width using high resolution image sensors), the satellite records would still require calibration using in situ traditional measurements.

Despite the challenges of using remote sensing techniques to monitor river discharge, several promising experiments using active and passive remote sensors were conducted in the late 1990s, paving the way for new approaches to monitoring river discharge and, more extensively, environmental data (Vörösmarty et al., 1996b; Smith et al., 1996; Alsdorf et al., 2000; Birkett, 1998).

Problem definition

Hydrological studies, water resources, flood risk management, and ecological habitat management all require precise river discharge measurements. However, due to technical difficulties and metrological questions, measuring and monitoring stream discharges is a difficult and time-consuming task. Aside from the usual field deployment issues, rivers present unique technical challenges such as floods.

River discharge time series, which were originally recorded to predict floods and water scarcity, became indispensable in the design of hydroelectric dams. Currently, discharge monitoring aids in detecting climatic and environmental change because river water discharge and water quality are functions of many climatic, biological, geological, and topographic variables that coexist in the basin. Climate change is altering the pattern of atmospheric precipitation distribution in time and space, as well as the occurrence of extreme weather events. The global upgrading of river gauging networks is critical for revealing hydrological trends and changing atmospheric patterns. In this way, discharge monitoring stations and the resulting time series may be invaluable in revealing the role of important environmental variables.

In many practical applications, discharge estimation in natural rivers is performed using the velocity-area method, which is based on: (i) discrete point sampling of flow velocity along transects in a specific cross-section of interest; and (ii) derivation of both average flow velocity and associated wetted area (Le Coz et al., 2012). This method, which traditionally employs a large number of highly specialized personnel, is extremely expensive and time-consuming. Multiple field campaigns are frequently conducted on the same cross-section of a river with the goal of deriving the flow rating curve (Figure II), which requires a consistent dataset of paired measures of discharge and river stage, with a consequent need for field campaigns conducted at different times of the year to ensure good flow regime representativeness. Cross-sections may change over time because of

vegetation growth and riverbed movement, necessitating frequent replications of field campaigns and periodic flow rating curve recalibrations.

Figure II – Typical river discharge measurement with a current meter (National Park Service U.S. Department of the Interior)

It is possible to categorize the uncertainties of river discharge measurements according to the following error sources, taking into account the thorough literature review (more than 140 publications) conducted by Pelletier (1988): sampling the cross-sectional area, sampling the mean velocity in time, sampling the mean velocity in space (both vertically and transversally), sampling river stages, instruments errors (including a variety of effects), and differences in the discharge computation. It has been determined that significant sources of inaccuracies in discharge measurements using rating curves come from errors in river stage and velocity measurements made during surveys. These latter are sometimes insufficient to assess discharge during severe flood conditions, necessitating extrapolation. This final factor is related to how challenging is to sample discharge-stage couples using conventional methods and equipment when there is high flow, particularly given the elevated hazards to operator safety.

Any hydrological assessment relies on flow rating curves, but the amount of discharge measurements that can be collected on a given cross-section typically limits how well they can be calibrated (Fulton and Ostrowski, 2008; Di Baldassarre and Montanari, 2009). Moreover, rating curves of alluvial rivers can change over time (Westerberg et al., 2011), and this suggests that repeated, time-consuming, and expensive field measurements are required, which may not always result in a sufficient dataset. Flow rating curves are typically created by using curve fitting techniques to data of river stage and discharge. The most common equation (Eq. I) used to describe the relationship between stage and discharge is (Mosley and McKerchar, 1993; Clarke, 1999):

$$Q = C(h + a)^n \qquad \text{(Eq. I)}$$

where C, n, and a are calibration parameters.

This equation is fitted to the N observations of (H, Q) neglecting the origin of these data (i.e., the procedure used to derive discharge). In fact, this data are originally obtained from a river survey aimed at measuring the averaged flow velocity and the associated wetted area of the cross-section. Both features vary with river stage and can be expressed as a function of H, but the wetted area can be easily measured at higher river stage values with topographic surveys, providing a critical constraint for the extrapolation of the flow rating curves at the higher values of H.

Although various and valid options, such as the use of Doppler instrumentation, radar, and remote sensing observations, are frequently considered, these rarely reduce the problems associated with both expensive equipment and the need for lengthy and laborious field campaigns conducted by expert personnel. There is a growing recognition that advancements in flow monitoring toward simpler and more accessible methods with higher spatial and temporal resolution are still urgently needed.

Objectives

Traditionally flow measurements have been performed using the velocity-area method, which obtains the discharge by integrating the individual discharge contributions within the difference surfaces into which the cross-section of a river is discretized. It is a measurement that needs the knowledge of the cross-section geometry as well as numerous measurements of the current velocity along different verticals and at different depths. The velocity-area method can be applied continuously with ADCPs or discretely with current meters (often mechanical or electromagnetic). The traditional method that relies on using these instruments has significant execution issues and needs the use of highly qualified individuals for a sizable amount of time. Moreover, it is frequently hard to conduct such measurement campaigns and ensure acceptable safety conditions for operators during specific flow circumstances, such as during high flow or flooding events.

Discharge measurements are also connected to the rating curves established for river sections. They are characterized as the correlation between the discharge in a certain river cross-section and the relative water level above the hydrometric zero. Depending on the hydraulic regime this relationship is always identified, though with varied degrees of accuracy. The rating curve must have the qualities of being unique and stable over time to be properly evaluated. The rules of hydraulics always ensure uniqueness. On the other hand, the issue comes with the stability of the rating curve over time because a number of variables, both of natural and anthropogenic origin, can affect the morphology of the river channel and, as a consequence, the hydrometric regime that is established in the channel during extreme events.

Having a rating curve available in a specific section of a river allows an immediate and real-time estimation of the discharge flowing in that section from the simple continuous measurement of the stage levels. However, to define a trustworthy rating curve, a thorough campaign of flow measurements and the corresponding water heights must be conducted to gather a sufficient number of

representative points for all potential flow situations and to then apply regression techniques. Once the equation from the rating curve is created, a continuous "planned management" effort is needed because of the hydraulic and morphological unpredictability of the riverbed and the requirement to control and update the rating curve over time.

It frequently occurs that, despite lengthy measurement campaigns, the measured stage-discharge combinations do not adequately cover the range of flow rates, or, again, that during floods, measurements are impractical due to the inherent limits of conventional measuring instruments. Such circumstances can significantly reduce the rating curves range of validity and reliability and make it more common to extrapolate higher discharges from them.

Among the measurement techniques that today can easily complement, or even replace, traditional approaches and allow to overcome many of the associated difficulties, are the optical techniques. The objective of such techniques is to obtain the surface velocities of a field of motion in which a trackable material is present, whose movement can be easily followed from a graphical point of view. A distinction can be made between those techniques developed for small-scale applications (i.e., laboratory experiments) and those for large-scale ones. To the first category belong PIV (Particle Image Velocimetry), which uses a Eulerian approach for the estimation of the surface velocity field, and PTV (Particle Tracking Velocimetry), which instead uses a Lagrangian approach. Evolutions of the small-scales techniques for applications at larger scales, such as the natural rivers, are called LS-PIV (Large-Scale PIV) and LS-PTV (Large-Scale PTV).

In both optical techniques, it is operationally necessary that a suitable tracer (naturally present or artificially introduced) is floating on the water surface and moving along with the water flow, with the ability to describe the movement of the surface liquid particles. The movement of the tracer over time is then recorded resulting in sequences of images that are subsequently processed to estimate the surface velocity field of the current. In the “processing” phase, the recorded images are processed using specific software freely available on the web and generally open source. A statistical cross-correlation analysis is usually applied with which the displacements of the tracer particle patterns between successive frames are estimated. If the geometric resolution of the images and the temporal resolution of the sequence (i.e., frame rate) are known, it is possible to derive the instantaneous surface velocity fields, from which an average (time-averaged) velocity field can be derived over the entire analysed image sequence. Finally, it is possible to carry

out a final step, which can be performed if the bathymetry of a section contained within the recorded area is known. The discharge is then obtained by calculating the depth-average velocity from the average surface velocity field by making simplified assumptions on the vertical distribution of the velocity and multiplying this result with the wetted cross-sectional area.

Economically inexpensive, extremely adaptable, non-invasive, and able to quickly supplement or replace conventional measurement methods, optical techniques are becoming widely used to monitor rivers. Additionally, combining optical approaches with conventional methods would enable the achievement of a dual goal in the task of rebuilding the rating curves: (i) the ability to conduct measurements even in situations where using traditional methods would be impossible (such as during floods or when water levels are abnormally low), obtaining valuable data that can be used to reconstruct the rating curve by extending its range of validity; (ii) the chance to use measurements from optical techniques to validate the extrapolated rating curves.

The aim of this thesis is to demonstrate the potential of optical techniques by describing their typical characteristics and strengths. Since optical techniques represent an innovative approach in river flow monitoring, operational protocols for the extensive application of such methodologies are often lacking. For this reason, the research activity presented in this thesis has focused on analysing some of the fundamental parameters of optical techniques, allowing some useful guidelines to be derived for the optimal application in the field. The objective of these studies is to improve the expected response from optical techniques by acting on or modifying certain parameters that significantly improve the software's ability to describe the actual behaviour of the watercourse during the observation period. Open-field applications were also carried out and compared with results obtained with traditional approaches in order to verify the actual simplicity and convenience of adopting the innovative optical techniques.

Thesis structure

The thesis is organized as follows:

- Chapter 1 introduces the importance of river flow monitoring by describing the techniques and methodologies traditionally applied for discharge calculation. Rating curve and the type of relationship between discharges and water levels are described, as well as the problems and limitations encountered in its determination. Chapter 1 therefore gives an overview of the state of the art in the field of flow measurement.
- In Chapter 2, a detailed description of innovative techniques applied on a large scale is given. All the fundamental steps in the application of optical techniques are explained, distinguishing between Eulerian and Lagrangian methods.
- Chapter 3 contains the description of activities related to a measurement campaign carried out extensively over the entire region of Sicily, Italy. With particular emphasis on the LS-PIV technique, the field activities allowed the application of the optical approach for the assessment of the discharges flowing in several Sicilian rivers. The field activities spanned the entire PhD period, so the applicability of the optical techniques was evaluated over a sufficiently wide time span to experience different weather and environmental conditions, as well as different hydraulic regimes. Flow measurements with traditional techniques were also performed, obtaining benchmark values to compare the two approaches.
- Chapter 4 is dedicated to an in-depth analysis of some peculiar parameters of optical techniques. Explicit reference is made to the LS-PIV technique, exploiting the measurements made during the measurement campaign described in Chapter 3. Analyses are first carried out on several synthetically generated sequences

representative of a real watercourse. The images analysed refer to different scenarios: a totally ideal and a semi-real one. The particles move virtually under two different hydraulic conditions of the current (low and high velocity) and different conditions of tracer density, and size are also taken into account. Finally, the influence of two important parameters specific to recorded sequences is studied: video length and acquisition frame rate.

- Chapter 5 reports the influence of two fundamental elements on which the accuracy of discharge estimation by optical techniques depends. In particular, the density and distribution of the tracer on the liquid surface plays a key role in the adequate description of the motion of surface water particles. An absence or an excessive presence of tracer, or even a poor distribution of the tracer, leads to difficulties in the tracking of patterns by dedicated optical software. This means that the entire recorded sequence is often not suitable for processing as the density and distribution characteristics of the tracer are generally not kept constant during acquisitions. A methodology is therefore proposed to identify the best video portion to process based on the tracer characteristics, optimising the response of the optical software.
- Chapter 6 provides a preliminary analysis of the phenomenon of turbulence and its influence on the performance of optical software. Turbulence is an element that moves the operating conditions away from ideal conditions, and is almost always present in natural watercourses, as could be observed during measurement campaigns in open field. A current may be turbulent due to the presence of obstacles within the channels, or due to the high roughness of the streambed, or even due to flow velocities. The seeding phase may therefore be subject, as verified with the experience of the field measurement campaigns, to problems that cause the tracer to agglomerate and not distribute homogeneously over the liquid surface. Chapter 6 addresses the problem of turbulence from a numerical point of view and using tools typical of computational fluid dynamics. The results reported are from preliminary analyses, as the phenomenology of turbulence is a very complex and difficult problem to study. However, the results obtained are promising and indicate that the analyses carried out are heading in the right direction.

The thesis ends with a brief summary of the contents of the previous chapters, reporting the most important highlights and results obtained from the analyses presented. Finally, concluding remarks and future analyses for the further development of knowledge regarding optical techniques are given.

Chapter 1
Discharge measurements: state of art and innovative techniques

1.1. Introduction

The sum of all climatological, geomorphological, and geographic elements that coexist in a drainage basin results in streamflow. It is the only stage of the hydrological cycle where the water is contained in well-defined channels (Figure 1.1), making it possible to quantify the volumes involved with high accuracy.

Figure 1.1 - Central Arizona Project (CAP): an example of well-bounded open channel. The aqueduct is a diversion canal in Arizona (US) diverting water from the Colorado River (U.S. Bureau of Reclamation).

The foundation of effective water management is based also on the knowledge of accurate streamflow data, and the accuracy of the data ultimately lies on the initial field observations. Therefore, it is the duty of the hydrologist performing these measurements to guarantee raw data of acceptable quality. The accuracy of the field measurements is a key factor in the data successful processing and publishing.

The type of streamflow information required may be classified into two distinct categories. The first is required for planning and design, while the second is that required for current use, i.e., operational management. Although data for planning and design may not always be immediately useful, they are valuable in the long run for a variety of civil engineering projects as well as for forecasting and controlling floods. In addition to data on the stream environment, planning and design data are also employed to look at long-term trends. Since current use data are always necessary at first for operation and control, they have an instant high return value instead.

According to Newtonian physics of open channel hydraulics of water, river discharge is the volumetric rate of flow of water (volume per unit time) in an open channel, including any sediment or other particles that may be dissolved or combined with it. In cubic metres per second, this is the total volume of water flowing through the channel at any time.

About 2.5 percent of the Earth's water mass (~1.4 10^9 km^3) corresponds to freshwater. Rivers and freshwater lakes, that are, undoubtedly, the most accessible water sources, store ~0.007% of the total water available for human consumption. Besides their role and freshwater suppliers, rivers contribute to support dynamic and assorted life-sustaining systems, in the river themselves, and in estuaries and the contiguous marine environment. Despite the ostensible scarcity of freshwater and the almost insignificant relative presence of rivers in the freshwater budget, they supply ~50% of the water humanity has at its disposal to fulfil all its drinking needs, and ~57% of the water used for irrigation (UNESCO WWAP, 2021). These information put in the correct perspective the importance of freshwater resources for the future of humanity, particularly in a climate change scenario.

The changing of discharge of a river over time depends on a few, but important, factors. Water availability would be the main element influencing river flow in a drainage basin; hence weather and climate are significant factors to take into account (Von Storch, 2005). Even with an adequate water supply, drainage basin characteristics may have a significant impact on river discharge and runoff in

several ways. The hydrological regime, which in turn impacts the ecosystem-level processes that affect the availability of water resources, may be altered by human or natural activity in the natural systems (Vogel et al., 2015; Bonacci et al., 2015). The physical characteristics affecting river discharge and runoff, has been traditionally divided in two distinct classes: (i) conditions inherent in the natural landscape, and (ii) conditions in which nature has been transformed by the human use of the land. Basin elevation and orientation, topography (shape and slope), geology, and soil type are the more conspicuous natural features. Deforestation, agriculture, or urban developments are the practices having the most general influence on natural drainage, while dam construction and waterway alteration impact on river flow dynamics.

The most significant factor influencing riverine flow is climate, which takes into account both the short- and long-term availability of moisture as well as the daily weather patterns that determine when and how much water is transported to drainage basins by the atmosphere. Included are storm kinds, typical rain or snowfall length and intensity, distribution of precipitation over the drainage basin, and the consistency of precipitation over a number of years, all of which are thought to have been considerably altered by climate change. Climate change affects how often extreme climatic events occur and how frequently precipitation occurs, which gives river flow series non-stationary features. So, it is evident that climate has a major role in causing floods and droughts (Figure 1.2). However, the physical characteristics of the drainage basin regularly affect floods, sometimes working in concert with rainfall (e.g., increased runoff triggered by deforestation). Conversely, effective management of the vegetation cover may favourably contribute to preserving base flow in streams and rivers during droughts.

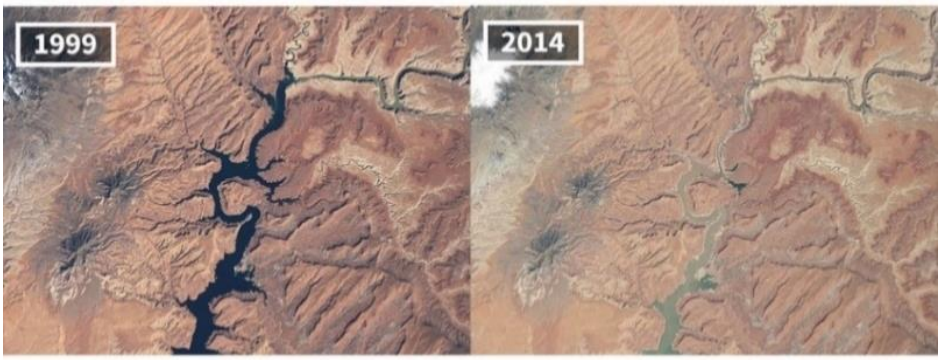

Figure 1.2 - Effects of the climate change on Lake Powell (Arizona, US). Prolonged droughts have caused a dramatic drop in the lake's water level. By May 2014 the lake had dropped 24% of capacity (NASA satellite images).

The current climate environmental crisis has given river monitoring a fresh perspective: river flow dynamics provide a trustworthy picture of the environmental causes and changes taking place in the drainage basin. Long river flow time series can enable obtaining a historical description on environmental changes, like climate change.

Since monitoring streamflow can potentially be used to study the impact of climate change on water resources, help understand trends of natural hazards, e.g., flash floods, landslides, and can be applied for the assessment of freshwater services or water retained by different landscapes (Naithani et al. 2001; Haritashya et al. 2006; Huntington 2006; Mata and Budhooram 2007; Chen et al. 2014), it is essential to understand how to carry out precise discharge measurement. Discharge can also be used as a tool to understand the contribution of water to economic development and human well-being (Acreman, 2001), enabling societies to allocate water to its highest social value (Moran and Dann, 2007). Efficient economic allocation of water ensures the availability of water resources for direct human use such as drinking, domestic use, agricultural use, etc., while efficient ecological water allocation ensures availability of resources for indirect human use in terms of provision of several ecosystem services that support human society (Acreman, 2001; Reddy et al., 2015). However, streamflow, in developed countries, is being monitored since late nineteenth century for better management and allocation of water resources (Barrow, 1998), while in developing countries, streamflow monitoring is largely understudied.

The measurement of discharge in a stream forms an important branch of Hydrometry, the science and practice of water measurement. Methods for streamflow monitoring are specific to stream types. Stream channels can be classified based on eight major variables: width, depth, velocity, discharge, slope, roughness of bed and bank materials, sediment load, and sediment size (Singh, 2003). Different methods are available to quantify and monitor the surface water flow. Barring a few exceptional cases, continuous measurement of stream discharge is very difficult. As a rule, direct measurement of discharge is a very time-consuming and costly procedure. Hence, a two-step procedure is followed. First, the discharge, in a given stream, is related to the elevation of the water surface (stage) though a series of careful measurements. In the next step, the stage of the stream is observed routinely in a relatively inexpensive manner and the discharge is estimated by using the previously determined stage-discharge relationship. The observation of the stage is easy, inexpensive, and if desired, continuous readings can also be obtained. This method of discharge determination of streams is adopted universally.

1.2. The stage-discharge relation

1.2.1. Overview

The stage and discharge of a stream are generally variable. A correlation between the stage and discharge is computed in order to generate a continuous record of discharge. The stage-discharge relation is a term used to describe this calibration. The rating curve is a crucial instrument in surface hydrology because a good stage-discharge relationship at the gauging station is crucial to the accuracy of discharge data values. Despite the appearance that creating rating curves is mostly an empirical effort, a solid theoretical foundation is required to develop a dependable instrument for deriving from measured water height to discharge.

The rating curve has been and continues to be an important tool in hydrology for estimating discharge in natural and/or artificial open channels. Since the early nineteenth century, it has been common practise to measure the discharge of streams at appropriate times, typically using a current meter or other methods (Rantz et al. 1982; ISO 1100-1, 1998; SIMN, 1998). A curve of discharge against stage can then be produced by fitting these data with a power or polynomial curve,

while the matching stage is simultaneously monitored in the meantime. The conventional and straightforward method for determining current discharge is to monitor the water level using gauges and then estimate the flow discharge using the stage-discharge relationship. Direct measurements of discharge in open channels are notoriously expensive, time-consuming, and occasionally unfeasible during floods.

The definition and application of stage-discharge curves dates back to the early XX century. Jones (1916) first suggested a way to adjust stage-discharge relations by taking the slope of the surface water into account in the beginning of the previous century. In the same period (1918) the "Ufficio Idrografico del Magistrato della Acque di Venezia" (Venice Warer Authority) provided instructions to define the stage-discharge relations for a watercourse. A great portion of the modern practices used worldwide were developed by the United State Geological Survey (USGS). The methods that are currently in use are widely described in USGS publications of Corbett et al. (1943), Dawdy (1961), Bailey and Ray (1966), Rantz (1963), Rantz et al. (1982), as well as in the World Meteorological Organization (WMO) Publication n. 519, Operational Hydrology Report n.13 (1980), and in the International Organization for Standardization (ISO) Regulation n. 1100-2 1998 (ISO, 1998). Other sources are the National Engineering Handbook (Pasley et al., 1972), the "Manuale per il monitoraggio idrografico" (Becchi et al., 1994), and the book "Streamflow Measurement" by Herschy (1995).

Enough discharge measurements must be taken, and then a rating curve can be developed by plotting the measured discharges against the appropriate stages and creating a smooth curve representing the relationship between the two parameters. To establish the rating curve as quickly as possible, discharge measurements are performed across the range of stage variation. During the analysis period, the ISO regulation 1100-2 (ISO, 1998) recommends at least 12-15 discharge measurements. Lower and medium stage discharges are usually simple, but higher stage discharges can take some time and require careful extrapolation. If the channel is stable, fewer measurements may be needed; however, very few rivers have completely stable characteristics. Calibration cannot thus be performed once and for all but must be repeated as frequently as the rate of change in the stage-discharge relation requires. The number of discharge measurements required to define the stage-discharge relation at any time is thus determined by the stability of the relation. Because of random shifts in the stream geometry, several discharge

measurements per month may be required to define the stage-discharge relation in sand-bed channels, for example.

To maintain a permanent and stable stage-discharge relationship, the stream channel at the gauging station must be capable of stabilising and regulating the flow past the station so that the discharge through the measuring section remains constant for a given stage. The shape, reliability, and stability of the stage-discharge relation are normally controlled by the station control, which is a section or reach of channel at or downstream from the gauging station. A station control is a critical depth control in open channel hydraulics, also known as a section control, if a critical flow section exists a short distance downstream from the gauging station, or a channel control if the stage-discharge relation is primarily determined by channel irregularities and channel friction over a reach downstream from the station. A control is considered permanent if the stage-discharge relation does not change over time; otherwise, it is considered impermanent and is commonly referred to as shifting control. The geometry of the station control eliminates all downstream effects on the discharge at the measuring section. The cross-sectional area and shape of the stream channel, the channel sinuosity (meanders and loops), the channel expansions and restrictions, the stability and roughness of the streambed and banks, and the vegetation cover are all factors determining the channel conveyance.

The following is the general procedure for determining the stage-discharge curve. The discharge measurements are plotted on an arithmetic graph, with discharge on the horizontal scale and gauge height on the vertical. If a discharge measurement was not taken at a steady stage, the mean gauge height during the measurement is used. The plotted observations are labelled in chronological order, and if necessary, rising and falling stages during the measurement are indicated by distinguishing symbols. The relationship should be defined by a sufficient number of measurements distributed appropriately across the stage range, taking into account the shape of the stage-discharge relation. The number and spacing of the observations should ideally be chosen to correspond to the relative frequency of flow at each stage. That is, the number of observations at various subranges is proportional to the probability of discharge at these same ranges, encompassing the entire discharge range for which the relation is plotted. In practise, however, it is preferable to have as many observations as possible at the extreme ranges, both at low flow and high flood stages. The relationship curve is drawn evenly and smoothly through the scatter of plotted data points (Figure 1.3).

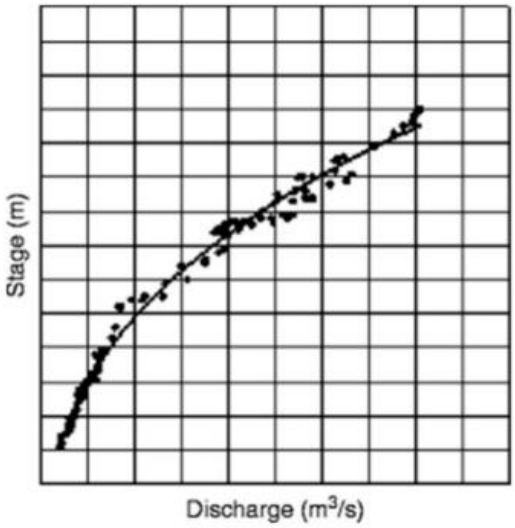

Figure 1.3 - Example of stage-discharge relation. Black scattered points are the stage-discharge pairs measurements; solid black line is the fitting curve. (Kumar, 2011)

Although all discharge data are verified and approved before being plotted, observations that plot more than, say, 5% of the discharge off the curve should be reviewed once again for potential errors. Particular attention is paid to the need to adjust or weight the gauge height, to the instruments rating, and to errors in the computation. With respect to the latter, it is useful to make a plot of the cross-sectional area of flow and the mean velocity against gauge height for each discharge measurement. Such plots reveal the presence of an error and where it is located in the computation, either in the velocity or in the cross-sectional area.

Fitting a median curve to observe or measure data points can be accomplished in a variety of ways. This can be done quite satisfactorily by visual estimation of the plot using drafting curves, which are typically designed to conform to parabolic equations. Because stream discharge varies as some power of flow depth, the trend of discharge measurements plotted on graph paper frequently follows a specific drafting curve. When fitting a median curve to observations using visual estimation (ISO, 1998), the criterion is that there are roughly the same number of plus and minus deviations. A deviation is considered negative when the measurement is above the curve and positive when the measurement is below the curve. The stage-discharge curve can often be determined by plotting the

logarithms of stage against the logarithms of discharge. The use of logarithmic graph paper eliminates the need to compute logarithms, and observations are plotted in the same manner as before. There are certain important advantages in using the logarithmic method:

- the logarithmic form of the rating curve can be developed into a straight line by adding or subtracting a constant value (datum correction) to the gauge height logarithmic scale;
- the straight-line graph can be described by a simple mathematical equation that is easily handled by pocket calculator or computer;
- the straight-line graph may be conveniently analysed for uncertainties;
- a percentage distance of the curve is always the same regardless of where it is located. Thus, a measurement that is 10% off the curve at high stage will be the same distance away from the curve as a measurement that is 10% off at low stage;
- it is easier to identify the range in stage for which different controls are effective;
- the gauge height scale may be conveniently altered by halving, doubling, or adding a percentage to the scale. The curve will merely shift position but retain the same shape;
- the curve can be easily extrapolated, if necessary, but caution is required in extrapolation at either the top or the bottom end of the curve. If the curve is a single segment and the control is stable, then extrapolation may be performed with more confidence than if the curve is made up of several segments.

The most used stage-discharge relation treats the discharge as a unique function of the stage. This relation typically follows a power curve (Herschy, 1995; ISO 1998; Kennedy, 1984; Rantz et al., 1982). The stage-discharge relation may be expressed by an equation (Eq. 1.1) of the form:

$$Q = C(h + a)^n \qquad \text{(Eq. 1.1)}$$

where Q is the discharge, h is the gauge height, C and n are constants, and a is the stage at zero flow (datum correction). Eq. 1.1 may be transformed by logarithms to Eq. 1.2:

$$logQ = logC + nlog(h + a) \quad \text{(Eq. 1.2)}$$

which is in the form of the equation of a straight line (Eq. 1.3):

$$y = nx + C \quad \text{(Eq. 1.3)}$$

where n is the gradient and C is the intersection of the line on the y-axis.

By plotting Q against $(h + a)$, on double logarithmic graph paper, a straight line is obtained (Figure 1.4).

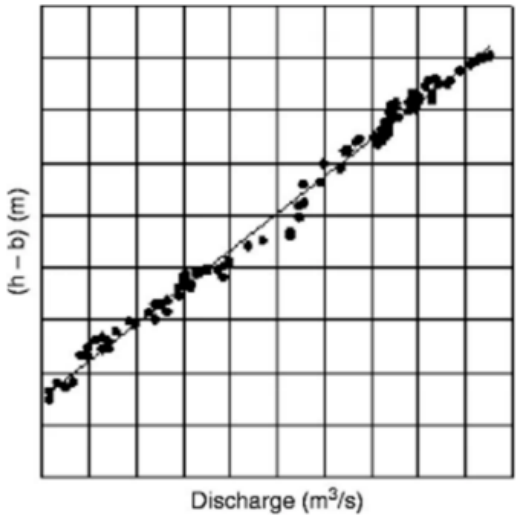

Figure 1.4 – Example of stage-discharge relation in a logarithmic plane. Black scattered points are the stage-discharge pairs measurements; solid black line is the fitting curve. (Kumar, 2011)

Often, two or more connected straight lines are needed to fit the data, and it is usually possible to determine the approximate location of the break points of each rage. The actual break points can be determined either by solving the two equations for Q and h or by purely graphical means. The equation for Q cannot be expected to apply throughout the entire range of stage for very irregular channels or non-uniform flow. Sometimes the curve changes from a parabolic to a complex curve, and the constants and exponents vary across the range. The logarithmic rating equation therefore is seldom a single straight line or a gentle curve throughout the entire range of stage at gauging station. If the section changes at various stages, it may be necessary to fit two or more equations. If, however, too many changes in the parameters are necessary to define the relation, it is possible that the logarithmic method may not suitable, and a curve fitted by visual estimation can be employed.

The first derivative (Eq. 1.4) of the equation for Q is a measure of the change in discharge per unit change in stage, that is the first derivative gives the first-order differences of the discharge series. The first derivative is:

$$\frac{dQ}{dh} = Cn(h+a)^{n-1} \qquad \text{(Eq. 1.4)}$$

Second-order differences (Eq. 1.5) are obtained by differentiating again. The second derivative is:

$$\frac{d^2Q}{dh^2} = Cn(n-1)(h+a)^{n-2} \qquad \text{(Eq. 1.5)}$$

An examination of the second derivative shows that the second-order differences increase with stage when n is greater than 2 and decrease with stage when n is less than 2.

Normally in graphical analysis the dependent variable, Q, would be plotted on the vertical axis and the independent variable, h, plotted on abscissa. It has been a tradition in stream gauging, however, that this procedure is reversed while still retaining Q as the dependent variable and taking n, the slope, as the cotangent

instead of the tangent. The geometry or shape of the channel section is reflected in the slope, n, of the stage-discharge equation. This property is a useful indicator when carrying out a preliminary survey at a new site. The following are approximate relations between n and channel sections:

i) for a rectangular channel section, $n = 3/2$
ii) for a concave section of parabolic shape, $n = 2$
iii) for a triangular or semi-circular section, $n = 5/2$

When the exponent n approaches to $3/2$ rating is also known as Guglielmini rating-curve (Ufficio Idrografico del Magistrato di Venezia, 1914).

Changes in channel resistance and slope with stage, however, will affect the exponent n. The net result of these factors is that the exponent in the equation of Q for relatively wide rivers with channel control will generally vary from about 1.3 to 1.8. For relatively deep narrow rivers with section control, the exponent n will almost always be greater than two and may often exceed a value of three.

The lowest point on the low water control corresponds to the datum correction (a), which is the value of the stage at zero flow. Unless the gauges are expressly placed to the lowest level of an artificial control or the crest of a measuring structure, this stage typically does not correspond with the gauges' zero. Therefore, for artificial controls and in situations where the control is precisely defined by a rock ledge, the point of zero flow can be clearly identified. Subtracting the depth of the water over the lowest point on the control from the stage indicated by the gauge reading yields the stage of zero flow. The position of the point of zero flow is best determined at time of low water, when rivers can often be waded. It should be noted that when a quantity has to be added to the gauge heights in order to obtain a straight line, a is taken as positive, that is the zero of the gauges is in this case positioned at a level above the point of zero flow. Conversely, when a quantity has to be subtracted from the gauge heights, a is taken as negative and in this case the zero of the gauges is positioned at a level below the point of zero flow. When the zero of the gauges coincides with the level of the point of zero flow, then a is zero.

Scientific literature contains other hypotheses about the topic. For instance, several papers suggested fresh methods for extrapolating curves for discharge ratings. Support Vector Machines (SVM; Cristianini and Shawe-Taylor, 2000), which operate on the principal of linear regression on a higher dimensional feature space, are recommended by Sivapragasam and Muttil (2005) for the extrapolation

of rating curves. However, Bhattacharya and Solomatine (2000) had already defined stage discharge relations using Artificial Neural Networks (ANNs), which nowadays are popular in many fields of water-related study. An evaluation of an ANN-based strategy against a traditional statistical stage-discharge model demonstrated its advantages. Deka and Chandramouli (2003) tested several modern approaches to the problem: a neural network model, a modularized neural network model, a conventional curve-fitting approach and a fuzzy neural network model are compared using a case study. Overall, the fuzzy neural network model gives the best results. Manfreda (2018) introduces an approach for calculating rating curves based on the product of current velocity and wetted cross-sectional area, both of which functions of river stage.

$$Q = V(H - h_o)\Omega(H - h_o) \qquad \text{(Eq. 1.6)}$$

where $V(H - h_o)$ and $\Omega(H - h_o)$ are the fitting functions describing the relationship existing between velocity, wetted area, and water stage.

The approach can be usefully employed in all those cases where few data are available, exploiting these to obtain, with an appropriate regression, the average velocity values from which to calculate the function $V(H - h_o)$. Regarding the relationship $\Omega(H - h_o)$, information about variation in the magnitude of the wetted area with increasing water level can be obtained directly from topographic surveys of the measurement section. This implies that it is possible to know the cross-sectional wetted area information even for water levels related to high flow conditions, i.e., those for which rating curves are usually extrapolated.

The sensitivity of a stage-discharge relation is a measure of how much an increase in stage will counteract an increase in discharge. When a relatively large increase in discharge results in a relatively little rise in stage, the relationship is said to be non-sensitive. The opposite is true when a relatively small increase in discharge results in a relatively large increase in stage. The accuracy of the flow data reflects the degree of sensitivity, which impacts the station's record at all flow phases. As a result, a sensitive stage record can be transformed into a discharge record more precisely than a non-sensitive one. For instance, reading water level accurately to 5 mm at a sensitive station would be sufficient, but at a less sensitive station, the accuracy needed might be 1 mm to get the same accuracy of discharge.

Sensitivity varies with discharge at every station and, for the most part, tends to fall as discharge rises. It should be estimated for each station at the same level in order to provide a true comparison.

The uncertainties in the discharge records from these stations as a result of the uncertainties in the empirical stage-discharge ratings have been studied by several authors. Numerous papers address issues like the impact of uncertainty on peak discharge evaluation or the definition of the rating curve (Clarke, 1999; Parodi and Ferraris, 2004; Aronica et al., 2005). Rating-curves are empirical; hence uncertainty analyses are typically restricted to a statistical analysis of such curves.

1.2.2. Extrapolation of rating curves

The stage-discharge relation's ability to be applied in cases of extremely high flow is crucial. The defining of the upper and lower portions of the rating-curve typically lacks discharge measurements. This data extrapolation is susceptible to a considerable error that could have significant effects on flood management (upper curve) and water resource planning (lower curve).

It is frequently essential to extrapolate the rating curve in both directions. If the zero-flow point has been found, the curve can be roughly interpolated between this point and the measurements of the lowest discharge. However, it is not a good idea to extrapolate too far in this direction if the point of zero-flow is not available. Extrapolation is almost always required in the upper portion of the curve.

For shorter extensions, logarithmic extrapolation has proven to be a reliable technique. However, special techniques must be required if extended extrapolations must be made. The most popular techniques for extrapolating rating curves are listed below.

1.2.2.1. The stage-velocity-area method

The extension of the stage against the mean velocity curve is the most effective technique. If the cross-section is regular and no bank overflow occurs, a plot with stage as the ordinate and mean velocity as the abscissa results in a curve

that tends to become asymptotic to the vertical at higher stages. This curve can therefore be stretched without making many errors because the rate of increase in velocity at the upper stages rapidly decreases. Additionally, the area can be read off at any stage by displaying the stage-area curve (with stage as the ordinate and area as the abscissa) for the same cross-section as that from which the mean velocity was determined. Discharge is obtained by dividing the area by the mean value of velocity.

The area is obtained by a field survey up to the highest stage required and is therefore a known quantity.

1.2.2.2. The Manning equation method

The uniform flow equation as developed by Manning, expressed as Eq. 1.6:

$$Q = \frac{1}{n} A R^{\frac{2}{3}} S^{\frac{1}{2}} \qquad \text{(Eq. 1.6)}$$

where n is a constant, A is the area of the cross-section, R the hydraulic radius, S the slope of water surface, and Q the discharge, may be used for extrapolation of rating curves. In terms of mean velocity, the equation may be written as Eq. 1.7:

$$v = \frac{1}{n} R^{\frac{2}{3}} S^{\frac{1}{2}} \qquad \text{(Eq. 1.7)}$$

For the higher stages, the factor $\frac{1}{n} n S^{\frac{1}{2}}$ become approximately constant (K); thus Eq. 1.6 and Eq. 1.7 can therefore be rewritten as Eq. 1.8 and then Eq. 1.9:

$$Q = K A R^{\frac{2}{3}} \qquad \text{(Eq. 1.8)}$$

$$v = KR^{\frac{2}{3}} \qquad \text{(Eq. 1.9)}$$

By using various values of v from the known portion of the stage against the mean velocity curve and the corresponding values of R, values of K can be computed by velocity equation for the range in stage for which the velocity is known. By plotting these values of K against the gauge height, a curve is obtained that should asymptotically approach a vertical line for the higher stages. This K-curve may then be extended without much error and values of K obtained from it for the higher stages. These high stage values of K combined with their respective values of A and $R^{\frac{2}{3}}$ using Q-equation will give values of the discharge Q which may be used to extrapolate the rating curve.

A and R are obtained by field surveys and are supposed known for any stage required.

1.2.2.3. The Stevens method

The so-called Stevens method is a variation of the Manning equation method. It is based on the Chezy formula for uniform flow (Eq. 1.10):

$$Q = AC(RS)^{\frac{1}{2}} \qquad \text{(Eq. 1.10)}$$

For shallow streams with a relatively small depth-width ratio, the mean depth D does not differ much from the hydraulic radius R. Then, by substituting D for R, Eq. 1.10 may be written as Eq. 1.11:

$$Q = CS^{\frac{1}{2}}AD^{\frac{1}{2}} \qquad \text{(Eq. 1.11)}$$

At higher stages, the slope S in most cases may be considered constant. Then, by plotting $AD^{\frac{1}{2}}$ against Q, an approximately straight line is obtained which is readily extended. Both A and D are obtained by field surveys and are therefore known factors.

1.2.3. Difficulties and uncertainties in defining stage-discharge relation

In natural channels, the resistance coefficient varies with bed and flow conditions, the cross-section changes with sediment deposition and erosion, and the water-surface slope fluctuates with irregular flow. Numerous factors that vary the shape and position of the rating curve or cause loops in the rating curve can alter the relationship between stage and discharge. Principal factors that affect the rating curve include (Herschy, 1995; Kennedy, 1984; Rantz et al., 1982): (i) changes to the channel cross-section due mainly to scour and fill; (ii) growth and decay of aquatic vegetation; (iii) loaf or debris jams (an accumulation of logs and other organic debris which blocks the flow of a stream of water); (iv) variable backwater; rapidly changing discharge; (v) discharge to or from overbank areas; (vi) ice. Variable backwater, rapidly changing discharge, and flow to or from overbank areas all result in looped or non-unique ratings and are typically addressed through including additional parameters, such as an estimate of the water surface slope or the rate of change of the water surface at the gauge. So, when the type of flow differs significantly from the steady flow state, the simple stage-discharge relation is no longer sufficient to define the discharge. Another parameter should be included, i.e., the slope of water surface. Essentially, in these conditions the ordinary approach, i.e., using the single-valued stage-discharge rating for the computation of discharge records, is not applicable: the discharge rating under conditions of variable backwater and for highly unsteady flow cannot be defined by stage alone.

In general uncertainties in stage-discharge relations could be ascribed to different potential sources of uncertainty:

- natural uncertainties associated with the inherent randomness of natural processes; they include the effect of processes such as

turbulent fluctuations, wind, temporal changes, in resistance or geometry, sediment concentration, and similar physical processes that can affect the flow but are not measured for gauges;

- knowledge uncertainty, which reflects the result of inadequate understanding of the true physical processes and can be reduced by improved knowledge of the physical processes and parameters. This includes improper assumptions in formulation of the relation between stage, discharge, and other parameters; neglection of important parameters; incorrect specification of parameter, and similar errors. This is expected to be the largest source of error in most stage-discharge relations;
- data uncertainties. These include errors in measurement of stage, discharge, geometry, and other characteristics of the flow and channel, transcription errors, and inadequate spatial or temporal sampling.

It has been attempted to quantify and/or decrease uncertainty in stage-discharge relations in a large number of papers and studies. Nevertheless, the state-of-the-art in determining the uncertainty in stage-discharge ratings consists mainly of statistical analyses of the deviations of observations from a "best-fit" rating curve or equation (Herschy, 1995; ISO, 1998). The analysis is generally performed on logarithmic plane. The standard error of estimate s_e may be calculated from the following equation (Eq. 1.12) (ISO, 1998):

$$s_e = \sqrt{\frac{\sum(lnQ - lnQ_c)^2}{k-2}} \qquad \text{(Eq. 1.12)}$$

where Q is the measured discharge, Q_c is the discharge calculated from the rating curve equation, and k is the number of observations. Each segment of the rating curve should be subjected to a separate statistical analysis, according to the ISO standard. When many observations are available, like more than 20, it is possible to derive the 95% confidence interval. In such a way two parallel lines (in logarithmic graph) on either side of the rating curve segment at a distance of $2s_e$ from it can be described. In other words, 95% of the observations on average will be contained within this limit.

This method ignores the potential improvements in the connection that may be produced by integrating hydraulic components and simply takes into account the statistical features of the discharge data used to establish the relation.

1.2.4. Representation of stage-discharge relation

A stage-discharge relation can be represented in various format:

(i) Graphic format through a plotted curve;
(ii) Table format, using generally two columns (one for stage and one for discharge);
(iii) Equation format, by mathematical expression for different stage ranges.

The first step before making a plot of stage versus discharge is to prepare a list of discharge measurements that will be used for the plot. At a minimum this list should include from 12 to 15 measurements, all made during the period of analyses (ISO, 1998). These measurements should be equally distributed over the range of gauge heights experienced, but this is not always achievable because different is the frequency of the various heights (frequency of occurrence of course reduces as height increases).

The list of discharge measurements should also include low and high measurements from other times that might be useful in defining the correct shape of the rating and/or for extrapolating the rating. Extreme low and high measurements should be included wherever possible. For each discharge measurement in the list, the following items should be included at least:

- unique identification number;
- date of measurement;
- gauge height of measurement;
- total discharge;
- accuracy of measurement;
- rate-of-change in stage during measurement, a plus sign indicating rising stage and a minus sign indicating falling stage.

Other information might be included in the list of measurements, but it is optional.

For scales that are simple to read and have the required precision, the rating curve may need to be plotted in two or more segments if the range of gauge height or discharge is wide. Separate curves for low water, medium water, and high water may be produced as a result of this method. It is important to check that the individual curves merge to generate a smooth, continuous combined curve.

Both a logarithmic plot and a rectangle (arithmetic) coordinate plot are used to visualise the discharge and stage measurements. A graph with numeric scales is simple to use and understand. These scales, which have a benefit over logarithmic scales in that zero values of gauge height and/or discharge can be shown, are perfect for depicting a rating curve. However, for analytical purposes, arithmetic scales have practically no advantage. A stage-discharge relation on arithmetic scales is almost always a curved line, concave downward, which can be difficult to shape correctly if only a few discharge measurements are available.

On the other hand, there are a few analytical benefits to using logarithmic scales. As a result, the majority of stage-discharge relations or portions of them are often graphically analysed using logarithmic plotting graph. To effectively utilise this approach, the effective gauge height of zero discharge should be subtracted from gauge height in order to convert it to the effective depth of flow. A rating curve segment, then, will tend to plot as a straight line. In addition, this feature allows the analyst to calibrate the stage-discharge relation with fewer discharge measurements. Finally, it is simple to calculate the rating curve's slope by dividing the horizontal distance by the vertical distance. For shape and analytical purposes, a stage-discharge relation is often first written on logarithmic plotting graph.

The graphic format of a rating shows the stage-discharge relation visually and this is the form used for the initial rating analysis. Every point corresponds to a pair of stages and discharges. Typically, it is better to draw the discharge (the dependent variable) as the abscissa with the concavity pointing downward. The discharge measurements are numbered sequentially in chronological order to make it easier to identify time trends.

Rating curves can be shown as tables, which can then be plotted as piecewise linear curves. But using analytical formulas like Eq. 1.1 to depict stage discharge relation is a more appropriate method for hand calculation. The National Hydrographic Service of Italy used to provide stage-discharge relationship in both

formats in its Hydrological Annals. The first range of ratings, corresponding to measurements, is provided in a table format that can be represented in a piecewise linear curve (Figure 1.5). The extrapolation range is instead expressed in analytical format using Guglielmini formulas (Ufficio Idrografico del Magistrato di Venezia, 1914).

SCALA NUMERICA DELLE PORTATE

Altezza idrometrica *m*	Portate *mc/s*	Altezza idrometrica *m*	Portate *mc/s*	Altezza idrometrica *m*	Portate *mc/s*	Altezza idrometrica *m*	Portate *mc/s*
Dalle ore 0.00 dell'1.1 alle ore 0.59 del 12.2				Dalle ore 1.00 del 12.2 alle ore 24:00 del 31.12			
0,46	0,00	1,80	16,54	0,54	0,00	1,90	21,75
0,98	2,24	2,00	23,60	1,06	2,18	2,10	29,51
1,02	2,64	2,20	34,43	1,10	2,84	2,30	40,84
1,06	3,05	2,40	47,26	1,18	4,18	2,50	56,88
1,10	3,47	2,60	66,50	1,22	4,94	2,70	79,16
1,20	4,53	2,80	91,82	1,50	11,03	2,90	105,91
1,40	7,36	3,00	120,00	1,70	16,05	3,00	120,00
Per H > 3,00 Q = 108,71 (H - 1,93)$^{3/2}$				Per H > 3,00 Q = 108,71 (H - 1,93)$^{3/2}$			

Figure 1.5 – Rating curve in table-format. Table extracted from a Hydrological Annal (National Hydrographic Service of Italy).

1.3. Measurement of discharge

1.3.1. Overview

Methods for streamflow monitoring have been grouped into four categories (based on John, 1978; Martin, 2006; Herschy, 2008; S¸ Şengörür et al., 2014): (i) direct measurement methods, (ii) velocity-area methods, (iii) formed constriction or constricted flow methods, and (iv) non-contact measurement methods. Each of them is explained below.

1.3.2. Direct measurement method

1.3.2.1. Timed volume or volumetric streamflow method

This method is used for streams where the entire flow converges into a single channel (Hauer and Lamberti 2007). The time required to fill a container of a known volume is recorded and later used to calculate the average flow rate. For reliable and accurate results, container must be of a large size and the flow rate measured at least five times, with more than three replicates for the stream width and depth recorded (Ely 1994; Pfeffer and Wagenet 2007). The flow rate is the ratio of average stream cross section area and average time taken to fill the container. This method is accurate, cost and time effective, non-polluting and requires limited resources and technical knowledge (Najafi et al. 2012). However, this method is suitable only for small and narrow streams (Weight 2001; Shope et al. 2013).

1.3.3. Velocity-area methods

Velocity-area methods are based on the principle of the continuity of fluid flow. These methods are used for instantaneous measurement of streamflow and to establish the stage-discharge relationship (Harmel et al., 2009).

1.3.3.1. Float method

In the float method, an object of low density is allowed to float for a known distance in the stream, and the time taken by the float is measured and water speed calculated. The speed of water and the cross-sectional area is used for calculating the water flow in the stream. To overcome error, 5-10 floats should be recorded. The floats should ideally be made of materials such as a water-soaked block of wood, or other natural material that has less per unit area mass and can be easily spotted from a distance (Harrelson et al. 1994; Harwell and Asquith 2011). This is

a simple, non-polluting method and does not require extensive resources and high skills (Hauer and Lamberti 2017). However, the results are often inaccurate because vertical turbulent motion causes the difference between the velocity of different surfaces of streams and float does not represent the actual flow (Hilgersom and Luxemburg 2012). This method is suitable for small and straight streams or canals with low flow (Hudson, 1993); its applicability for larger streams is questionable. To overcome this, the integrated float method has been developed (Herschy, 1995; Hilgersom and Luxemburg, 2012), where a float is released at the bottom of a river or canal. The float is assumed to rise with a constant velocity, so the depth-integrated horizontal velocity can be determined from the float's displacement as it surfaces (Hilgersom and Luxemburg 2012).

1.3.3.2. Dilution gauging method

Dilution gauging method measures streamflow on the basis of rate of diffusion of a tracer that can be either a chemical or a radio isotope (Comina et al. 2014; Dingman 2015). Chemical tracers, such as common salt (NaCl), can be used by using an electrical conductivity (EC) meter or an ion electrode (Flury and Wai 2003). Streamflow is calculated by multiplying average cross section area and velocity of the flow. The method is inexpensive. It is an absolute method because the discharge is computed from volume and time only (Herschy 2008). It is used in turbulent flow conditions where conventional methods are difficult to apply (Gordon et al., 2004). However, the method can report erroneous results due to the loss and incomplete mixing of the tracer arising from the difference in velocity in the upper and lower surfaces of the stream. Special training is needed to apply this method in the field. In certain areas, it is difficult to obtain the permission to inject tracers into streams as it can pollute water.

1.3.3.3. Trajectory method

In the trajectory method, all the flow in a stream is diverted into a pipe (Yan 1996). Flow from a horizontal pipe can be estimated using either the California pipe method developed by van Leer (1924) or the trajectory method

developed by Greve (1928). This flow measurement technique is based on measuring brink depth at the end of the pipe. The diverted water is discharged with pressure so that the rate of flow can be estimated from measurements of the jet (Rohwer 1943). At least two measurements of the discharging jet are required to calculate the rate of flow of the water (Yan 1996; Liu et al., 2014). The method provides reasonably accurate values of discharge only for certain ranges of size and flow conditions and can be applied to streams where discharge can be diverted through a pipe (Hudson 1993). This method can be adapted for the measurement of discharge in small open channels where flow can be directed to a pipe (Liu et al., 2014). This method needs trained manpower and involves complicated calculations.

1.3.3.4. Current meter method

The current meter method depends on defined channel geometry for the calculation of flow velocities (Hamilton and Moore 2012). The current meter measures a point velocity or a velocity field directly. The cross-sectional geometry (channel geometry) is needed to convert the velocity to a discharge. In this method, stream channel cross section is divided into vertical subsections. Area for each subsection is calculated by measuring the average width and depth. The velocity of flow at a point is proportional to the rate of rotation of the rotor during a fixed period of time (Soupir et al. 2009), if a mechanical current meter is employed. The discharge is a product of area and measured velocity and is calculated for each subsection. Total discharge is the sum of discharge of subsections. The current meter method is accurate, time effective and suitable for hilly terrains (USGS 2007) and so can be used commercially (USDA 2001). Current meters are expensive and can be used only for a short period.

1.3.3.5. Acoustic Doppler current profiler method

Acoustic Doppler current profiler method (ADCP) transmits sound into the water and receives echoes from particles suspended in the stream. The difference in the frequency of the transmitted sound and echoes is used to calculate the velocities

of the particles and the water in which they are suspended (Costa et al., 2000, 2006). Mounted on a ship or a boat, ADCPs provide the quasi-continuous vertical profile of horizontal current (Muste et al., 2004; Chauhan et al., 2014). It measures boat speed and direction by tracking the river bottom and compensate for the boat movement in the computation of water velocities (Oberg and Mueller 2007). ADCPs can be classified into two classes based on the techniques used to configure and process the acoustic signal-narrow-band and broadband (Lu and Lueck, 1999; Lee et al., 2014). ADCP methods measures the stream discharge faster and yields accurate results because ADCPs measure a much larger portion of the water column (Mueller and Wagner, 2009). It is non-invasive but costly and needs trained personnel, since if used with inappropriate techniques it may give inaccurate results and is suitable only for large streams and rivers in flat terrains (Visbeck, 2001; Flener et al., 2015). However, the ADCP equipment may be deployed using tethered boat, or small powered launches or catamarans, where, with the aid of two operators, this method can be used for small rivers (Herschy 2008; Flener et al., 2015).

1.3.3.6. The electromagnetic method

The electromagnetic method measures point velocity of a stream by using an electromagnetic meter. Continuous records of velocity at one point in a cross section and of the stage readings are used to calculate the stream discharge records (Egusa et al., 2013). This method works according to Faraday's law of electromagnetic induction, the motion of water flowing in a stream cuts the vertical component of the earth's magnetic field and an electromotive force (EMF) is induced in the water. This EMF can be sensed by electrodes (probes) on each side of the stream and is found to be directly proportional to the average velocity of flow in the cross section (Herschy, 2008). This method gives accurate results, but special training is needed to use the probes (Ryckborst and Christie 1977).

1.3.4. Formed constriction methods

These methods are less influenced by the roughness of the stream and the backwater influence, compared to the velocity-area methods. All formed constriction methods are generally appropriate for small streams.

1.3.4.1. Weir method

In this method, stream discharge is estimated using a formed check-dam or weir made of plywood, or other wooden boards, and reinforced concrete, in the cross section of a stream (Rickard et al. 2003). Weirs are classified into two general categories: broad crested and sharp crested (Chaudhry 2008). Broad crested weirs can only be used to calculate instantaneous flows (Gonzalez and Chanson 2007). Sharp crested weirs are constructed in a variety of shapes such as V-notch, rectangular and Cipolletti weirs (Martin 2006). Flow rate can be measured by using a predefined table or discharge can be estimated using a weir equation, which considers the flow rate, height of water and width of the crest (Ghodsian 2003; Emiroglu et al. 2011). This method requires skilled workers (Peterson and Cromwell 1993) and considerable drop between the upstream and downstream surfaces, which is often not available in flat grade ditches. Frequently, it is necessary to construct a pool or stilling area above the weir, so the water loses its velocity. Weir installations in earthen ditches can be troublesome and results can be affected by installation and construction (Peterson and Cromwell 1993). This method is time consuming, expensive and installation of weirs may alter the habitat for local species (Rickard et al., 2003). Siltation affects the reliability of the results (Hudson 2004). A premeasured flow rate is needed before constructing a weir (Martin 2006). The weir must be sized to accommodate the range that needs to be measured. In many cases, the natural range of flow is too large to be captured by a single weir. Compound weirs can be used to expand the measured range of flows. Weirs are one of the most accurate methods of measuring water flow (Peterson and Cromwell 1993) and may form an important component of a Water Management Plan.

1.3.4.2. Flume method

A flume is an artificial open channel flow section that restricts the stream area and changes its slope, which increases the velocity and changes the volume of the water flowing through the flume (Ancey et al., 2008). There is no impoundment, but the height of water in the flume is measured with a stilling well (Mutz et al., 2007). The discharge can be calculated by measuring the height of water in the flume. A series of type flumes ("HS" type for small flows, "H" type for average flows, and "HL" type for large flows) are used for measuring intermittent runoff, Venturi flume for measuring irrigation water and San Dimas Flume for debris laden flows in mountain streams (USFWS 2006). For water flow calculations, tables given by Bos (1976) and Hudson (1993) can be used. Flumes give accurate results when properly manufactured and installed (Hudson 2004) and do not need calibration, but accuracy gets affected by approach velocity of liquid and siltation (Hudson 2004). This method is not suitable for streams with large number of debris, sediment or solids. Construction and installation are difficult (Shieh et al. 1996; Baffaut et al. 2015). Flumes are not practical except for small streams and are more limited than weirs regarding the range of flows that can be measured. Additionally, flume construction is more difficult than weirs.

1.3.5. Non-contact measurement methods

Most of the above-mentioned methods are feasible in accessible terrains. The non-contact methods can be used for the streams which are not easily accessible. These methods are based on the principle of radar system and may be used to make continuous, near-real-time flow measurements during high and medium flows.

1.3.5.1. Remote sensing method

Remote sensing method estimates river discharge from space, using ground measurements and satellite data to construct empirical curves that relate water

surface area to discharge (Bjerklie et al. 2005). The sensors used in this method can be (i) passive, in which the sensor receives energy naturally reflected by or emitted from the earth's surface; and (ii) active, in which the sensor provides its own illumination and records the amount of incident energy returned from the imaged surface (Xu et al., 2004). Three general approaches are used to estimate stream discharge: (i) direct measurement of water surface level from radar altimeter waveform data; (ii) determination of water surface elevations at their point of contact with the land surface using high-resolution satellite imagery and topographic data; and (iii) correlation of satellite-derived water surface areas with ground measurements of stage or discharge (Smith 1997; Revilla-Romero et al. 2014). Satellite data could provide unprecedented global coverage of critical hydrologic data that is logistically and economically impossible to obtain though ground-based observation networks (Koblinsky et al. 1993; Xu et al. 2004; Batra et al. 2006). Remote sensing is an expensive method but cannot directly estimate the stream discharge (Costa et al., 2000). Larger errors occur in flooded forests because trees are highly reflective in the visible and near-infrared range (Ward et al., 2013). Floating emergent macrophytes also affect the accuracy of the results in tropical systems (Hess et al., 1995, Birk and Ecke 2014). This method can be used for both flat and hilly terrain, but it can estimate the discharge of only larger streams (Immerzeel et al., 2009).

Satellite remote sensing of river discharge is a much newer approach, with nearly all work done since the mid-1990s. The methods used have different variants, but a common approach is to simply correlate remotely sensed water levels (from altimetry) or inundation areas (from imaging) acquired at or near a gauging station with the simultaneous ground data (Smith et al., 1995; Al-Khudhairy et al., 2002; Townsend and Foster, 2002; Kouraev et al., 2004; Xu et al., 2004; Coe and Birkett, 2004; Brakenridge et al., 2005; Ashmore and Sauks, 2006; Calmant and Seyler, 2006; Papa et al., 2007). This is conceptually like the traditional method, except that a satellite-derived rather than ground-derived measurement is used, and (in the case of imaging systems) flow area or width, rather than depth, is the variable of choice. Another approach is to merge the satellite data with topographic information (Brakenridge et al., 1994, 1998; Sanyal and Lu, 2004; Bjerklie et al., 2005; Matgen et al., 2007), or output from hydraulic models (Horritt and Bates, 2002; Overton, 2005; Roux and Dartus, 2006; Leon et al., 2006; Schumann et al., 2007).

Strictly speaking, all remote sensing discharge methods are dimensionally incompatible with the traditional cross-section framework. In planform, flow width

and depth measured at a field cross-section possess dimensions of length, whereas even the finest-resolution satellite sensors sample a two-dimensional area on the ground. For river discharge estimation, the remote sensing community has largely treated its two-dimensional measurements as equivalent to the one-dimensional values of classical at-a-station hydraulic geometry. In the case of water level variations sampled by profiling altimeters, or flow widths extracted from image transects, the area effect is simply ignored. For discharge retrievals based on inundation area, the dimensional problem is often resolved by defining some river reach. Flow inundation areas measured within reach are then divided by the reach length to yield one-dimensional units, dubbed “effective width” (Ashmore and Sauks, 2006).

1.3.5.2. Optical methods

Optical methods consist of two basic techniques: Particle Image Velocimetry (PIV) and Particle Tracking Velocimetry (PTV). An accurate description of the techniques will be presented in the subsequent sections of this thesis, and a general description is given below for understanding how they work.

In the PIV and PTV methods, the position of the fluid is represented through the light scattered by liquid or solid particles illuminated by a laser light sheet (Prasad 2000; Tauro et al. 2016). In most of the studies, liquid or solid particles must be seeded with tracer particles that are small and light enough to move with local flow velocity (Brossard et al., 2009). A flat terrain in which flow need to be calculated, is illuminated twice by means of two superimposed laser light sheets. The light scattered by the liquid or solid particles is recorded on two separate frames on a CCD camera sensor (Bosbach et al., 2009). The time intervals between the two laser pulses, image magnification produced by camera calibration and projection of the local flow velocity vector onto the place of the light sheet are used to calculate the small interrogation areas. These small interrogation areas produce one displacement vector. The velocity is the ratio of the particle displacement divided by the time interval between images (Harpold et al., 2006; Stamhuis 2006). The main advantage of PIV is that it provides high-resolution flow velocity information of a (small) flat surface at one time (Stamhuis 2006). This method requires special training and expensive instruments to take measurements and can be applied only in flat terrains (Adrian and Westerweel 2011). PIV gives

accurate results as compared to other methods but does not take direct measurement; hence, validation of results is needed for this method (Hauet et al., 2008).

What was described is generally related to discharge measurements under controlled conditions, i.e., in the laboratory.

1.3.5.3. Radar technology

Radar technology enables the measurement of surface velocity by transmitting radio waves toward the liquid surface at a specific angle. The liquid surface of an open channel is never perfectly flat, and even the smallest waves on the surface reflect radar waves back to the sensor (Costa et al., 2006).

If the surface is moving, the frequency of the reflected radio waves is changed by the Doppler effect, and the receiver in the radar sensor is able to measure even small changes in frequency. The difference in frequency is then automatically processed returning the surface velocity measurement (Plant and Keller, 1990). The sensor is able also to detect the direction of the flow.

The low power consumption of the sensors also makes the equipment suitable for continuous, real-time monitoring where there is no power supply. One or more surface velocity radars can be combined together with a level gauge to make a complete chain of flow measurement of high accuracy.

The versatility of the equipment allows it to be used in multiple applications, from the hydrological field to water cycle management in general, regardless of the fluid characteristics as it is non-contact technology. The measurement system is suitable from clean water to wastewater, in circular, ovoid pipelines or canals of various shapes and sizes.

To achieve optimal measurement accuracy, it is important to choose the installation site carefully. The flow at the installation site should, as with all measurement systems, be as uniform as possible. Reliable measurements are obtained if the channel has an appropriate straight section, free of bends and dimensional variations in cross-section. The flow must be free of turbulence or eddies and must be at a suitable and sufficient distance from weirs, gates, or waterfall.

For optimal operation and best measurement performance, the sensor should be oriented upstream so that the water flows toward the sensor. The covered area of the radar beam depends on the positioning height of the sensor relative to the liquid surface and the angle of inclination relative to the horizontal plane. The inspection area can be approximated to an ellipse.

The radar sensor for surface velocity measurements is typically mounted on a bridge or other existing structure crossing the channels. No specific structures are needed to build, and no flow interruption is generally required.

The height of the sensor above the liquid surface and the inclination of it determine the area of the surface covered by the radar beam. The radar beam covers an elliptical area on the liquid surface. The radar velocity sensor processes thus the average velocity of the stream flowing through the inspection area. However, in the presence of turbulent flow, fluctuations in measured data and reduced overall measurement accuracy may be recorded. The uniformity of the liquid flow is the key factor in achieving stable and accurate measurements. Turbulence should always be avoided.

1.3.6. Most used instruments

1.3.6.1. Mechanical current meters

A current meter measures the water velocity at different vertical locations along a transverse portion of a watercourse, and the area to which each measurement refers is identified. The average watercourse discharge in the chosen segment is calculated by multiplying the flow velocity by each corresponding area and adding these results.

The ISO standard ISO-748:2007(E) (ISO 2007) specifies the requirements for the accurate measurement of the mean velocity for various vertical locations, the computation of the discharge using various graphical or numerical methods, and the selection of the fewest possible vertical locations. In each situation, some flexibility is required to adapt these requirements to the various circumstances that are experienced at each location throughout time.

The general characteristics of current meters measurements include their simplicity, excellent precision (particularly when the watercourse is not too deep or

during a flood), and repeatability. The riverbed may have specific conditions, or there may be turbulence and high flow rates, which typically happen during flood conditions. It is impossible to carry out measurements with the necessary number of vertical data points to ensure respectable precision under these circumstances. The method frequently underestimates the discharge through the section, and the inaccuracy associated with this technique is frequently larger than 50%. Additionally, it has been demonstrated (Whalley et al., 2001) that the performance of current meter can vary substantially and frequently exhibit considerable variances at very low speeds. The measurements in these circumstances are frequently improved by increasing the number of vertical measurements or the number of points along the same vertical line. In every case, a larger number of vertical points results in better resolution and, therefore, more accurate calculations for the watercourse.

The current meter is still the most universally used instrument for velocity determination. The principle is based upon the relation between the speed of the water and the resulting angular velocity of the rotor (propeller or micro-propeller). By placing a current meter at a point in a stream and counting the number of revolutions of the rotor during a measured time interval, the velocity of the water at that point can be determined. The number of revolutions of the rotor is obtained by various means depending on the design of the meter but normally this is achieved by an electric circuit though the contact chamber. In all types of design, the electrical impulses produce either a signal which registers a unit on a counting device or an audible signal in a headphone. Intervals of time are measured by a stopwatch or by an automatic timing device. Latest developments in current meter design include the introduction by the USGS of an optical head pick-up which improves low velocity response. This new pick-up system utilises a pivot bearing in the head and is actuated by a rotating fibre-optic bundle. The system generates four counts per revolution.

Current meters can be classified generally as those having vertical axis rotors and those having horizontal axis rotors, the former being known as cup-type current meters and the latter as propeller-type meters.

The cup-type current meter (Figure 1.6a) consists of a rotor revolving about a vertical shaft and hub assembly, bearings, main frame, a contact chamber containing the electrical contact, tail fin and means of attaching the instrument to rod or cable suspension equipment. The rotor is generally constructed of six conical cups fixed at equal angles on a ring mounted on the vertical shaft. This

assembly is retained in the main frame by means of an upper shaft bearing and a lower pivot bearing.

The propeller-type current meter (Figure 1.6b) consists of a propeller revolving about a horizontal shaft, ball-bearings in an oil chamber, the body containing the electrical contact, a tailpiece with or without a vane and a means of attaching the instrument to the suspension equipment. The meter may be supplied with one or more propellers which differ in pitch and diameter and therefore may be used for various flow speeds.

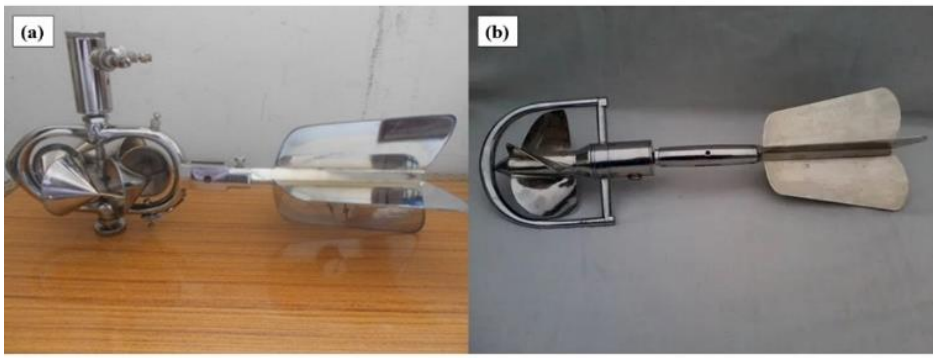

Figure 1.6 – Cup-type current meter (a) and propeller-type current meter (b) (Nune Instruments)

Both types of current meter are available in miniature form (mini meters) for use in very small depths of flow. There is generally no significant difference between the accuracies of the velocities registered by cup-type and propeller-type meters, but the comparative characteristics of each meter can be summarized as follows:

- Cup-type current meter:
  - this is a robust instrument requiring little maintenance; the rotor is replaceable in the field without affecting the rating;
  - it operates at lower velocities than the propeller-type meter;
  - the bearings are well protected from silty water;
  - a single rotor serves for the entire range of velocities;
  - when held rigidly by rod suspension and pointing upstream at right angles to the measuring section the meter will indicate a

velocity which may be greater or less than the oblique stream velocity, if present, depending on the direction of the oblique flow. When supported on a cable, the meter will indicate the actual oblique velocity provided the meter is balanced and free to align itself with the stream.

- Propeller-type current meter:
  - this meter disturbs flow less than the cup-type meter;
  - the propeller is less likely to become entangled with debris than the cup-type meter;
  - bearing friction is less than for vertical shaft rotors because any bending moment on the rotor is eliminated;
  - a propeller-type current meter used in oblique flow with a component propeller will register the velocity normal to the cross-section when held rigidly by road suspension at right angles to the cross-section;
  - propeller-type current meters are not susceptible to vertical currents as cup-type meters and therefore give better results when used for measurements from boats.

In order to determine the velocity of the water from the revolutions of the rotor of the rotating-element current meter, a relation is established between the angular speed of the rotor and the speed of the water which causes it to turn. This relation is known as the current meter rating.

The usual method of rating a current meter is to tow it through still water and observe the time of travel and the number of revolutions as the meter levels a given distance. The number of revolutions per second and the corresponding velocity are then computed. When these two quantities are plotted against each other on graph, a series of equations will usually be necessary to fit the points.

For a propeller-type meter the calibration equation (Eq. 1.13) would be:

$$v = kn \qquad \text{(Eq. 1.13)}$$

where v is the velocity in metres per second, n is the rate of revolution of the propeller in revolutions per second, and k is a constant. Owing to frictional

causes, the relation between v and n is not linear near to the minimum speed of response of the meter.

The complete calibration of the current meter is expressed by one or more equations in the form of Eq. 1.14:

$$v = b + kn \qquad \text{(Eq. 1.14)}$$

where b is the intercept on the velocity axis when $n = 0$.

1.3.6.2. Electromagnetic current meters

The electromagnetic current meter (Figure 1.7) employs the Faraday principle of electromagnetic induction whereby a magnetic field (in the velocity sensor) induces an electro potential in a moving conductor (the water). An alternating current is passed through a coil in the velocity probe which in turn sets up an alternating field in the probe head and surrounding water. Movement of water past the probe causes an electric potential in the water which is detected by two electrodes in the probe. This potential is then amplified and transmitted through the connecting cable to the display unit where the velocity signal is digitised and displayed in metres per second at present intervals in the range 2-60 seconds as required. The velocity may be also continuously displayed. The range of velocities of a typical electromagnetic current meter is normally zero to 4 m/s. The meter is battery powered. Maintenance of the meter is minimal and consists of keeping the velocity probe's electrodes always clean. This can be done by using a mild domestic detergent solution before use. The aim is to ensure good "wetting" of the surfaces of the electrodes. The velocity probe should be connected to the stainless-steel rods whenever possible to obtain good "ground earthing". Because of the principle of electromagnetic induction, the meter will not operate successfully in very low-conductivity solutions (e.g., in laboratories) unless a small amount of common salt is added to the water.

Figure 1.7 – Electromagnetic current meter. (RS Hydro)

1.3.6.3. Acoustic Doppler Current Profilers

The Acoustic Doppler Current Profiler (ADCP) measures water velocity using sound. The ADCP transmits sound in the ultrasonic range (above the range heard by the human ear). Commercial ADCPs use a low frequency of around 30 kHz, and the common range for riverine measurements is between 300 and 3000 kHz. The ADCP measures water velocity using a principle of physics discovered by Doppler in 1842. Doppler's principle relates a source's change in frequency to the relative velocities of the source and observer. An ADCP employs the Doppler principle by reflecting an acoustic signal off small particles of sediment and other material (referred to collectively as scatterers) in water. Doppler velocity is measured parallel to the direction of the transducer emitting the signal and receiving the backscattered acoustic energy. Three or four beams pointing between 20 and 30 degrees from vertical are typical for boat-mounted ADCPs. A three-dimensional velocity measurement requires three beams. An additional error velocity can be measured if a fourth beam is present.

Transducers are deployed beneath the water's surface and aimed downward in a boat-mounted system. The velocity of the water relative to the boat can be calculated by measuring the velocity of the water from a moving boat. ADCPs used

in this manner account for the boat's velocity through bottom tracking or the use of a global positioning system (GPS). Bottom tracking measures the Doppler shift of acoustic signals reflected from the streambed to determine the velocity of the boat; thus, the water velocity relative to a fixed reference is computed by correcting the measured water velocity with the measured boat velocity (Figure 1.8).

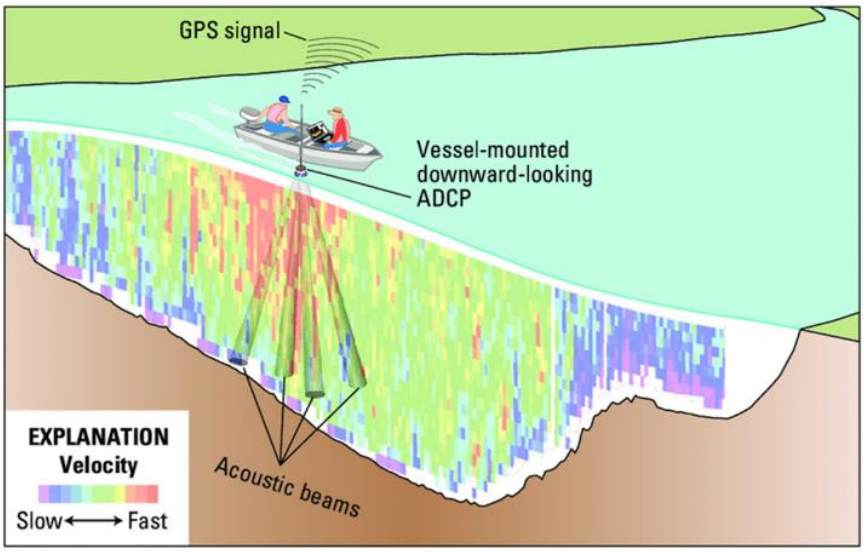

Figure 1.8 – ADCPs operating principle. The instrument is moved across the river acquiring depth-velocity data and the position of the streambed. (Mueller et al., 2013)

ADCPs can be classified into two groups based on the techniques used to configure and process the acoustic signal: (i) narrowband, and (ii) broadband.

Narrowband is typically used in the hydroacoustic industry to describe a pulse-to-pulse incoherent ADCP; however, the narrowband ADCPs also can operate in a pulse-to-pulse coherent mode for short ranges. This means that in a narrowband ADCP, only one simple pulse is transmitted into the water, per beam per measurement (ping), and the resolution of Doppler shift takes place during the duration of the received pulse. The velocity measurements made using the narrowband technology are noisy (have a relatively large random error). Narrowband systems compensate for the large random error by pinging fast (up to

20 Hz) and averaging many pings together before reporting a velocity. Typical response from a narrowband system is a velocity-profile measurement every 5 seconds.

Broadband systems use a ping consisting of two or more synchronized acoustic pulses that are encoded with a pseudo-random code. The encoded pulse allows multiple velocity measurements to be made with a single ping, thus reducing the random noise associated in the measured velocity. Broadband systems are more difficult to configure because of the effect of the lag between the two pulses and because the processing of the complex pulse is slower than a narrowband system; however, the complex pulse results in a much lower random error, and the pulse pair allows configuration of the instrument to minimize random error for particular measurement conditions.

The physics of sound generation from a transducer, as well as its propagation, absorption, attenuation, and backscatter in the water column, result in specific limitations and properties of ADCPs. The quantity and characteristics of particulate matter (such as sediment and aquatic life) in the water column can have a significant impact on the ADCP's ability to measure velocity accurately. Because there is no suspended particulate matter to reflect acoustic energy, pure water is acoustically transparent. In order to measure velocity, water must contain enough particulate matter to return enough acoustic energy to the ADCP. As a result, in very clear streams, there may be insufficient material in the water column for an ADCP to measure water velocity. High sediment loads, which are common during times of high flow, can have the opposite effect. High sediment concentrations near the streambed can make it difficult for the ADCP to distinguish the streambed from the suspended-sediment concentration, resulting in inaccurate water depth and (or) invalid boat velocity measurements. Furthermore, high sediment concentrations in the water column can attenuate the acoustic signal before it can travel through the water column and back to the transducer, preventing the ADCP from performing a measurement.

ADCPs are referred to as profilers because they provide velocity measurements throughout the water column. The ADCP divides the water column into depth cells (also known as bins in some software and references) and reports a velocity for each depth cell; however, an ADCP cannot measure velocities at the water surface due to the draught of the instrument and the required blanking distance, nor can it measure near the bed due to side-lobe interference (Figure 1.9a). The draught of the instrument deployment, the effect of transducer

mechanics, and the flow disturbance around the instrument all contribute to the length of the unmeasured area at the water's surface. Because the ADCP must be deployed beneath the water's surface, it cannot measure water velocity above the transducers. The required instrument draft is controlled by the need to prevent the instrument from coming out of the water and to prevent entrained air from traveling under the instrument; therefore, the required instrument draft depends on the shape of the instrument mount, the boar, and the relative water velocity (water velocity past the instrument). ADCPs cannot measure the water velocity near the streambed due to side-lobe interference. Most transducers that are developed using current technology emit parasitic side lobes off of the main acoustic beam (Figure 1.9b). The acoustic energy in the side lobes is much less than in the main beam. In comparison to the energy transmitted, the amount of acoustic energy backscattered from scatterers in the water column in the main beam is very small. The streambed reflects much more acoustic energy than the scatterers in the water column. The magnitude of the energy reflected from the streambed in a side-lobe reflection is close enough to the magnitude of the energy reflected from scatterers in the main beam to cause potential errors in the measured Doppler shift. The percentage of the water column affected by side-lobe interference varies from 6% for a 20-degree system to 13% for a 30-degree system.

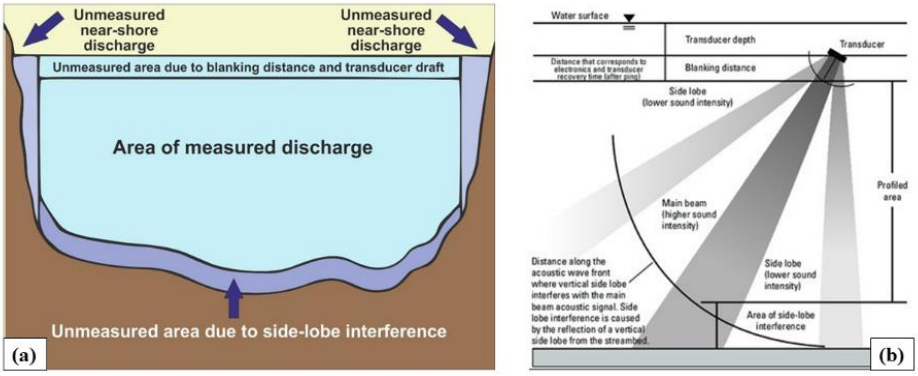

Figure 1.9 – Parts of the cross-sectional area that remain unmeasured by ADCPs (a); side-lobe effect affecting the measure of ADCPs (b). (Kim et al., 2015)

The frequency and the techniques used to configure and process the acoustic signal are important in determining the maximum and minimum water

depths that can be measured. Lower frequency ADCPs typically can measure deeper than higher frequency ADCPs, but also require larger depth cells and a longer blanking distance. The operational mode of some ADCPs determines the location of the first and last valid depth cells and the acceptable size of the depth cells. The ADCP cannot measure the velocity in the upper and lower portions of the water column because of the draft, blanking distance, and side-lobe interference; therefore, the discharge in these areas must be estimated from data collected in the measured portion of the water column. For this reason, it is recommended that a minimum of two depth cells be measured in the water column. The shallow-water limitation of an instrument is, therefore, the summation of the draft, blanking distance, location of the first depth cell, location of the last depth cell, the depth-cell size, and the range of the side-lobe interference.

An ADCP can be mounted on either side, off the bow, or in a well though the hull of a manned boat. The ADCP should not be mounted close to any object containing ferrous metal or sources of strong electromagnetic fields, such as generators, batteries, and boat engines. A good rule of thumb is that an ADCP should not be mounted any closer to a steel object than the largest dimension of that object. This is a general rule, however, and large variations in the magnetic fields are generated by different metals. Even stainless steel varies appreciably in the amount of ferrous material contained in the steel. The local existence of large magnetic fields can cause errors in the compass calibration phase in those instruments equipped with GPS.

ADCP mounts for manned boats should:

- allow the ADCP transducers to be positioned free and clear of the boat hull and mount;
- hold the ADCP in a fixed, vertical position so that the transducers are always submerged while minimizing air entrainment under the transducers;
- allow the user to adjust the ADCP depth easily;
- be rigid enough to withstand the force of water caused by the combined water and boat velocity;
- be constructed of non-ferrous materials;
- be adjustable for boat pitch-and-roll;
- be equipped with safety cable to hold the ADCP in the event of a mount failure.

A tethered boat can be defined as a small boat attached to a rope, or tether, that can be deployed from a bridge, a fixed cableway, or a temporary bank-operated cableway (Figure 1.10). The tethered boat also should contain waterproof enclosure capable of housing a power supply and wireless radio modem for data telemetry. A second wireless radio modem attached to the field computer enables communication between the ADCP and field computer without requiring a direct cable connection. The radio modems should reliably communicate with the ADCP using the ADCP data-acquisition software.

Figure 1.101 – Tethered ADCP boats. (Communication Technology srl)

Tethered ADCP boats have become a common deployment method. Certain considerations need to be made when making tethered ADCP boat measurements. Tethered boats are used in a variety of settings, but primarily they are used from the downstream side of bridges for convenience. Bridges piers can cause excessive turbulence during high streamflow, especially if debris accumulations are present on the piers and the piers are skewed to the flow. Attention should be paid to the cross section to ensure that no large eddies that could cause flow to be nonhomogeneous. Possible alternatives to measuring off the downstream side of bridges include using bank-operated cableways or having personnel on each bank hold a rope attached to the platform to pull the platform back and forth across the river. Bank-operated cableways may be as simple as a temporary “rope and pulley” apparatus or may involve the use of a small temporary cableway with a motorized drive for toeing the tethered boat back and forth across the stream.

When the water velocity is slow, controlling the tethered boat may become difficult, especially when handling instruments from a bridge. This lack of control may be exacerbated by wind, which may push the boat in an undesired direction, without following the average water motion. Boat handling can be improved by attaching a sea anchor to the back side of the boat to increase the effect of the current and its pull on the tether. Make sure that this anchor is far enough behind the boat to not disturb the flow and potentially bias the velocity measurements. When the water velocity is fast or when the boat is deployed from a high bridge, it is not uncommon for a tethered boat to be pitched upward at the bow. This increased pitch is caused by increased vertical tension on the tether in faster flows, hull dynamics, and an incorrect setting of the angle for the bail for those boats equipped with a rigid bail. The bail connects the tether to the boat and can be either a rigid design or a flexible rope bail. Large pitch angles may introduce some bias in depth measurements and should be minimized as much as practical. Adding a sounding weight on the tether near the location where the tether is tied to the boat will help decrease the pitch angle. In addition, increasing the length of the tether helps reduce the pitch angle. It is possible to lose control of a tethered boat because of a system-component failure. For example, a boat tether or tether attachment point could break. ADCP operators using tethered-boat deployments should have redundant attachment points for the tether on the boat and have a contingency plan for retrieving the boat in the event of a failure that causes a loss of boat control.

1.4. Measurement of stage

1.4.1. Overview

The height of the water surface above a recognised datum plane determines a stream's stage. The gauge height is the elevation of the water relative to some arbitrary or specified gauge datum. Gauge height is often used interchangeably with the more general term “stage” although gauge height is more appropriate when used to indicate a reading on a gauge. Stage or gauge height is usually expressed in metres. The determination of stage is one of the most important measurements in hydrometry. It can be stated that, in methods of streamflow measurement where a correlation is established between stage and discharge, the

uncertainty in the measurement of stage has a significant effect on the overall uncertainty in the record discharge.

The non-recording reference gauge is the basic instrument for the measurement of stage whether at a regular flow measuring station or at a site where only direct reading of water level in the stream or as an inside gauge to indicate the level in a stilling well, and is used for setting and checking the water level recorder, for indicating the stage at which discharge measurements are taken, and for emergency readings when the recorder is out of action. There are various forms, the choice being decided by the site conditions and the specific use to which it will be put. The reference gauge may be read visually one or more times a day if a water level recorder is not part of the installation. The disadvantages of a non-recording reference gauge in this case are the need for an observer and the loss of accuracy of the estimated continuous graph of stage unless observations are taken many times a day. In some large rivers, with long sloping shallow banks, however, it is not always feasible to install a water level recorder and resort must be made to visual observation of the reference gauge.

Typically, the reference gauge is either an inclined gauge or a vertical staff gauge. Standard porcelain enamelled iron plated portions that are each around 150 mm wide and 1 m long and graduated in units of 10 mm make up vertical staff gauges in most cases (Figure 1.11).

Figure 1.11 – Non-recording staff gauge with 10mm-graduation.

The sections are screwed to a backing board which is fastened to a suitable support. Slotted holes in the plates are provided for final adjustment in setting the gauge. The gauge is located near the edge of the stream so that a direct reading of the water level may be made. If this is not possible because of excessive turbulence, wind effect or inaccessibility, the observations are made in a suitable permanent stilling bay in which wave action is reduced and the level of the water surface follows that of the stream. The staff gauge is located at or near to the current meter measuring section without affecting the flow conditions and in a position where there is least possible damage from drift. Bridge abutments or piers are generally unsuitable locations. To enable the observer to make readings as near as possible to eye level, convenient access is necessary and in this connection a flight of steps is normally desirable. A suitable backing for a vertical staff gauge is provided by a board fixed to a wall having a vertical face parallel to the direction of flow. The board is securely attached to the surface of the wall to present a vertical face to receive the graduated gauge plates. Staff gauges may usually, however, be fixed to piles or driven firmly into the riverbed or riverbanks or set in concrete in order to avoid movement or being washed away during floods. Anchorages are designed to extend below ground level to a level free of any disturbing effects. Provision is made in all cases for easy removal of the gauge plates for maintenance or adjustment. Where the range of water level exceeds the capacity of a single vertical gauge section, additional sections are installed on the line of the cross-section normal to the direction of flow. An inclined, or ramp, gauge usually consists of heavy timber securely attached to a permanent foundation. The graduations of an inclined gauge are either marked directly on the surface of the timber or carried on manufactured gauge plates designed to be set to specific slopes. Except where use is made of manufactured gauge plates, an inclined gauge is calibrated in situ by accurate levelling from the station benchmark. An inclined gauge is installed to follow the contours of the bank; sometimes a gauge with a single slope is adequate but more usually it is necessary to install an inclined gauge in several sections each with different slope. As in the case of the staff gauge, it is usually convenient to construct a flight of steps alongside the incline gauge to facilitate both installation and reading. Reading of the gauge may be improved using a small portable stilling box which helps to dampen wave action. A properly designed inclined gauge is less prone to damage than a staff gauge and normally allows more accurate readings of water level to be made because of its better resolution and its convenience in reading.

It is possible to mention also about two other kinds of gauge: the float-tape gauge and the electric-tape gauge. The float-tape gauge is used mainly as an inside stilling well reference gauge for a water level recorder and consists of a float attached to a counterweight by means of a stainless-steel tape. The tape is normally graduated in metres and 10 mm divisions and passes over a pulley. The float pulley consists of a wheel about 150 mm in diameter and is grooved on the circumference to accommodate the tape and mounted on a support. An arm extends from the support to a point slightly beyond the tape to carry an adjustable index. The tape is connected to the float by means of a clamp which is also used for adjusting the tape reading if the adjustments necessary are too large to be accommodated by the adjustable index. A 250 mm diameter copper float and a 1 kg lead counterweight are normally used. The electric-tape gauge, like the float-tape gauge, is used as either an outside or inside reference gauge. It is commonly used at measuring structures as an outside gauge to measure the head over a weir or through a flume where it is operated from a datum plate set into an abutment wall. A staff gauge fixed to the wall of a weir or flume, although useful as a spot check, is difficult to read to the required accuracy because of its awkward location. A typical hand-held gauge consists of a graduated reel of steel tape and a 9 V (PP3) battery. The gauge is lowered until it contacts the water surface which completes an electric circuit and causes a buzzer to sound. The gauge is read to the nearest millimetre against a datum plate.

Generally, the datum of the gauge may be nationally recognised datum such as mean sea level or an arbitrary datum plane chosen for convenience. An arbitrary datum is selected for the convenience of using relatively low numbers for gauge heights. To eliminate the possibility of minus values of gauge height, it is usual to select the datum, for operating purpose, below the elevation of zero flow on a natural control. Where an artificial control is part of the installation, the gauge datum is usually set at the elevation of zero flow. This also applies to measuring structures. As a rule, a permanent datum is maintained so that only one datum for the gauge height record is used for the life of the station. An exception occurs at gauge sites where low flow stages have a negative gauge height. In this situation a change in gauge datum to eliminate the negative numbers is normally carried out. This avoids possible confusion involving the algebraic sign of the gauge heights.

The record of stage is normally produced by a water level recorder (“logger”) actuated by a float and counterweight spring system working within a stilling well, the movement of the float being used to operate a recording mechanism such as a pen or head which can produce either an analogue record on a

chart or digital record. Essentially the recorder consists of a time element and a water height element which operate together and produce on the chart or tape a record of the rise and fall of the water surface with respect to time. The time element consists of a clock actuated by a spring, weight, or electrical mechanism, driving in the case of an autographic recorder either a chart drum or a recorder pen, or in the case of a digital recorder, rotating a cam which initiates the recorder pen. The water height element consists of a float, combined with a counterweight device, and some form of mechanical linkage to connect either directly or through reduction gearing to the recording device. An encoding or digitising device is used to convert the analogue measurement of water level to a digital output. The recording device can be a pen or pencil, in the case of an autographic record. In solid-state loggers, water level data is transmitted from the sensor (float and tape) via a shaft encoder to a solid-state medium in the form of a cartridge, cachette or similar module.

With technological development, additional methods for measuring water levels in a watercourse have been designed. These allow for continuous monitoring of water levels and enable real-time transmission of acquired data through electronic circuits that send the data to an easily accessible database.

One of these new technologies is the measurement of levels through ultrasonic sensors. The instrument transmitter emits an ultrasonic wave to the liquid surface. The liquid surface reflects the signal. Based on the time the signal travels, the device calculates the distance between the bottom edge of the sensor and the surface.

The possible influence of the surrounding atmosphere on the velocity of sound is generally automatically compensated by the transmitter by inputting specific values and measuring the environmental temperature.

Ultrasonic levels measurement is a methodology that does not involve direct contact with water. This represents an advantage of the method, because it is not necessary for water level measurement operators to immerse themselves inside the watercourse, or to have to get dangerously close to the banks for reading the hydrometric gauge.

Technology similar to that of ultrasonic sensors is applied by radar water level measurement methods.

The radar measuring instrument generally consists of a case with the electronic parts, an antenna, and a sensor. Short radar pulses lasting about 1 nanosecond are emitted from the antenna of the radar sensor. These are reflected by the water and received by the antenna as echoes. The radar waves propagate at the velocity of light.

The travel time of the radar pulses from emission o reception is proportional to the distance and thus to the water level. The water level thus determined is converted into a corresponding output signal and indicated as detected value.

As with ultrasonic measurement, there is no contact with water during level measurement. The main difference between these two measuring modes is the type of wave emitted. Ultrasound emits a mechanical wave that requires a medium to propagate at the velocity of sound, while a radar emits an electromagnetic wave that propagates at the velocity of light, even in a vacuum.

Chapter 2
Optical techniques

2.1. Introduction

The human senses are limited and subjective, so observers may make completely opposite qualitative observations on the same phenomenon. This would not allow comparisons to be made between phenomena of similar nature, which, moreover, are generally located differently in both space and time. The use of measurement was developed to allow recording and comparison of observations not only carried out in different places and times, but also by different observers.

The description of a flow is one the examples of the millions of natural phenomena that humans have been trying to study for centuries, and that currently continue to be a challenge for the scientific community. One of the most famous nature and environmental scientists that history has ever known is certainly Leonardo da Vinci, who managed to provide contemporary scientists with an enormous amount of information on flows by making mere observations. Leonardo did not only study fundamental flow phenomena, but in particular those of engineering interest. A huge number of documents are stored in Milan (Italy) at the National Museum of Science and Technology; they consist of graphic sketches, often accompanied by written explanatory notes, about complex flow phenomena, such as the unsteady flow patterns.

A great step forward in the investigation of flows was made with Ludwig Prandtl, one of the most important representatives of fluid mechanics. Prandtl was a promoter in using visualization techniques to extract information about a flow; He designed and utilized flow visualization techniques in a water tunnel to study aspects of unsteady separated flows behind wings and other objects. Prandtl's water channel has been rebuilt by DLR's School_Lab (Deutsches Zentrum für

Luft- und Raumfahrt School Lab). As shown in Figure 2.1, the channel was composed of two section, upper and lower, separated by a horizontal wall. The water was recirculated in the upper open channel through the lower closed duct. Two-dimensional surfaces of various shapes could easily be installed in the middle of the channel emerging out of the water. The flow could be observed from the upper section thanks to the distribution of a suspension of mica particles on the surface of the water.

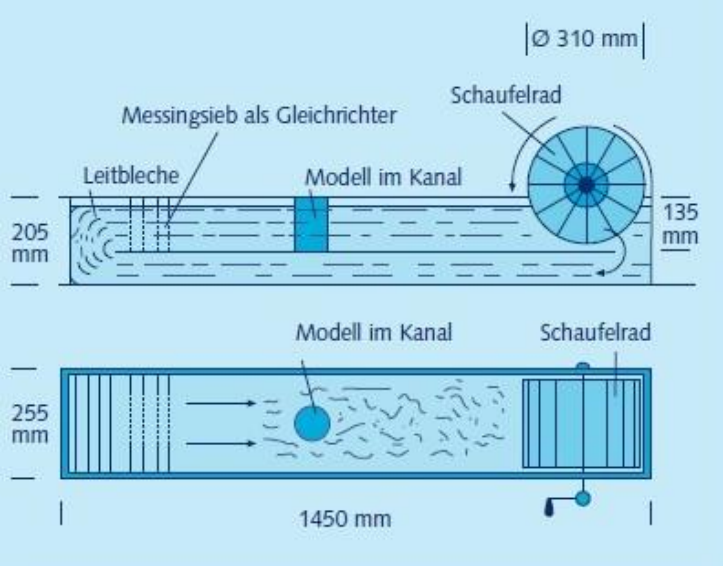

Figure 2.1 - Sktech of Prandtl's water channel as used by DLR's School Lab. (DLR School Lab)

In 1904, during a lecture at the III Internationaler Mathematiker Kongress, Prandtl introduced the concept of the boundary layer for the first time, moreover he described the set-up of his water channel (Figure 2.2), in which the water was moved with a paddle wheel and presented photographs of vortices arising from the interference between the flow and objects with different shapes (Prandtl, 1904).

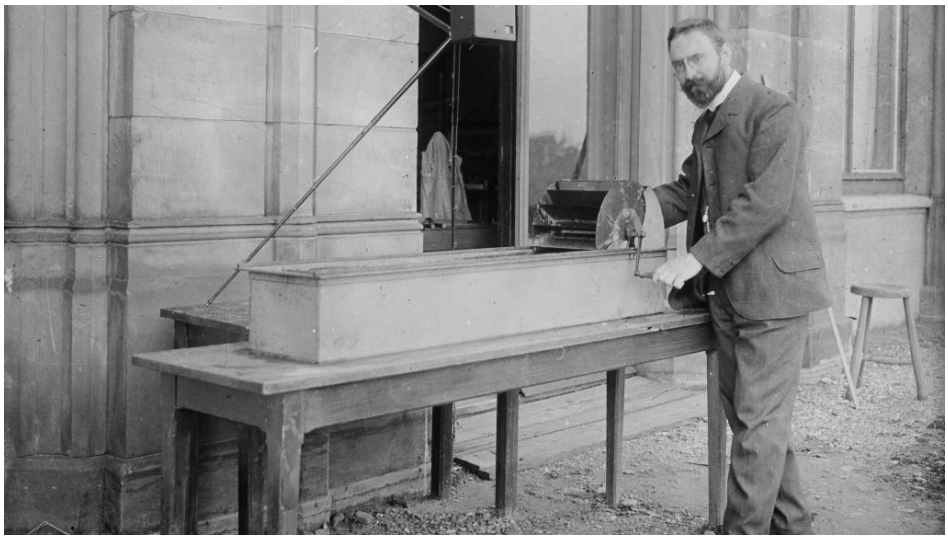

Figure 2.2 – Prandtl in 1904 running his open channel model through the paddle wheel. (DLR School Lab)

Prandtl conducted a number of additional tests with the water channel due to his fascination with the flow phenomenon. Prandtl was able to alter numerous experiment parameters, such as the angle of incidence, flow velocity, and steady-unsteady flow, which allowed him to obtain new understanding of many fundamental aspects of unsteady flow phenomena. In 1927, during the Wilbur Wright Memorial Lecture in London, He illustrated (Figure 2.3) in detail the turbulence phenomena showing photographs of unsteady flows (Prandtl, 1927).

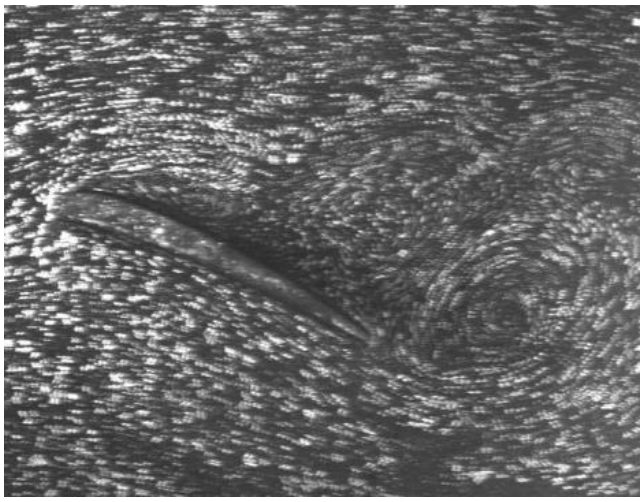

Figure 2.3 – Separated flow behind a wing (replica of Prandtl experiment). (Raffel et al., 2018)

Prandtl's primary method of substantiating his theories and presenting the flow phenomena he researched was hence photographic documentation. However, at that time, the flow field could only be qualitatively described.

Keeping with Prandtl's method, which allowed for the explanation of flow phenomenology through photographic images, it is now able to acquire extremely accurate quantitative evaluations of a wide range of quantities that are directly related to water flows. The Prandtl approach received a significant boost from the rapid technological advancement of today, which helped it develop its characteristics and give rise to the well-known optical methods known as Particle Image Velocimetry (PIV) and Particle Tracking Velocimetry (PTV).

2.2. Optical methods

2.2.1. Overview

According to Tauro et al. (2017), optical-based techniques have a lot of potential for river flow monitoring since they make it simple and inexpensive to collect a wide variety of measurements in real time, at any flow rate, and with high spatial resolution. A new generation of optical sensors, digital cameras, and

approaches are becoming more and more readily available, which is another factor influencing how quickly these techniques are evolving. Digital fixed gauge-cams located close to rivers, mobile devices used by operators positioned on the banks and on bridges, and even cameras mounted on unmanned aerial vehicles (UAVs) have all seen major advancements in monitoring techniques in recent years (Eltner et al., 2018; Manfreda et al., 2018).

Over the past two decades, research into large-scale image velocimetry has grown year after year, with an increasing focus on the use of software packages. The lab-based image velocimetry method (Lindken et al., 2009), which was initially developed to undertake hydraulic studies in controlled, laboratory environments, shares many concepts with this technique. The basic ideas behind the lab-based method involve the seeding of the flow with neutrally buoyant particles, which are then lit with laser light and their motion is captured on camera before the particle displacements are calculated using either PTV or PIV (Willert et al., 1996). Although large-scale image velocimetry frequently employs these similar tracking techniques in uncontrolled outside settings, some aspects are modified because of need and for the output optimization. Lab-based image velocimetry has been widely adopted with standardized published procedures (Gollin et al., 2017; Cerqueira et al., 2018). However, because to the adaptable nature of large-scale image velocimetry, procedures and approaches may differ depending on the hydrological setting, ambient circumstances, and platform of acquisition. As a result, standardisation has become a more challenging task (Perks, 2020).

The Large-Scale Particle Image Velocimetry (LS-PIV) and the Large-Scale Particle Tracking Velocimetry (LS-PTV) techniques have gained widespread acceptance for use in natural river flow monitoring among the various image-based methods (Fujita et al., 1998; Fujita et al., 2007; Tauro et al., 2014; Perks et al., 2020; Pearce et al., 2020). Both methods, which are based on the study of floating tracers, were initially created for controlled laboratory research. They essentially apply the fundamental principles of the Particle Image Velocimetry (PIV) and Particle Tracking Velocimetry (PTV) methods to large-scale cases. While LS-PTV utilises a Lagrangian point of view, LS-PIV adopts an Eulerian point of view. The two techniques have a number of common characteristics, as noted in Raffel et al. (2018) and Gollin et al. (2017), but their primary differences are in the methods used to evaluate the recordings: while LS-PTV reconstructs the track of individual particles transiting in the field of view, LS-PIV estimates the velocity at image sub-regions (Tauro et al., 2017). It is important to point out that other methods of image

velocimetry have also developed in the recent years, and it is worth mentioning the Kanada-Lucas-Tomasi Image Velocimetry (KLT-IV) (Perks, et al., 2016), the Optical Tracking Velocimetry (OTV) (Tauro et al., 2010), the Space-Time Image Velocimetry (STIV) (Fujita et al., 2007).

The surface velocity field is obtained indirectly by measuring the velocity of floating tracer particles in the flow, which are either naturally present or artificially introduced and are assumed to move with the local flow velocity. Cameras record the dynamics of the liquid surface over a series of consecutive frames, reconstructing the local flow velocity beginning with the identification of tracer particle displacements between pairs of subsequent frames. Unlike the LS-PTV, the LS-PIV divides all frames into small, regular sub-regions known as Interrogation Areas (IAs); local distribution patterns and displacements are typically determined by cross-correlating the IAs of consecutive frames.

Measurements with optical techniques typically include the following four main phases:

1) "seeding", i.e., introduction of a flow tracer with suitable geometry and density in an area of the river with good lighting, utilising particles that accurately depict the motion of the river without significantly interfering with it; this is only necessary if the properties of naturally occurring flow tracer are not suitable for the purpose (e.g., sparse concentration with non-uniform dispersion, inappropriate dimensions, etc.);
2) "recording", i.e., taking pictures with a sufficient temporal resolution;
3) "processing", i.e., elaboration of captured images, which may also include estimation of the tracer displacements between pairs of subsequent images and pre-processing techniques (such as image stabilisation, orthorectification, and manipulation to increase tracer brightness and the contrast between tracer and water) if necessary;
4) "evaluation", i.e., processing velocity data afterward to define the velocity field across the whole study region.

Combining the bathymetry of a river cross-section with the determined surface velocity field and using simplified hypotheses for vertical velocity profiles, it is possible to estimate the discharge (Hauet et al., 2008).

Pattern recognition-based monitoring methods have a number of advantages over more conventional ones. First, the simplicity: field campaigns are

quicker, easier, and do not require personnel with specialised expertise. Additionally, because the instruments are not submerged in the stream, there is less flow disturbance, which reduces the danger of operator injury and damage during floods. Secondarily, affordability: recent technical developments have made it possible to purchase low-cost cameras with high resolution capabilities as well as tools for significant image processing and storage. Many user-friendly, widely accessible software products based on LS-PIV and LS-PTV include FlowManager (Podlinski et al., 2007), RIVeR (Patalano et al., 2017), FUDAA-LSPIV (Le Coz et al., 2014), and PIVlab (Thielicke and Stamhuis, 2014).

The following steps can be used to describe the important phases of large-scale image velocimetry workflows: (i) capture optimization; (ii) pre-processing; (iii) image processing; and (iv) post-processing.

Capture optimization steps (Figure 2.4) are about the proper equipment selection, setup, and preparation for capturing accurate image sequences (e.g., maximising tracer visibility, minimising environmental noise, etc.).

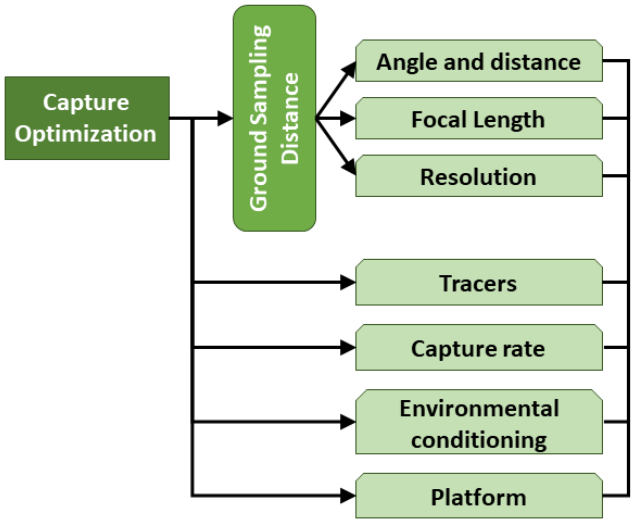

Figure 2.4 – Steps required for capture optimization.

Pre-processing steps (Figure 2.5) may be defined as those that guarantee stable video, with images modified to reduce noise and to increase the signal (e.g., visibility of surface tracers).

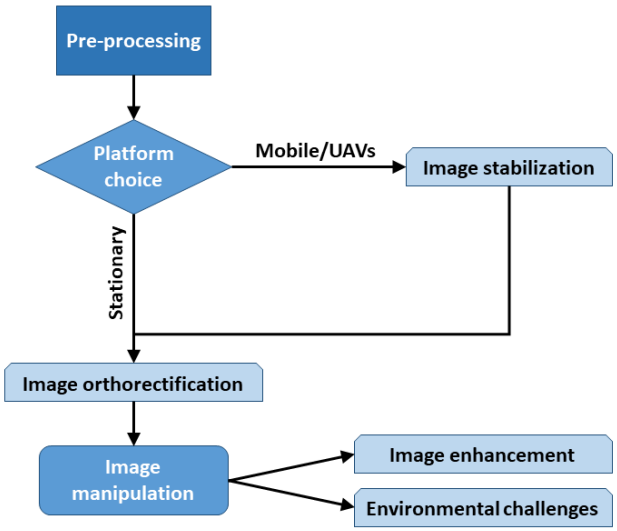

Figure 2.5 – Steps required for pre-processing step.

Processing (Figure 2.6) uses 1D or 2D analysis of feature displacements throughout a specified field of view.

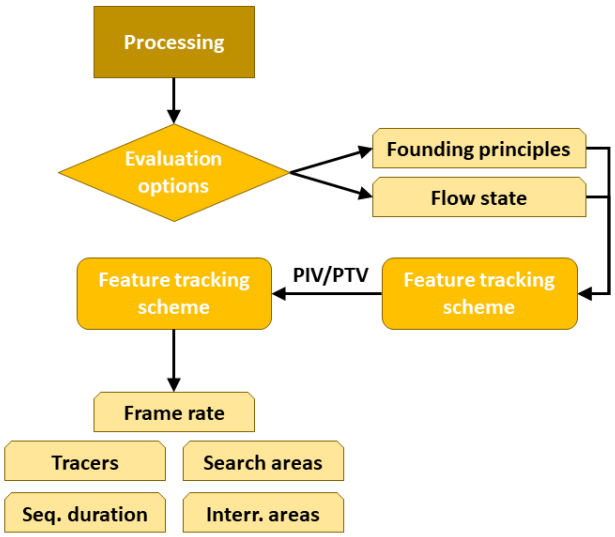

Figure 2.6 – Steps required for the processing step.

Post-processing steps (Figure 2.7) verify the estimated data and remove incorrect measurements. When paired with cross-section measurements, the filtered dataset could be used to assess discharge.

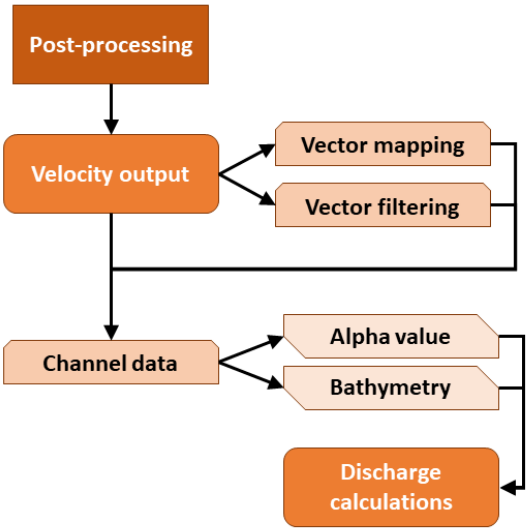

Figure 2.7 – Steps required for post-processing.

2.2.2. Capture optimization

2.2.2.1. Ground sampling distance

The distance between the centroid of two adjacent pixels is the ground sampling distance (GSD) of imagery. GSD is an important factor in large-scale velocimetry analysis, since elements that are smaller than the GSD are difficult to resolve. For example, if an image has a GSD of 1 cm/px it may contain elements with length up to 1 cm. Elements that are smaller than GSD might not be appear in the image and may not be useful for image-velocimetry elaborations. It is crucial to know GSD values (cm/px) in advance to guarantee a camera system capable of resolving elements visible on the free surface.

A lot of acquisition parameters play an important role in how the video is captured when it is taken at nadir (Figure 2.8). The height (H) of picture acquisition can be estimated using the desired GSD (Eq. 2.1).

$$H = \frac{IwP \times GSD \times F}{SW} \quad \text{(Eq. 2.1)}$$

where

H	height of the camera with respect to the liquid surface [m]
IwP	image width [px]
GSD	ground sampling distance [cm/px]
F	focal length [mm]
SW	sensor width [mm]

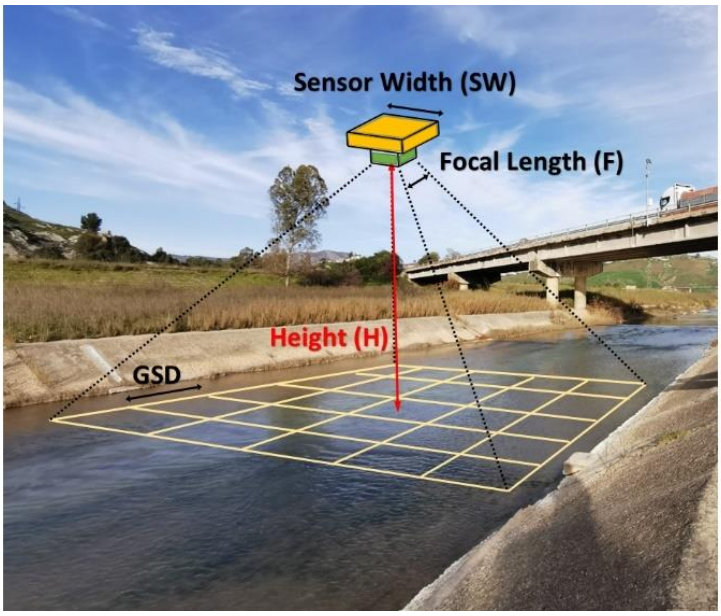

Figure 2.8 – Schematics of GSD at nadir angle.

The camera angle may have an impact on GSD values. The length between the camera and the background of the image is extended when the camera is at a non-nadir angle, in addition to increasing the coverage (Figure 2.9). A change in the camera's pitch will really produce an image grid with a trapezoidal form, with the background scaled proportionally to the angle and distance from the source. Due to this, the GSD varies across the field of view (FOW), and the background of

the image is comparatively poorly resolved. Eqs. 2.2, 2.3, 2.4, and 2.5 can be used to calculate the GSD (cm/px) in cases of oblique picture acquisition.

$$GSD = \frac{L \times 200}{IwP} \quad \text{(Eq. 2.2)}$$

$$L_v = H \frac{\sin(\theta \pm \alpha_v)}{\sin(90 - (\theta \pm \alpha_v))} \quad \text{(Eq. 2.3)}$$

$$L_h = H \frac{\sin(\theta \pm \alpha_h)}{\sin(90 - (\theta \pm \alpha_h))} \quad \text{(Eq. 2.4)}$$

$$\Theta° = \tanh\left(\frac{SW}{F}\right) \quad \text{(Eq. 2.5)}$$

where

L	length both horizontally (L_h [m]) and vertically (L_v [m])
IwP	image width [m]
α_v	angle of tilt seen in the roll axis
α_h	angle of tilt seen in the pitch axis
$\Theta°$	angle of capture, calculated by using SW and F

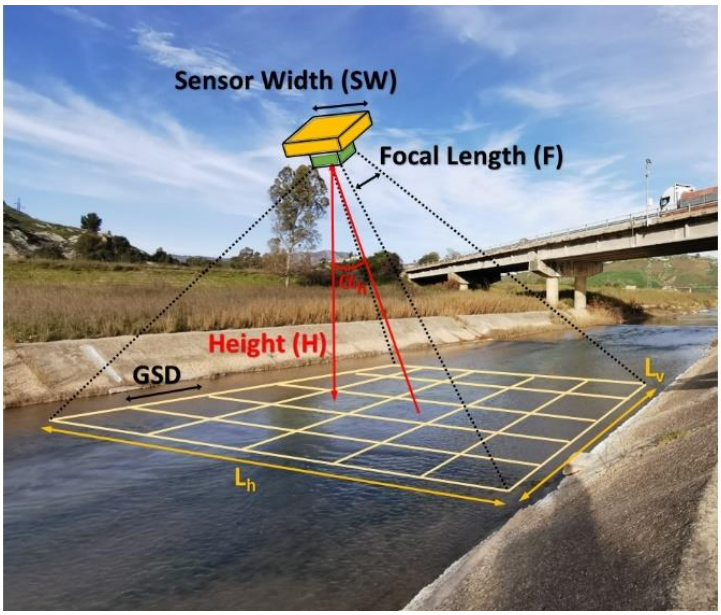

Figure 2.9 – Schematics of GSD at an oblique angle.

In general, the closer the camera sensor is to the nadir for both stationary and mobile platforms, the better. The impact of stage variations in the camera FOV is a crucial factor to take into account when a stationary camera station is installed. As the stage gets bigger, the distance between the water surface and the camera gets smaller, with a reduction of the amount of area inside the FOV (Detert, 2021).

Finally, the image resolution has a significant impact on the GSD (i.e., number of pixels in an image). Using the highest resolution possible to reduce the GSD requires time and computational costs when performing image velocimetry analysis. The lack of guidelines regarding the optimal resolution for the image acquisition has led researchers to use intuition to define the most appropriate configuration (Dal Sasso et al., 2018). Ultra-HD and 4K videos could be used to enhance tracer visibility and to enable the tracking of small tracers. As a general rule, the optimal resolution should be chosen based on the visibility of the tracer material in the field. The traceable features should be clearly visible in the recorded images and should occupy an area that is at least 1 pixel or more. In this context, the use of UAVs allows for greater flexibility because the recording height and thus the resolution can be varied as needed.

2.2.2.2. Tracers

Tracers have been used for a long time in hydrology and geophysics. They allow for integrated investigations of the hydrological system through the observation of flow and transport processes in diverse environmental compartments (Leibundgut et al., 2009). Tracers are widely used for investigating, quantifying, and monitoring several physical processes, including overland flow (Dunkerley, 2003), surface and sub-surface flow (Planchon et al., 2005; Hassan, 2003; Replogle et al., 1966; Waldon, 2004), water travel time (Holecek and Vocel, 1965), water aging (Botter et al., 2009), runoff formation (Lyon et al., 2008), and concentration time (Leibundgut et al., 2009; Pilgrim, 1975).

Based on the substance or object released into the water, traditional tracers can be roughly divided into four types. These categories are known as "isotopes," "chemicals," "buoys," and "dyes."

Isotopes can exist naturally in water or be introduced artificially into streams. Because water composition changes during the hydrological cycle, it can be used to identify catchment flow patterns. Artificial radioactive isotopes can be easily found by non-invasively measuring their radiation emission as they decay over time. However, safety regulations regarding the release of radioactive isotopes are often tight, and costly equipment is needed for their preparation and detection (Pilgrim, 1975; Pilgrim 1966). According to Botter et al. (2009) and Lyon et al. (2008), isotopes are primarily used to distinguish between event and pre-event flow in hydrographs and to calculate the transit times of river basins (Holecek and Vocel, 1965; Pilgrim, 1975; Pilgrim, 1966; Calkins and Dunne, 1970; Wienhöfer et al., 2009). They are frequently employed for transport phenomena, groundwater dynamic measurements, and aquifers (Torgersen and Kennedy, 1999).

Numerous chemicals are employed in surface hydrology, including potassium iodide (Holecek and Vocel, 1965), salt tracers (Calkins and Dunne, 1970; Wienhöfer et al., 2009), nitrates and lithium (Botter et al., 2009). Their low cost, ease of preparation, extremely low toxicity, and minimal absorption of suspended sediment are their key benefits. On the other hand, sampling is required to determine the tracer concentration in streams. Consequently, the total detection process does not offer continuous data, is significantly influenced by severe weather, and necessitates the presence of supervisory operators.

Even though drifter buoys are mostly used in oceanography (Johnson and Pattiaratchi, 2004), Stockdale et al. (2008) conducted tests to determine stream flow velocities and catchment travel times for hydrological purposes. Buoys are comparatively large components that may transport GPS and other electronics. As a result, they are ineffective for monitoring flow in microchannel networks.

Dyes have been used in stream water and groundwater hydrology for over 100 years (Hassan and Ergenzinger, 2003; Hubbard, 1982; Wienhöfer et al., 2009). For instance, they are effectively employed to look into hydraulic connections and flow channels because of their improved detectability. Generally speaking, dye tracers are very adsorptive, non-conservative, and visible (Leibundgut et al., 2009; Hassan and Ergenzinger, 2003; Hubbard, 1982; Wienhöfer et al., 2009). In other words, they are significantly influenced by losses from infiltration processes and suspended sediments, necessitating high dye concentrations. Electrical conductivity tests and ion exchange chromatography are typically used to detect dye tracers, both of which need sampling. Fluorescence can occasionally be used to improve dye tracer detection (Leibundgut et al., 2009; Replogle et al., 1966; Waldon, 2004).

In addition to the tracers mentioned above, related research on PIV in fluid dynamics and hydrology has incited the development and characterization of particle tracers for flow studies (Adrian, 2005). For instance, fluorescent microparticles specifically designed for PIV laboratory studies have been created; these tracers exhibit high efficiency and detectability at almost every flow velocity and water depth (Angarita-Jaimes et al., 2008; Meselhe et al., 2004). Fluorescent polymer nano and microspheres have been used to study near-wall fluid motion (Jin et al., 2004) and mixing processes in multiconstituent and multiphase fluid systems (Angarita-Jaimes et al., 2008). In Jin et al. (2004), beads are detected through PTV which gives better results than PIV for microfluidic and low-density systems. Despite their good detectability, the use of fluorescent microparticles is largely limited to turbulent flow studies in small-scale laboratory experiments (Angarita-Jaimes et al., 2008; Jin et al., 2004).

An example of fluorescent particles designed for potential in-situ LS-PIV measurements is reported in (Pedocchi et al., 2008). It is therein show that reflection reduction is a remarkable advantage of fluorescent particles in large-scale hydraulic experiments. The tracer is detected through common PIV and due to the properties of fluorescent material, good images are obtained in the vicinity of laser-reflective surfaces. Unfortunately, only laboratory research on stratified flows have employed the proposed particle tracers for in-situ applications (Martin et al.,

2009). Additionally, the porosity of the resin composition limits the experimental viability of these particles in underwater activities. As shown in, particles do in fact have a tendency to absorb water after being released, which causes them to quickly become denser (Weitsman and Elahi, 2000). As a result, beads precipitate after losing their inherent buoyancy.

The method described in Tauro et al. (2012) uses commercially available high visibility particle tracers to quantify flow. The use of commercial particles in field studies is limited by a variety of issues, including their high cost, their plastic polyethylene composition, which may be harmful to the environment, the inability to adjust their visibility properties, which limits their applicability outdoors, and their good detectability in lab conditions. In Tauro et al. (2013), a novel approach for synthesising low-cost eco-compatible fluorescent particles was presented in order to overcome some of these problems.

For large-scale flow measurements other high-visibility particle tracers have to be take into consideration. In particular, beads of various sizes for LS-PIV measurements have been produced using light-coloured, kid-friendly dough. Due to their quick biodegradation, these environmentally sustainable tracers can be widely used in rivers and streams. These particles produce uniformly seeded water surfaces and, hence, precise velocity maps.

Generally speaking, tracers are thermally or optically distinct elements that are present on and advected by the water surface. Natural particles (e.g., foam, turbulent structures) may be present in the liquid surface for successful image velocimetry analysis. According to Meselhe et al. (2004), 10–30% of the surface should be traceable throughout the process, but the spatial and temporal distribution of tracers can also have an impact on how well image velocimetry performs. Recent research has recommended that the density, dispersion, and spatial variance of tracers are crucial factors influencing the effectiveness and applicability of image velocimetry methods (Pizarro et al., 2020a; Pizarro et al., 2020b; Dal Sasso et al., 2020, 2021).

Artificial tracers may be used in situations where the spatial distribution of natural tracers is not optimal. It is usually used an eco-friendly material, such bark or a polymer that is able to rapidly deteriorate. They should be inert, easily distinguishable, and have no effect on water quality (Detert and Weitbrecht, 2015). Other important factors are the size and the shape of tracer. It should be larger than the size of the pixel (GSD) (Dal Sasso et al., 2020), with a stable shape (and size) over time (Tsubaki et al., 2011; Tauro et al., 2017).

2.2.2.3. Camera frame rates

The frequency at which successive images are recorded is known as frame rate, which is typically expressed in frames per second (fps) or hertz (Hz).

Commercial cameras often have default frame rates that are usually adequate for capturing sequences for image velocimetry applications. Although 24 and 30 frames per second are the most typical frame rates, but modern cameras may also record images at 60 hertz (Hz). Since the acquisition frame rate is typically not a restriction, the most crucial factor is to guarantee that the frame rate remains constant throughout the acquisition (Perks, 2020; Detert, 2021).

Generally, a high frame rate is great for shot motions, even if is not always a good choice, especially in terms of capacity to stock the huge amount of frames also for brief videos. It is important to keep in mind that if a downgrade of the frame rate is necessary, a loss of frames may occur. For example, if a video is recorded at 60 fps, frames could be lost if a 24 Hz frame rate is used, just because 24 does not divide 60 equally; this problem does not appear if the 60 Hz frame rate is downgraded to 30 Hz, for example.

In the practical use, it is possible to take into account these main differences between 60, 30, and 24 fps recording frame rate (Figure 2.10):

- 60 fps is a high frame rate used to record films and applied for slow motion. It is commonly used for HD videos going for 720p to 8k resolution. A 60 fps video takes many frames per second; it shows more detail and more texture than the other frame rates;
- 30 fps is standard for web-based videos;
- 24 fps can be used for standard videos. It is generally the accepted and standard frame rate for showing feature films, TV, and cinema. It is at this rate that there is enough continuous motion of frames that create the idea of proper movement for the eye to see.

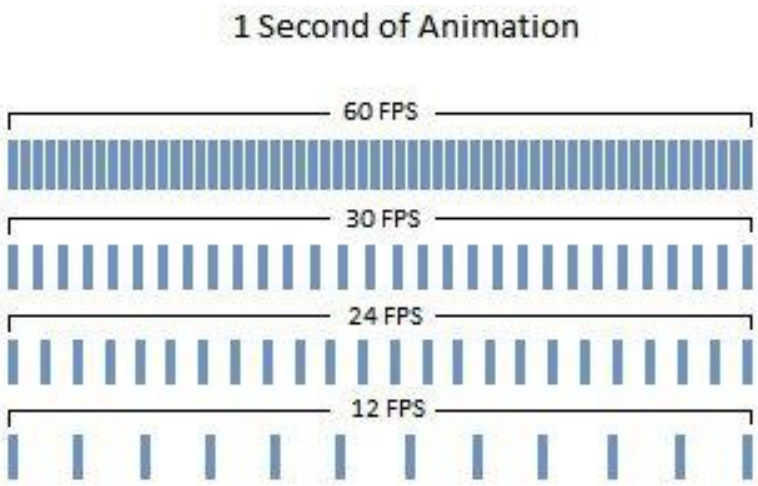

Figure 2.10 – Example of how many frames are contained in 1 second of recorded video considering different values for the frame rate. (http://gocamera.it)

2.2.2.4. External environmental conditions

Analyses of image velocimetry may be affected by difficult-to-control environmental influences, such as the presence of wind, rain, various lighting conditions, and glare. For example, when there is a low flow, wind shear may result in a surface movement that is not related to the real flow velocity (Le Coz et al., 2010). Recent research on the effects of wind showed that, normally, when wind opposes flow direction and when its size is significant relative to the flow, surface velocity deviates by an average of 3% and can reach a maximum of 8% (Pearce et al., 2020). The impacts of precipitation are not fully understood but have been reported to blur imagery (Fujita et al., 2007). A false sense of colour gradients throughout the area of interest is created by uneven lighting and glare on the river surface (Hauet et al., 2008; Zhang et al., 2013).

The effects of these external environmental factors are currently unknown, including the effect they have on the accuracy of image velocimetry results. It is a good practice to minimize the exposure to wind, precipitation, and glare fluctuations by modifying the acquisition methods used. For instance, using a polarising filter may be advantageous when there is a lot of glares. NIR cameras,

on the other hand, may act to reduce the intensity of the brightness difference and may visualise the tracers more clearly. It should be emphasised, nonetheless, that the use of NIR sensors in some situations may result in the loss of visible tracers because the water attenuates the NIR signal (Zhang et al., 2013). Although future research will try to give correction factors for observable external environmental circumstances (such wind shear), their effects should be minimised whenever possible since these relations have not yet been established.

2.2.2.5. Platforms

Considering fixed stations, they provide a time-series of photos that may be used to calculate surface velocities. The typical aim in commissioning fixed stations is to monitor river flows to create and extend discharge rating curves (Hauet et al., 2008). As seen in the case studies of Perks (2020), networked cameras can be used to stream imagery across a network to be processed either near real-time or at a later date.

As an alternative, video can be recorded using Unmanned Aerial Vehicles/Systems (UAVs/UASs) or helicopters in that situations that are difficult to access, hazardous to the operator, or where the area of the inundation exceeds the field-of-view of the stationary monitoring station. These approaches have been beneficial for understanding turbulent flows in rivers for sediment transport (Thumser et al., 2017), capturing flow data at ungauged sites (Kim et al., 2008), and determining river velocities during periods of high flow (Perks et al., 2016).

Although UASs are currently the main focus of mobile methods, it is important to note that there are other methods of mobile image velocimetry. Prior to UAS being reasonably attainable, mobile methods could be conducted using telescopic poles, as demonstrated in Le Coz et al. (2010) and Dramais et al. (2011). Secondly, an important revelation of mobile image velocimetry is the use of software on mobile phones (Hain et al., 2016; Caldwell et al., 2019).

The use of satellite images as a capture method is a more recent and promising discovery, but it is still in its early stages of development. In order to provide an example of good image quality, Kääb et al. (2019) tracked river-ice and water velocities using satellite data with a resolution of 3 m utilising PlanetScope satellite photography (Planet Labs Inc., 2021), taking each frame at 90-second

intervals. High-resolution image sequences and films with a resolution of less than or similar to 1 m can be obtained from satellite data storage (like PlanetScope).

2.2.3. Pre-processing

2.2.3.1. Stabilization

Image stabilisation is necessary due to the movements of mobile platforms (Perks et al., 2016; Bolognesi et al., 2017) and random movements of fixed cameras caused by vibrations by wind or traffic (when installed on a bridge) (Perks, 2020). Figure 2.11 illustrates how appears a stabilized image after applying the stabilization algorithm. It removes in each frame the borders of the entire initial image (shown as the black areas around the borders of the image) to only display the areas that are constant. Modern stabilisation techniques may use the camera GPS location or stable features in the area of interest to establish a steady frame of reference for further analysis (Ljubicic et al., 2021).

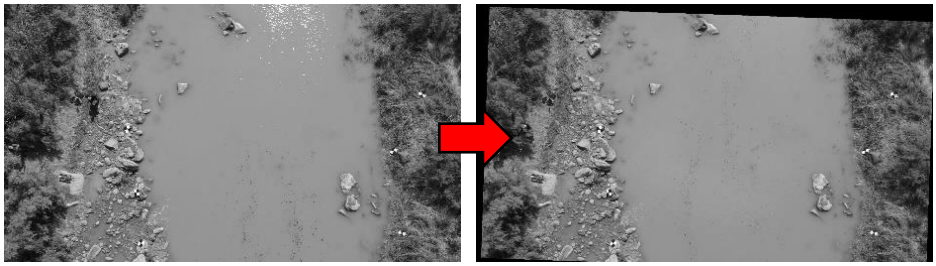

Figure 2.11 – Result of the stabilization process. The original image (left-side) is modified maintaining the portion of frame that is constant and removing the rest of frame (black areas).

Stabilized frames are often referenced to either the initial frame, or a subsequently stabilized frame. This may be achieved using a 3D stabilization technique (e.g., structure-from-motion; SfM), or more commonly a 2D motion estimation technique, e.g., single-step discrete Fourier transform algorithm (Guizar-Sicairos et al., 2008; Rodriguez-Padilla et al., 2019).

Stabilization techniques can be manual or automatic. Manual methods rely on a selection of static reference points which are then automatically processed to determine displacement between frames (Rodriguez-Padilla et al., 2019), while automatic methods select features and then track displacements using binary feature matching techniques (e.g., Harris Corner Detection and FAST) (Muja and Lowe, 2012; Mingkhwan and Khawsuk, 2017). A general process for stabilization techniques includes: (i) breaking videos into sequential frames, (ii) selecting of static features manually or automatically (i.e., feature detection), (iii) feature matching and outlier rejection, (iv) derivation of transformation function, and (v) image reconstruction.

For fixed stations stabilization is not necessarily required, unless the camera experience movement (e.g., oscillations generated by vibrations, or wind). Unstabilized image sequences may produce significant errors when mobile platforms are used. An example of this is given in Detert (2021), where it was shown through a re-analysis of earlier experiments that accounting for residual movement reduced errors by 20–30%.

2.2.3.2. Orthorectification

If the image is being collected at nadir orthorectification is not necessary. Orthorectification is a process to remove perspective distortion and to represent accurate real-world distances.

Typically, images of the river surface are taken from a bridge or riverbank at an angle that is perpendicular to the free surface plane. Such images need to be corrected using a suitable image transformation technique (Mikhail and Ackermann, 1976). Generally, a conventional photogrammetric relation is applied to produce orthoimages using known coordinates of ground control points (GCPs) in the map (X, Y, and Z) and the image (x and y) coordinate systems. The mapping relationship between the two systems is expressed through Eq. 2.6 (Fujita et al., 1998):

$$x = \frac{A_1X+A_2Y+A_3Z+A_4}{C_1X+C_2Y+C_3Z+1},\ y = \frac{B_1X+B_2Y+B_3Z+B_4}{C_1X+C_2Y+C_3Z+1} \quad \text{(Eq. 2.6)}$$

where the eleven mapping coefficients can be determined by the least square method using the known GCPs coordinates. A minimum of 6 GCPs are needed for conducting the transformation. The control points are surveyed in the field using specialized equipment.

When the GCPs are situated on a plane similar to the river surface, 2D transformations are possible. A minimum of four GCPs at the river free-surface elevation are needed for the 8-parameter plan-to-plan perspective projection used in 2D transformations (Fujita et al., 1998; Detert and Weitbrecht, 2015; Detert et al., 2017; Detert, 2021). Where there are significant elevation differences between GCPs and the river surface, 3D transformations are applied. The orthorectification matrix will have 11 unknowns, making it possible to solve it only with six or more GCPs (Jodeau et al., 2008). However, the accuracy of orthorectification can only improve with the number of GCPs (Detert and Weitbrecht, 2015; Detert et al., 2017; Detert, 2021).

The orthorectification can be explicit or implicit. Orthorectification transformations can be applied to the raw images (explicit), or to the vector fields arising after image velocimetry analysis (implicit). Higham and Brevis (2019) suggested that orthorectification of the velocity vector field is more effective especially with PIV cases. On the other hand, explicit orthorectification has the advantage of ensuring the same dimension to each pixel prior to processing (Perks, 2020).

2.2.3.3. Graphic enhancement

The process of changing the graphic characteristics of the acquired images, to remove any interferences and to improve the visibility of tracers, is called graphic enhancement. The first step in this process is to convert multiband imagery to single-band imagery (Fujita et al., 2007; Dobson et al., 2014). However, this is not required when footage is captured using a thermal camera (Patalano et al., 2017; Kinzel and Legleiter, 2019). In order to convert multi-band picture to grey scale, saturation and hue levels are removed and only luminance levels are kept (Perks, 2020). Image manipulation after that is optional but might be useful.

Frequently used image enhancement techniques include: (i) intensity normalization, (ii) histogram equalization, (iii) contrast limited histogram equalization (CLAHE), and (iv) binarization (Thielicke and Stamhuis, 2014). One of the most important processes is to enhance images through contrast enhancement steps (Dellenback et al., 2000). Enhancing the contrast image makes tracers more shining against their surroundings, improving tracking and tracer detectability.

For images where tracers are barely distinguishable, normalization may improve the contrast of the colours. Histogram equalization is the process of enhancing contrast by averaging out the brightness variation across the band. This has been shown to be effective in situations where a colour band shows a cluster of contrast level (Fujita et al., 2004). Image binarization typically uses threshold algorithms to split histograms into two parts (Malepati, 2010; Tensmeyer and Martinez, 2020). Binarization process can be helpful when tracers are scarce in the background.

It is useful to remove the background from images or eventually the influence of the riverbed. To do this, it is possible to use the double-frame background removal process (Honkanen and Nobach, 2005; Patalano et al., 2017). Subsequent frames are analysed and what remains stationary between the two frames is defined as background and noise, and then removed from the image, leaving only the tracer. Detert and Weitbrecht (2015) tried to use a variety of manipulation techniques to produce clear tracers. The study employs grey scaling, a Gaussian filter to reduce background noise, after which it sets the intensity of pixels below a particular threshold to zero and then conducts CLAHE.

2.2.4. Image processing

2.2.4.1. Basic principles

The fundamental concepts that govern image velocimetry algorithms come from either Lagrangian or Eulerian approaches (Hirt et al., 1974). PTV methods are based on the Lagrangian framework, while PIV methods are based on the Eulerian one. The working principles of the two approaches change based on how velocimetry data are seen and recorded (Durst et al., 1984).

In the Lagrangian scheme the velocity vector of a tracer particle can be described at any given point in space and time (Price, 2006). The Eulerian approach evaluates the velocity of a tracer particle as a function of a fixed space and time, having the water passing through a control volume.

The LS-PIV algorithms for estimating velocities are the same with those used in conventional high-density image PIV. In essence, the image intensity distribution in a collection of pictures is processed using a pattern matching technique. The similarity index for patterns enclosed in a small interrogation area (IA) fixed in the first image is calculated for the same-sized window within a larger search area (SA) selected in the second image. The window pair with the maximum value for the similarity index is assumed to be the pattern's most probable displacement between two consecutive images. After determining the distance between the centres of each small window, velocity can be calculated by dividing it by the time difference between consecutive images. This searching procedure is repeated for all IAs in the image.

As a similarity metric, the image velocimetry algorithm employs the cross-correlation coefficient (Fujita et al., 1998). Cross-correlation is calculated between an interrogation area (IA) in the first image and interrogation areas within a search area (SA) in the second image. The pair of particles showing the maximum cross-correlation coefficient is selected as a candidate vector. In this method the cross-correlation coefficient, R_{ab}, is defined as Eq. 2.7:

$$R_{ab} = \frac{\sum_{x=1}^{MX}\sum_{y=1}^{MY}\{(a_{xy}-\overline{a_{xy}})(b_{xy}-\overline{b_{xy}})\}}{\left\{\sum_{x=1}^{MX}\sum_{y=1}^{MY}(a_{xy}-\overline{a_{xy}})^2 \sum_{x=1}^{MX}\sum_{y=1}^{MY}(b_{xy}-\overline{b_{xy}})^2\right\}^{1/2}} \qquad \text{(Eq. 2.7)}$$

where MX and MY are the sizes of the interrogation areas, and a_{xy} and b_{xy} are the distributions of the grey-level intensities (ranging from 0 to 255 for an 8-bit image) in the two interrogation areas separated by the time interval dt. For improving the measurement accuracy, subpixel peak detection methods using Gaussian fitting or parabolic fitting is applied to the cross-correlation distribution (Fujita et al., 1998).

When using natural tracers, problems with PTV motion can occur because natural tracers are not completely stable in structure and are capable of deformation, breaking-up, agglomerating, and interacting with one another.

2.2.4.2. Particles detection

For determining flow velocities, PIV (Figure 2.12A) and PTV (Figure 2.12B) use different principles. PIV uses a Eulerian approach, looking at tracers passing through or along a control area, in order to calculate instantaneous velocity vectors. PTV, on the other hand, calculates flow velocity using the Lagrangian method, focusing on individual particles and tracking their movement through space.

PIV obtains particle displacements by searching (SA) and interrogation (IA) areas within an image. Small window interrogation areas are tracked within larger search areas (Muste et al., 2008). This method produces accurate results (Creutin et al., 2003; Muste et al., 2008), because it infers displacement from surface particle patterns, being less sensitive to the transformation of individual elements.

Individual particles are tracked in PTV-based approaches. This technique has been shown to perform well when seeding density is low (Lloyd et al., 1995; Tauro et al., 2017). However, tracers that change shape, size, or disappear from the frame may have an adverse effect on analysis. The greater the number of tracers successfully tracked, the greater the likelihood of producing an accurate representation of surface velocity. The uncertainty of the individual tracer detection and tracking process may also rise in the presence of very high tracer density (Zhang et al., 1997). There are a range of particle detection and tracking algorithms available for PTV. For feature detection, Good Features to Track (GFTT) (Shi and Tomasi, 1994), FAST (Rosten and Drummond, 2006), and SIFT (Lowe, 1999). For tracking algorithms, cross-correlation can be used, but there are also other such as Kanade-Lucas-Tomasi (KLT) (Perks, 2020), and variations of the Nearest-Neighbour algorithm (Tauro et al., 2019).

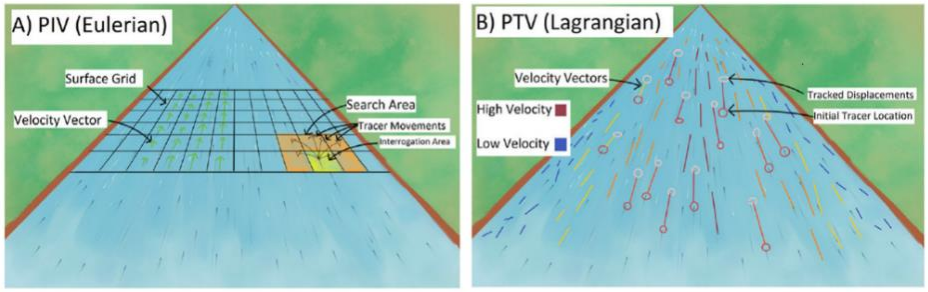

Figure 2.12 – Schematics of general PIV (A) and PTV (B) mechanics. (Jolley et al., 2021)

2.2.4.3. Fundamentals of cross-correlation for PIV

Particle images must be methodically investigated in order to produce a quantified two-dimensional vector field from recorded images. In order to do this, the recorded images are sampled using an interrogation window, whose size determines the measurement's spatial resolution. In order to improve spatial resolution, the interrogation regions can be close together or, more frequently, have a partial overlap with their neighbours. To account for flow gradients, the interrogation regions form can vary from square.

Historically, two methods have been developed: first, an auto-correlation method, followed by a cross-correlation method. The auto-correlation method required images to be double exposed, whereas the cross-correlation method required images to be single exposed. After determining the correlation peak using either of these methods, the displacement information is obtained. Because it was impossible to advance the film quickly enough between the two exposures, the auto-correlation analysis technique was developed for photography-based PIV. A double-exposed image's auto-correlation function has a dominant central peak and two symmetric side peaks. This includes two issues: (i) the flow direction is unclear, despite the fact that the particle displacement is known; (ii) for extremely small displacements, the side peaks can partially overlap with the central peak, reducing the range of observable velocities. Image shifting methods utilising rotating mirrors (Landreth and Adrian, 1988; Lourenco, 1993) and electro-optical techniques (Landreth and Adrian, 1988) have been developed to solve the directional ambiguity problem.

Due to these difficulties, cross-correlation analysis using singly exposed pictures is the favoured technique. First, using an interrogation window, two picture subsamples are recovered from the images at the same location: $f(i,j)$ and $g(i,j)$. Then, on these two examined locations, a cross-correlation process is carried out. In the interrogated regions, this approach yields a cross-correlation distribution with the pixel domain that has a dominating peak that corresponds to the shift of the particles, denoted by (dx, dy). Lastly, using calibration parameters, the pixel shift (dx, dy) is transformed into a velocity.

Due to the nature of cameras, after an image is taken, it gets pixilated and thus discretized. Each pixel's intensity value is read via an analog-to-digital converter and quantized as a result; typically, this is done with an 8-bit converter for a total of 256 (2^8) quantized levels. The discretized cross-covariance can therefore be mathematically expressed within a discrete domain as Eq. 2.8 (Westerweel, 1993; Westerweel, 1997):

$$C(r,s) = \frac{1}{M*N}\sum_{m=1}^{M}\sum_{n=1}^{N}\left[f(m,n) - \bar{f}\right]\left[g(m+r,n+s) - \bar{g}\right] \quad \text{(Eq. 2.8)}$$

where $f(m,n)$ and $g(m,n)$ represent the first and second subsampled images, respectively, M and N represent the number of rows and columns within the images, $C(m,n)$ represents the discretized correlation function, (r,s) represents the location at which the correlation is calculated, and $\bar{f}$ and $\bar{g}$ represent the mean image intensity of the interrogation windows, f and g, respectively.

Willert (1996) also suggests using another discretized cross-covariance description that inherently accounts for the in-plane loss-of-pair term (Eqs. 2.9, 2.10, 2.11, and 2.12):

$$C(r,s) = \frac{C_{II}(r,s)}{\sqrt{\sigma_I(r,s)}\sqrt{\sigma_{II}(r,s)}} \quad \text{(Eq. 2.9)}$$

$$C_{II}(r,s) = \sum_{m=1}^{M}\sum_{n=1}^{N}\left[f(m,n) - \bar{f}\right]\left[g(m+r,n+s) - \bar{g}(r,s)\right] \quad \text{(Eq. 2.10)}$$

$$\sigma_I(r,s) = \sum_{m=1}^{M}\sum_{n=1}^{N}\left[f(m,n) - \bar{f}\right]^2 \quad \text{(Eq. 2.11)}$$

$$\sigma_{II}(r,s) = \sum_{m=1}^{M}\sum_{n=1}^{N}[g(m+r,n+s) - \bar{g}(r,s)]^2 \qquad \text{(Eq. 2.12)}$$

where $\bar{g}(r,s)$ is the average of g coincident with the interrogation window, f.

Willert and Gharib (1991) suggested employing fast Fourier transforms (FFT) to greatly speed up the cross-correlation computations as doing so would lower the number (N) of computing operations for each questioned region from N^4 to $N^2\log_2 N$, reducing the heavy computational burden. Furthermore, computational efficiency can be increased by utilising the symmetry properties of real-valued images, which state that the real part of an FFT is symmetric while the imaginary part is anti-symmetric. Once the cross-correlation peak is identified, the interrogation window systematically interrogates the rest of the image pair, yielding a two-dimensional vector field.

2.2.4.4. Sub-pixel peak finding methods

Previous equations show that the discretized cross-correlation domain will exist only at integer values because the image domain is discretized. This means that the peak value within the cross-correlation domain, which corresponds to particle shifts within the interrogated region, can only be measured to an integer with an uncertainty of ±1/2 pixel. While this may not seem significant, it is important to realize that, for example, for window sizes of 32x32, and maximum particle shifts of 1/3 of window size, the uncertainty of a maximum particle shift of 10 pixels, is at best 5%. Given that vorticity and strain rates are differentially calculated from the velocity, their uncertainties will be about 10% which is unacceptable. As such, methods were developed to obtain sub-pixel accuracy.

Initially, centroiding, defined as the ratio of the first order moment to the zeroth order moment, was used, which required the correlation domain to be thresholded to define the region containing the correlation peak (Alexander and Ng, 1991). Unfortunately, this method strongly biased the displacement measurements towards integer values, creating a severe peal-locking effect on processed data (Westerweel, 1997). Fortunately, more reliable methods were also created, which used curve-fitting to achieve sub-pixel precision by fitting the

greatest peak and its two side-peaks independently in the x- and y-directions. These three-point estimating curve-fits have typically been either parabolic or gaussian, with the latter function being more often employed. Since the particle images, which are well approximated by Gaussian intensity distributions, likewise produce a Gaussian intensity distribution when they are coupled, its widespread usage has been justified. Its estimation is therefore much better predicted using a Gaussian curve fit, rather than a parabolic curve fit, which has also been shown through calibration experiments (Lourenco and Krothapalli, 1995). Furthermore, its peak-locking effect is dramatically reduced.

2.2.5. Post-processing

2.2.5.1. Vector validation

Using statistical approaches to identify and remove inaccurate outputs (e.g., outliers), post-processing may help in decreasing errors. If a vector is considered inaccurate, it is removed and replaced using a 2D interpolation (Stamhuis, 2006). Some common PIV statistical corrective methods are: Penalised Least-Squares Method (Tang et al., 2018), Kriging Regression (De Baar et al., 2014), and Proper Orthogonal Decomposition Outlier Detection (POD-OC) (Wang et al., 2015).

A very basic method to filter erroneous vectors is to choose proper thresholds (upper and lower ones) for velocities. All velocities that possess a value out of the range defined by the thresholds are removed and substituted with the "Not a Number" label.

For the case of PTV results, finding erroneous vectors is more difficult due to the lack of a gridded system. Duncan et al. (2010) constructed the Universal Outlier Detection Scheme (which can be used for both PIV and PTV), but it is a development of the algorithm from the Westerweel and Scarano (2005) study for PIV correctional algorithms.

After removing outliers and inconsistent vectors, the missing ones can be replaced by interpolating the data with surface interpolation algorithms.

2.2.5.2. Discharge assessment

Computing discharge is the prevalent use of image velocimetry techniques. Discharge evaluation is possible if the geometry of a transect of the river is known. If PTV techniques is used, the river surface must have a good amount of tracers for the discharge estimates to be as precise as possible. Eventually, measurements can be interpolated or extrapolated using polynomial, cubic, or the constant Froude methods (Perks, 2020). Traditionally, discharge may be calculated using a velocity-area method, taking into account some specific factors, such as depth-average velocities influenced by the alpha coefficient (Le Coz et al., 2010). Vertical velocity profiles can be calculated using an ADCP when computing alpha values, although Creutin et al. (2003) find that using 0.85 is a valid assumption when this is not feasible (Kim et al., 2008; Le Coz et al., 2010; Perks, 2020).

More recently, mobile image velocimetry methods have been used to calculate the Gauckler-Manning-Strickler coefficient (K) for cross-sectional roughness in rivers as an alternative to approximated alpha values (Bandini et al., 2021). Using both Manning's linear equations and the mean-section technique for calculating discharge from depth-average vertical velocity, the approach concurrently solves for K and discharge.

2.3. UAS-based image velocimetry

Image velocimetry techniques began to appear in the 1980s from laboratory and industrial uses, and they were later modified for river flow monitoring (Fujita et al., 1998). Optical approaches for river flow monitoring are becoming increasingly popular among researchers and are being considered at the operational level for the following reasons: conventional contact measures need skilled operators and are hence time-consuming and expensive.

The growing accessibility of affordable technology is the driving force behind the rising popularity of optical measures for river monitoring. Additionally, the development of such approaches was supported by the rise in the number of applications based on unmanned aerial systems (UASs), which made it possible to

access any point within a river system (Manfreda et al., 2018; Tmusic et al., 2020; Velez-Nicolas et al., 2021).

By combining depth-integrated water velocity profiles with cross-sectional areas, surface velocity data may be utilised to estimate river flow. One way is to use the linear relationship between the maximum and surface flow velocities to determine the mean flow velocity along each profile (Moramarco et al., 2017). On the other hand, 3D river cross-section reconstructions can be performed by Structure from Motion (SfM) algorithms (Eltner et al., 2018). Moreover, this data can also be exploited to measure water level elevation using Machine Learning Algorithms (ML) used for automatic segmentation of water surfaces (Eltner et al., 2021). However, difficult lighting conditions or water conditions (e.g., vegetation, turbidity) can severely affect automatic water line detection. Alternative methods use drone-based eco-sounder (Bandini et al., 2018), onboard radar altimetry (Bandini et al., 2021) and LIDAR (Light Detection and Ranging) systems (Kinzel and Legleiter, 2019) for the same purposes in extended morphological river conditions (e.g., turbid waters, obstructed river view).

The use of UASs for optical flow measurements in unfavourable flow conditions highlights the possibility to monitor floods, ungauged or inaccessible areas (Perks et al., 2016). Moreover, the possibility to capture videos from different flight heights and with nadir or oblique camera angles allows one to observe large and dynamic rivers (Strelnikova et al., 2020), as well as identify the water surface patterns from different points of view (Fujita and Kunita, 2011). UAS remote-controlled systems allow the real-time definition of acquisition frequency based on water flow velocities (Dal Sasso et al., 2018). The possibility of using filters, polarisers, and changing the flight height based on imposed resolution allows for adapting footage acquisition based on environmental settings (e.g., sunlight, reflections, shadows) to maximise the caption of different patterns in time (Liu et al., 2021).

Despite widely acknowledged UAS capabilities, UASs have significant drawbacks. The most significant are related to (i) the UAS maximum payload, which limits the ability to use multiple sensors and communication hardware; (ii) national flight regulations, which limit the use of UAS, particularly in urban areas; and (iii) the need for continuous power supply for frequent flight missions, as well as the inability to fly in extreme meteorological conditions. Furthermore, the key constraints such as wind speed and local favourable light conditions throughout the capture.

In the most recent decades, numerical and field-based research have been conducted to assess image-based velocity measuring systems. These studies generally adopt deterministic (Dal Sasso et al., 2020; Pearce et al., 2020) or statistical (Rozos et al., 2020) approaches for studying the error sources in outdoor applications. The main objectives concern the definition of parameter settings (e.g., camera frame rate, the size of regular sub-regions for cross-correlation approaches) to obtain accurate surface velocity estimations. Several studies enhanced the influence of some sources of errors on image velocimetry in outdoor applications strictly related to mobile platforms (e.g., UAS or handheld cameras). Detert (2021), for instance, evidenced that the stabilization issues and neglected, or poorly executed, camera calibration during field measurement could potentially induce significant errors on a frame-by-frame displacement calculation. According to these findings, Ljubicic et al. (2021) explored different commercial and ad-hoc tools for image stabilization algorithms, highlighting the influence of stabilization errors on image velocimetry performances and the beneficial effects of stabilization algorithms for these purposes. For calibration and geo-rectification purposes, optical data features with known coordinates (Ground Control Points, GCPs) are usually taken into consideration. To overcome the need for GCPs, recent approaches use onboard radars or lasers to convert image unit (pixels) into metric units (Bandini et al., 2021; Tauro and Grimaldi, 2017).

Another well-known problem is the effect of ambient noise on the velocity signal during adverse weather circumstances, such as poor lighting, sunlight reflections, glare and shadows on the flow surface, river colour backdrop, and riverine flora motions, among others (Detert, 2021; Le Coz et al., 2010). Furthermore, highly frightened lighting or quick illumination fluctuations may provide various challenges in reconstructing lengthy and consistent feature trajectories (Pearce et al., 2020; Tauro et al., 2018).

The problems in obtaining reference surface velocity data commonly affect field research. In general, both contact (e.g., current metres or ADCPs) and non-contact (e.g., radars) instruments are used for this purpose (Perks et al., 2020). These instruments are often influenced by several assumptions linked to surface velocity calculations. Current meters and ADCPs, for example, cannot measure surface velocity, which is often extrapolated based on a velocity depth profile. For these reasons, several authors are using computer vision techniques to reproduce real environments with an imposed reference velocity.

Along with these problems, one of the more well-known difficulties for outdoor applications is the absence of surface tracking characteristics or uniformly dispersed materials over the cross-section. Low seeding densities or locally dispersed tracer clusters are possible in flows under natural circumstances. Particularly close to the riverbanks, these circumstances have the potential to produce significant variation and underestimate the flow velocity field. In order to quantify the geographical and temporal aspects of seeding during the video capture phase, Dal Sasso et al. (2020) and Pizarro et al. (2020) presented three metrics. These metrics are based on calculating the: (i) seeding density, (ii) index of dispersion of tracers, and (iii) coefficient of variation of tracer dimension to show their statistical relevance on image-based performances. Additionally, Pizarro et al. (2020) recently presented the Seeding Distribution Index (SDI) as a dimensionless metric that combines the properties of seeding and geographical distribution to synthesise the seeding conditions in the field.

Practically speaking, many experiments in the literature have been artificially seeded to make it easier to recognise moving patterns on the water surface (Perks et al., 2020). However, because operators must enter the area, repeated artificial tracer deployments are neither practicable nor safe. As a result, the current research is working to identify flow patterns such ripples, changes in colour intensity caused by suspended particles or light, and turbulence structures in order to maximise the information about the movement of the water. Several computer vision techniques that are features-detector-based, such as Feature Tracking Velocimetry (FTV, Cao et al., 2018), Optical Tracking Velocimetry (OTV, Tauro et al., 2018), Space-Time Image Velocimetry (STIV, Fujita et al., 2007) Surface Structure Image Velocimetry (SSIV, Leitao et al., 2018), and Kanade-Lucas Tomasi Image Velocimetry (KLT-IV, Perks, 2020), have been implemented for this purpose. The efficiency of these new emerging methods is promising, considering the possibility of monitoring flows without visible objects. More research efforts are needed to test algorithms in different environmental conditions and to discriminate the main differences of approaches. In turn, seeding limitation can be partially compensated using high-visibility tracers (Tauro et al., 2018) or thermal sensors that are less affected by water surface reflections and illumination conditions than RGB imagery (Tauro and Grimaldi, 2017). Thermal sensors allow for monitoring in daylight and night-time conditions (Fujita, 2017), but their current spatial resolution, low contrast, and price present a limitation for monitoring larger rivers or when a high level of detail is required. For this reason, pre-processing techniques based on image enhancement are needed to increase

image velocimetry performances and obtain realistic trajectories in rivers (Pearce et al., 2020; Tauro et al., 2018).

Additionally, a significant obstacle to optical approaches is the absence of data on the velocity profile along the vertical to calculate river discharge. It is customary in this situation to apply a conversion factor to compare surface and depth-averaged velocities (usually known as the alpha value). This factor depends on site-specific river hydraulic and geometric properties, and calibrating it necessitates extensive fieldwork under various flow conditions. In general, the presence of vegetation on the riverbank or secondary currents affects the form of the velocity profile (Moramarco et al., 2017). Bandini et al. (2021) investigated innovative approaches for the parametrization of this coefficient as a function of the Gauckler-Manning-Strickler coefficient based only on UAS observations of surface flow velocities and water surface slope.

UAVs are appealing platforms for fluvial monitoring because they provide (i) high spatial resolution, (ii) high accuracy, (iii) great flexibility, and (iv) cheap costs. The application of UAS observations on surface velocity calculations, morphology reconstruction, and river discharge monitoring across a wide variety of water and river morphology circumstances appears promising. These hydrological variables are critical for sediment transport analysis, flow dynamics simulations, inundation process reconstruction, flood and droughts predictions, and pollutant dispersion monitoring. Technical advancements and downsizing can significantly increase flight performance and multisensory applications, overcoming known UAS constraints, particularly for river bathymetry and water depth assessment. These developments, when paired with real-time data transfer to a cloud system, will result in faster data processing.

2.4. Common error contributions

The total measurement error in optical techniques is a result of a variety of factors, ranging from the recording procedure and setup to the assessment approaches. As a result, errors can be introduced in many different ways.

Every real measurement is subject to a finite measurement error. Thus, any measured value can be decomposed into a true but unknown value and the

measurement error δ_X which is as well unknown for each single measurement (Eq. 2.13):

$$X_{measured} = X_{true} + \delta_X \qquad \text{(Eq. 2.13)}$$

Therefore, the value of both quantities can only be approximated and characterized in a statistical sense from many independent measurements.

Measurement errors are typically divided into two types: systematic errors and random errors. Systematic errors, also called bias errors, can be caused by incorrect calibration or incorrect operation of the measurement system. They are typically constant and predictable if known. Thus, they can be compensated in principle if identified correctly. The magnitude of the systematic error ε of a measurement determines the accuracy. The random error of a measurement is characterized by its non-predictable nature. Random errors can change in magnitude and sign for each single measurement. They have a zero mean value and are usually described by their standard deviation σ (Eq. 2.14):

$$\sigma_X = \sqrt{\frac{1}{n-1}\sum_{i=1}^{n}(x_i - \langle x \rangle)^2} \qquad \text{(Eq. 2.14)}$$

The parameter x_i and $\langle x \rangle$ denote the individual measurements and the corresponding mean value, n is the number of samples and i the control variable. The standard deviation of the random error of a measurement determines the precision.

To determine systematic errors experimentally an independent measurement with higher accuracy is needed. To determine the standard deviation of the random error, a measurement must be repeated many times to ensure that the measured standard deviation converges towards its true value. Therefore, the repeatability and stability of an experiment must be well balanced with the uncertainty of the measurement techniques applied.

Many parameters, including particle image size, intensity and density, turbulent fluctuations, velocity gradients, noise level and interrogation window size, affect the uncertainty. In the last years, different methods were developed to quantify the uncertainty of optical velocity fields (Charonko and Vlachos, 2013; Christensen and Scarano, 2015; Kähler et al., 2016; Sciacchitano and Wieneke, 2016; Timmins et al., 2012; Wieneke, 2015; Xue et al., 2015). Two promising strategies have emerged. The first one is based on identifying all parameters that influence the measurement uncertainty and determining their effect on the overall uncertainty (Timmins et al., 2012). This requires that all relevant parameters and sensitivities are known. The second approach reduces the parameter space by analysing the correlation functions only. This is motivated by the fact that the correlation signal is a result of all parameters that contribute to the measurement uncertainty (Charonko and Vlachos, 2013; Wieneke, 2015).

A systematic error occurs for small particle images: the continuous intensity distribution of very small particle images in insufficiently sampled by the discretized digital camera sensor. Thus, if the low intensities of the pixel next to the one containing the maximum intensity of one particle image are in the order of the image noise level, the sub-pixel position is lost and cannot be reconstructed. However, for particle image diameters in the order of one pixel or less the bias error is still significant. It is important to note that the magnitude of the peak locking effect is very sensitive on the image interpolation approach. However, in comparison to the case without image deformation a strong improvement takes place. This is because the manipulation of the image by means of image deformation techniques allows the maximum of the correlation peak to shift towards the correlation plane centre. This leads to a symmetric correlation peak whose maximum can be estimated best by using the symmetric Gaussian fit function. This also explains why the random error is significantly lower for the multiple-pass evaluation with image deformation. The presence of this “peak-locking” or “pixel-locking” effect can be detected by plotting a displacement histogram (Kähler, 1997). Such a distorted histogram can serve as a good indicator that the systematic errors (due to small particle images) are larger than the random noise in the displacement estimates. However, a smooth histogram can also be present when the random noise is larger than the systematic error, so care must be taken regarding misinterpreting the histogram data.

To avoid significant bias errors due to peak locking it is important to have a particle image diameter of at least two pixels. Smaller sizes usually appear in the

case of low optical magnification or for camera sensors with large pixel spacing, which is typical for some high-speed cameras.

Chapter 3
Materials and methods

3.1. Introduction

Research activities carried out during the PhD course were accompanied, since the first year, by an intensive fieldwork activity. The direct experimentation of what has been learnt on a theoretical basis, allowed a close observation of the advantages, disadvantages, pros, and cons of the optical techniques, testing their capabilities directly in the field.

Field activities are to be framed within a specific scientific collaboration agreement between the Engineering Department (Dipartimento di Ingegneria – DI) of the University of Palermo and the Water Protection Department (Servizio tutela delle acque – S1) of the Basin Authority of the hydrographic district of Sicily (Autorità di Bacino del distretto idrografico della Sicilia – AdB), signed in January 2019.

The main objective of the signed agreement was to optimize the hydrometric network installed extensively throughout the region of Sicily. The hydrometric network, that consists of 125 hydrometric rods with manual readings and 57 recently installed telemetry hydrometric stations, aims to monitor the main water courses in Sicily, with specific installations also on those rivers of particular interest for the hydraulic protection of the territory.

The hydrography of the Sicilian region is rather peculiar, as Sicilian rivers are all of limited discharge and extension, when compared to the large perennial rivers of European nations or other regions of Italy itself. In Sicily, it is possible to identify several so-called “fiumare”, i.e., rivers of torrential character (torrents), characterized by a very low flow in the summer months, but which can reach

considerable discharge values during the rainy season (autumn and winter). The peculiarity of Sicilian streams and rivers is that, during the warmer months of the year, they can remain completely dry, although the disappearance of water may only be apparent, with water flowing below the riverbed. Being characterized by strong erosive action, torrents have a considerable capacity to transport solid material, especially during flash floods phenomena.

Given the importance of monitoring rivers and torrents, also for the reasons mentioned before, the Engineering Department (DI) of the University of Palermo has made a commitment to S1-AdB to develop a series of technical-scientific activities to carry out flow measurement campaigns using various techniques to reconstruct the rating curves at 38 telemetered hydrometric stations, properly identified through appropriate field procedures and protocols.

According to what has been established in the Technical Annex of the Agreement, the research programme consists of the following activities:

- literature review aimed at analysing new discharge measurement methods and identifying suitable protocols for measurement campaigns;
- research and field activities for the development of operational protocols for current measurement with different techniques;
- development of a methodology for the reconstruction of the rating curves at some hydrometric stations in telemetry;
- acquisition of stage-discharge measurements at some hydrometric stations subject to criticality;
- comparative analysis of various alternative discharge measurement techniques;
- other activities, which include, for example, the compilation of operational forms, intermediate reports, and documents updating activities for their administrative monitoring over time.

The Agreement originally stated that a total of 38 hydrometric stations were to be analysed, i.e., all those stations equipped with telemetered sensor operating at the date the Agreement was signed. To this purpose, a measurement campaign was originally planned, to include a maximum total number of daily trips for measurements, surveys, and/or inspections, to be carried out over the entire duration of the programme.

The Basin Authority office (S1 – AdB) has traditionally monitored watercourses in Sicily (Italy) using a standard and traditional approach. In particular, the S1 – AdB operators carry out the acquisition of discharge measurements using an electromagnetic current meter to measure the current velocity along transects aligned in a section of interest, according to the UNI EN ISO 748-2007 standard and following the numerous operational indications available in the literature or in other contexts. Among the main criticalities and problems associated with a traditional approach and encountered by the S1 – AdB staff, are the intrinsic difficulties relate to measurement campaigns, which require the use of highly specialized personnel, and a high burden in terms of cost and time, limiting the possibility of frequent discharge sampling. The conventional instruments cannot often be used in hydrometric conditions characterized by high discharges, as they can often pose certain risks to the operators. As stated in the previous chapters, the observation of the rating curves often reveals a lack of characteristic points for high values of discharge, leading to use the rating curves in extrapolation and with some levels, sometimes unacceptable, of approximation. Moreover, discharge measurement campaigns are often not accompanied by simultaneous topographical surveys of the hydrometric section under analysis, which are often, again, costly, and time-consuming. In such cases, the definition of the rating curve is based on prior knowledge of the riverbed geometry, acquired in previous campaigns, and on the assumption of geometric invariance of the section. This assumption does not always correspond to the reality, especially for unstable sections subject to erosion or silting phenomena. This therefore implies that the S1 – AdB staff collects flow measurements that may be representative of geometric conditions of the section that have undergone significant changes in shape over time. Another particularly important issue, for which the S1 – AdB has signed an agreement with the DI, is the upgrading of the specific rating curves of the Sicilian rivers. These curves are not currently updated. When necessary, curves can often be used whose last update is about 30 years old.

Based on these premises, new approaches and tools for measuring current velocity and assessing flow rate based on acoustic and optical techniques were considered within the scope of the activities under the Agreement between the DI and the S1 – AdB. Among the approaches, the use of the Acoustic Doppler Current Profiler (ADCP) was considered. ADCP allows for the complete reconstruction of both the velocity profile along a section and the bathymetry, which is useful for the estimation of the discharge. This method, when applied following the WMO (World Meteorological Organization) guidelines and standards, is considered the

one with the smallest uncertainty. A further low-cost, simple, and non-invasive method, that allows an accurate estimation of the surface velocity field of the current in a river, is based on optical techniques, fully described in the previous chapters. These techniques involve the acquisition of a sequence of images and their processing to derive the velocity field from the evaluation of the displacement between successive frames of a floating tracer that is assumed moving with the current. Common cameras in fixed installations on a bridge or with an operator, or cameras mounted on drones, can also be used for this purpose. Both natural tracers, such as leaves, branches, and floating particles, and tracers artificially introduced into the surface water flow with appropriate distribution and density can be used. For image processing, several software packages are now available, distinguishing between those based on the LS-PIV technique and those for LS-PTV. In the activities envisaged by the Agreement between DI and S1 – AdB, the LS-PIV method was applied extensively on several Sicilian watercourses, processing the images with software like PIVlab (Thielicke and Stamhuis, 2014) and FUDAA-LSPIV (Le Coz et al., 2014), acquiring images both from a fixed position and a drone in hovering status. It is also worth highlighting how the use of the drone (UAVs), in addition to allowing in some cases the acquisition of images to be processed with the LS-PIV technique, has also allowed for a rapid, efficient, and inexpensive topographical (3D) survey. The part of the section above the free surface, obtained with topographical surveys, suitably integrated with bathymetric reconstruction using ADCP, provides complete geometric information of the section. It is point out that geometrical information are fundamental for the definition of the rating curves.

The measurement campaign carried out within the framework of the Agreement was mainly carried out using the ADCP technique, taking a total of 156 discharge measurements in 28 different sections, making six to ten measurements in each section under investigation and not subject to any criticality, and at least three measurements for the remaining sections. A simultaneous measurement campaign using the LS-PIV technique was also carried out, for a total number of 31 measurements in 14 suitably selected sections, to assess the reliability, limits and potential of the optical methods compared to the acoustic ones, as well as the possibility of using it as an alternative method in cases where the use of the ADCP is problematic (e.g., flood conditions).

The intensive measurement campaign carried out almost during the entire PhD period, enabled the development of a high level of fieldwork experience from

which it was possible to obtain research insights with the production of the analyses that will be reported in the following paragraphs and chapters.

3.2. Measurements using acoustic technique: ADCP

As detailed in the previous chapter, the ADCP technique exploits the principle of the Doppler effect to measure the velocity and direction of the current by transmitting sound waves at a given frequency and determining the Doppler shift as a function of the return echo due to the presence of reflecting particles (e.g., silts, microalgae, etc.) passively transported by the river. The Doppler effect causes the frequency variation between the emitted and received signal, depending on the object the signal hits. Thus, the ADCP measures the velocity of solids suspended in the water and assigns the same velocity to the flow. The use of the ADCP technique allows for a reduction in the time required to measure flow rates in a watercourse, as well as the measurement of velocities at spatial and temporal scales. The minimization of measurement duration is beneficial both because it allows for a reduction in the time operators are required to stand on bridges, boats or within the course itself, minimizing the associated risks, and for the acquisition of measurements at those sites where flow conditions change rapidly. Some of the limitations of the ADCP technique are related, for example, to the possible effect of sediments on the backscattering of acoustic energy. The amount and characteristics of the sediment contained in the water column analysed by ADCP instruments can significantly influence the ability to measure velocities. In order to be able to perform a velocity measurement, the water must contain an adequate amount of sediment, since a reduced presence of suspended matter could provide insufficient information to accurately determine the flow velocity and, vice versa, an excessive presence of sediment makes the technique unusable for the attenuation of sound propagation intensity within the moving fluid. This critical aspect was sometimes found during the measurement campaign on a few rivers.

The instrument supplied to the DI is the StreamPro ADCP manufactured by Teledyne RD Instruments. It is capable of measuring discharge in rivers with depths between 12 and 200 cm. The vertical water column is divided into several cells, with a single cell thickness of at least 2 cm (max value of 10 cm). The

blanking distance (i.e., the depth below the transducer), for which velocity cannot be measured, is 3 cm. The data refresh rate is 1 Hz. The resolution is 0.1 cm/s. The measurable velocity is in the range ± 5 m/s. The transducer operates at a frequency of 2 Mhz and features a configuration with 4 beams (20° angle). The instrument transmits in Bluetooth-wireless mode with a handheld device equipped with dedicated software (StreamPro Software for Pocket PC and WinRiverII) and it is equipped with a floating platform. As the instrument traverses the cross-section, the bottom-tracking sensor detects the bottom and measures the vertical velocity profile and the local depth.

Discharge measurements with ADCP were carried out following the WMO (World Meteorological Organization) standards and considering the operational guidelines of the USGS (United States Geological Survey). The correct use of the ADCP instrument requires that the measuring section should be as regular as possible, avoiding asymmetrical geometries, with vegetation on the bottom and high turbulence situations. A Bluetooth connection is then established between the instrument and the Pocket PC. The acquisition parameters are then chosen, including:

- sensor depth (“Transducer depth”);
- cell size (“Cell size”);
- acquisition mode (“Profiling mode”).

In all measurements carried out by DI personnel, the sensor was placed at a depth of 5 cm below the free surface, whereas the other parameters depend on the conditions of the site under analysis.

It would be possible to set an immersion depth of 0 metres for the transducer, placing the sensor at the level of the liquid free surface, but this is not usually applied to prevent the sensor from coming out of the water when handling the instrument.

The water column can be discretized with cells of 5 or 10 cm. As a general rule, if the depths are less than 1 metre, the vertical column may be discretized with a maximum number of 20 cells, 5 cm each; if the section depths are greater than 1 metre and up to 2 metres, the vertical column may be discretized with a maximum number of 20 cells, 10 cm each. This allows, by sampling several velocity points, to describe as accurately as possible the velocity variations along the vertical. In any case, it is up to the ADCP user to understand what combination of cell sizes

the best solution is for describing accurately the vertical velocity profile of the river cross-section under analysis.

Velocity acquisitions are performed using either Profiling mode WM12 or WM13. The WM12 mode is used for rivers deeper than 1 metre and with average velocities greater than 0.25 m/s, as opposed to the WM13 mode used for rivers with velocities less than 0.25 m/s and depth within 1 metre. The main difference between the two profiling modes is the frequency at which sound pulses are sent from the transducer.

Acquisitions took place along transects of the rivers through the movement of the instrument by personnel from banks or bridges.

Figure 3.1 – Measurement activities moving ADCP along a transect.

For the measurement session to be successful, the following key aspects have been considered:

- detect a sufficient (at least 4) and preferably equal number of reciprocals transects (left to right or right to left), in order to minimize directional bias and ensure a sufficient degree of measurement accuracy;

- verify that the measurement activities along the transects has a duration (exposure) of at least 720 seconds, or more.

The fulfilment of these conditions ensured that discharge measurements could be collected with sufficient accuracy. In any case, in operational practice, the number of measured transects was always greater than 4 (from 6 up to 10 measurements), as the exposure time was always greater than 12 minutes. Since in the field it is not possible to carefully verify the reliability of measurements, this operational practice allowed for a redundancy of measurements, so that enough measurements are available even if some unreliable ones are removed.

As mentioned above, the movement of the ADCP was sometimes from the banks, sometimes from the bridges, depending on the accessibility conditions of the river or the current regime, in each case preserving the safety of the operators. This movement was possible thanks to the presence of two ropes suitably tied to the two sides of the ADCP, pulled alternatively by the operators to move the instrument from left to right and vice versa. The ADCP was moved by trying to keep the drag velocity extremely low, or at least below half the current velocity value. This way of operating ensures a better analysis of velocities along vertical, as the sound pulses have enough time to scan each portion of the river cross-section in detail, but also to avoid the measured velocities being affected significantly by the boat's dragging velocity.

3.3. Measurements using optical technique: LS-PIV

The Large-Scale Particle Image Velocimetry (LS-PIV) technique, used for the determination of the surface velocity of rivers, was extensively described in the previous chapter, and it is widely used in this thesis work. LS-PIV technique is considered a practical and low-cost methodology that complements traditional measurement techniques and offers the possibility of compensating for certain shortcomings and limitations of classical methods. Although it is framed as a promising technique for measuring discharge in a riverine environment, it is essential to point out the almost total absence of operational standards for the proper application of the technique.

The peculiarity of the LS-PIV technique is its ability to extract the kinematic information of a river surface quickly and efficiently from a sequence of images, captured by common devices such as smartphones and digital cameras. Unlike traditional techniques, LS-PIV, being optical, works in a non-intrusive manner. There is no need for operators to immerse themselves in rivers when measuring flow discharge and may expose themselves to the risks linked with non-ordinary flows. However, as will be seen below, it is essential that preliminary preparation activities are carried out on those sites in which the LS-PIV technique is to be applied. If this is not applicable in advance, appropriate surveys can always be carried out proper site surveys to apply the LS-PIV technique appropriately. The use of versatile and simple equipment allows the LS-PIV to be used in any environmental condition, even the most unfavourable ones, like flood events.

The Agreement between DI and S1-AdB made possible the extensive and full-scale application of the LS-PIV technique in Sicily. Considering the lack of operational protocols for the standard application of the technique, for the type of tracer to be used, its density and distribution on the liquid surface, and considering the peculiarities of Sicilian rivers and flow regimes, a sensitivity analysis was carried out on some fundamental parameters of the technique. These analyses were carried out from a numerical point of view, generating synthetic sequences of images representing both ideal and realistic river conditions. The problem was approached numerically as the virtual environment in which the synthetic images were created allows for a proper and independent management of the characteristics of the images to be generated, as well as the flow conditions to be imposed, and other parameters characteristic of the problem studied.

For this purpose, it was developed a script coded in MATLAB environment, capable of generating sequences of images simulating the movement of tracer particles, of fixed shape and diameter, uniformly distributed and with a given density. Analyses were carried out considering different cases of particle density and geometry, and particle velocity, to investigate the importance of the seeding phase and to derive useful information on the characteristics and density of the tracer to be adopted in the field according to the actual motion condition. As a further analysis, evaluations were carried out investigating two other fundamental parameters of LS-PIV technique: the frame rate (fps) and the duration of the video sequences (video length). The number of frames contained in one second and the overall amount of frames to be processed play an essential role in the graphical interpretation of the movement of the tracer on the liquid surface. A detailed description of the above-mentioned synthetic analyses will be given in Chapter 4.

The video length is a parameter on which further analyses have been carried out. In particular, the experience of the open field application of the LS-PIV technique has highlighted the difficulty of optimally managing the seeding phase, when this is necessary. The results obtained from the numerical analyses, which will be explained in Chapter 4, provided specific information on the optimum tracer density for the optimization of the description of the surface velocity field in a watercourse. However, these indications are often disregarded when the seeding phase takes place in reality. Various situations can adversely affect the success of the liquid surface seeding phase, such as the current regime, hydraulic turbulence, and errors in tracer dispersion by operators. The dispersion of the tracer on the surface is a further parameter to be taken into account since a uniform presence of tracer allows a more accurate description of the current motion. For these reasons it is possible that the video recorded during the recording phase may not be useful in its entirety in the LS-PIV analysis and for the purpose of calculating the surface velocity field. In fact, there will be portions of the video that will be characterized by a better density and distribution of the tracer, conditions that significantly improve the response of the LS-PIV software. Chapter 5 will show the analyses performed to understand the best video portions to be extracted taking into account the density and distribution parameters of the tracer when it is artificially introduced onto the liquid surface.

As there are no universally recognised standards the LS-PIV technique was applied by faithfully following typical workflow steps (i.e., seeding, recording, and processing), identifying an operational protocol that could be applied to each case study. LS-PIV discharge measurements were made using the following equipment:

- video recording devices (digital camera/drone);
- tracer material (wood chips/birch chips/natural tracer);
- topographic surveying devices (differential GPS and drone).

Regarding the seeding phase, the artificial tracer is made of floating, non-polluting, biodegradable, and environmentally sustainable material, consisting of wooden elements between 25 and 40 mm in size. Some measurements were also carried out using tracer naturally present on the liquid surface, such as foam or other floating elements. Images of the movement of the tracer were recorded, during the recording phase, in high definition with a digital camera (Nikon Coolpix 530) or with a mini drone (DJI Mavik) at a frame rate of 25/30 fps. However, the type of camera used is not so important. It is intuitive to choose devices capable of capturing high resolution images anyway, reducing graphic noise due to poor

camera resolution as much as possible, maximising the information contained within the frames. High resolution images allow the tracer to be better discretized against the background against which it floats and moves. The position of the recording devices was chosen appropriately in order to include within the field of view proper marker panels used as Ground Control Points (GCPs), whose coordinates were retrieved with differential GPS. Specifically, a 432-channel Stonex S500 global navigation satellite system (GNSS) receiver was used. The marker panels, approximately 38 cm in size, are made up of alternating black and white squares, making them easily identifiable during the pre-processing phases (i.e., stabilization and orthorectification) to which the recorded sequences are generally subjected. Here again, it is not essential that marker panels be used, as it is sufficient to have enough number of points (e.g., natural or artificial elements within the frames, such as rocks, trees, concrete elements, and similar) clearly visible inside the frames, whose coordinates are known precisely in a map coordinate system. During the measurement campaigns, from 6 to 9 markers were placed in a clearly visible position along the banks of the river, and a topographical survey of the areas surrounding the telemetry station was carried out for the definition of a detailed (5 cm resolution) Digital Elevation Models (DEMs). This information layer is a powerful tool through which a potentially infinite number of possible new GCPs of known coordinates can be derived. The map of a high-resolution DEM, as well as the geometric reconstruction of the river section containing the telemetry sensor, was carried out by acquiring aerial images of the area of interest using the DJI mini drone, model Spark, which, despite its small size, is equipped with smart flight control functions, mechanical stabilization, and a good digital camera. The elaboration of the 3-dimensional terrain model from digital photographs was performed using the 3DF Zephyr automatic digital photogrammetry software, which also required the survey and the successive georeferencing with differential GPS of several dozen homologous points, systematically identified in the various images, for creating hook points and be able to proceed with the alignment of the images. The DEM model of the areas of interest was also georeferenced in the WGS84 / UTM zone 33 N reference system.

Regarding image processing, it was decided to operate with two LS-PIV software: PIVlab and FUDAA-LSPIV. In particular, all the pre-processing operations of the acquired video sequences were performed using a dedicated module of the high-performance FUDAA-LSPIV software, which allows to extract the various frames from the recorded videos, to orthorectify and stabilize the images, exploiting the localization of the GCPs, that must be clearly visible in each

frame, and to enhance the images for processing purposes. The processing phase was carried out using the PIVlab software, which allows greater flexibility in the choice of parameters and processing procedures and reduced calculation times, while guaranteeing greater reliability of the results. Another advantage of the PIVlab software is that is coded in MATLAB environment, so the codes for starting the software are easily modifiable and adaptable to the requirements of the analyses to be produced, being able to apply processing operations cyclically and simultaneously to different video sequences. FUDAA-LSPIV, on the other hand, is a software developed in Java whose programming codes are not made available online, so it is possible to perform analyses on individual videos, without being able to automate the processes.

As the last step, by associating the surface velocity field derived from LS-PIV technique with the bathymetry of the section (obtained simultaneously with ADCP, or alternatively derived from DEMs) and adopting simplifying hydraulic assumptions on the vertical velocity profiles, the discharge was derived. The simplifying assumptions concern the vertical distribution of velocities along the entire measurement cross-section. It is generally accepted that this profile has a simplified shape and that there is a linear relationship between the average velocity at the surface and the average velocity at depth, with a zero velocity at the bottom. Velocity profiles along a vertical are almost never linear, so more recent studies have made it possible to obtain more accurate information on the relationship between the two average velocities (i.e., surface and depth) by deriving this relationship from the actual shape of the velocity profile.

3.3.1. PIVlab software

PIVlab software is one of the best known and most widely used software exploiting the theoretical basis of LS-PIV technology and was developed by the Energy and Sustainability Research Institute of Groningen, the Netherland (Thielicke and Stamhuis, 2014). It is a free and open-source tool, coded in MATLAB environment and characterized by a user-friendly graphical interface (GUI). However, the application can also be started via command line, and this is an advantage due to the possibility of automating processes and exploiting the potential of functions and tools already implemented in the MATLAB software.

PIVlab allows the import of the image sequences to be processed and it is also possible to choose how the software should perform the processing by being able to choose the processing style. In particular, two different styles are available:

- type 1, i.e., 1-2; 2-3; 3-4; etc.;
- type 2, i.e., 1-2; 3-4; 5-6; etc..

In the first case, each analysed image pair has one frame in common, i.e., the second image of each pair is the first frame of the next pair; in the second style, image pairs are considered individually, with no common frame.

After uploading the sequences, the typical workflow of the LS-PIV technique can be followed: (i) pre-processing, (ii) processing, and (iii) post processing. In fact, there are algorithms specifically implemented in PIVlab to apply pre-processing operations, cross-correlation analysis and, finally, filtering of the results obtained from the previous steps.

In terms of pre-processing algorithms, the software does not have algorithms for stabilizing and orthorectifying images, operations that are therefore carried out using other applications, but it does offer the possibility of applying various tools for graphically enhancing images and improving the contrast between the tracer and the background. Greyscale is always applied to images uploaded to the software as a default pre-processing to graphically enhance image contrasts, but if that is not enough, PIVlab offers the following algorithms:

- CLAHE (Contrast Limited Adaptive Histogram Equalization);
- Intensity Capping;
- High pass filter;
- Wiener2 denoise filter.

One of the graphical enhancement techniques often used is histogram equalization, through which the intensity values of each pixel are reassigned, distributing them as evenly as possible (Cheng and Shi, 2004). CLAHE is a variant of Adaptive Histogram Equalization (AHE) which takes care of over-amplification of the contrast in an image. CLAHE operates on small regions in the image, called “tiles”, rather than the entire image. When applying CLAHE, the parameter to be set is the number of pixels in the rows and columns that must make up the tiles, into which the images will be divided. When implemented into a LS-PIV workflow, it has been found that CLAHE can provide a 4.7 ± 3.2% increase in the detection of valid velocity vectors (Shavit et al., 2007).

A much less drastic algorithm is Intensity Capping, i.e., a graphical enhancement method whereby all the pixels exceeding a certain threshold intensity limit are replaced with the maximum value imposed (i.e., the threshold intensity value) (Shavit et al., 2007). Unlike CLAHE, the algorithm only acts on certain pixels, and not extensively on all those that constitute the frames, so the magnitude of the changes made is certainly smaller. Intensity Capping allows for a better detection of valid vectors by 5.2 ± 2.5% (Shavit et al., 2007).

A high pass filter is instead a method by which the high-frequency signal of an image is enhanced by removing the low-frequency signal. This in practice means that a smoothing filter is subtracted from the images, enhancing the high-frequency signal and thus giving a sharpening effect to the images (Raffel et al., 2018). Sharpening emphasises the contour of the objects contained within the frames, so the edges of the tracking particles are made more visible and thus traceable by the detection algorithm.

Since images are often subject to noise, PIVlab software also provides a denoise algorithm: the Wiener filter (Treitel, 1974). This filter is applied to images adaptively and depends on the local image variance. The Wiener filter locally applies a linear averaging filter, that will be performed using a neighbourhood of each pixel of fixed size. The strength of the averaging depends on the local variance in this neighbourhood. As a result, pixels in a region with higher contrast will be smoothed less, and pixels in a region with lower contrast will be smoothed more. The Wiener filter works well when the noise is “white”, i.e., a constant-power additive one.

There is a further methodology, properly implemented in PIVlab, for the graphical enhancement of images and the optimization of the information contained within the frames: the Background Removal. This method does not apply any filtering to the images but is based on subtracting the background image of the scene being recorded from the frames of the recorded sequences, so that the only information in the resulting images remains the moving tracer. This can be achieved by subtracting to each frame the successive one, or by obtaining a single background image, from the recording of the area of interest without a moving tracer and subtracting it from each frame of the sequences to be processed.

Prior to the processing phase to which the images of the video sequences are subjected, PIVlab software requires an image calibration phase. In particular, in order for results to be expressed in terms of velocity measured in metres per second (m/s), calibration is performed by identifying a reference distance, of known size,

and the time interval between successive frames (i.e., time step). The calibration step is indispensable for converting the velocities measured in pixels per frame into the velocities' units within the International System of Units.

For the processing phase, PIVlab software provides a choice of two different algorithms for applying statistical cross-correlation analysis and obtaining the displacement fields of the tracer particles: D-CC (Direct Cross-Correlation) and FFT-CC (Fast Fourier Transform Cross-Correlation). It is this part of the workflow that is the most sensitive for obtaining results with sufficient accuracy. The aim of cross-correlation algorithms is to identify the same patterns between consecutive frames, deriving the final displacement vector. The domain in which the algorithms solve the equations for the calculation of cross-correlation are different. In the D-CC the correlation matrix is computed in the spatial domain. The results from using this approach are more accurate, with a reduction in systematic and random errors, but it leads to the disadvantage of high computational times. Nowadays, however, it is possible to make use of parallel computing to speed up processing, thus taking full advantage of the D-CC approach. The difficulties arising from the use of D-CC are however solved using the FFT-CC approach, which solves the cross-correlation matrix in the frequency domain (Raffel et al., 2007). Unlike the D-CC approach where a single Interrogation Area of user-definable size can be used, in the FFT-CC approach a multi-pass analysis can be adopted to improve the geometric resolution of the results.

The position of the cross-correlation intensity peak to understand the most probable frame-by-frame displacement, with both approaches explained above, can be refined using peak finding techniques. There are two types of algorithms implemented in PIVlab: (i) 2·3-point fit, and (ii) 9-point fit. In the first case, a one-dimensional Gaussian curve (3-point fit) is fitted to the intensity distributions of the correlation matrix, while in the second case, a two-dimensional Gaussian curve (9 points fit) is used.

The final step of the LS-PIV workflow is the post-processing phase. PIVlab software has implemented two different levels of post-processing: (i) data validation, and (ii) data interpolation.

Data validation is crucial in order to eliminate erroneous vectors incorrectly estimated due to problems related to the environmental conditions in which the images were recorded. For example, the presence of sun-glint can lead to the estimation of inconsistent vectors due to the false movement of reflections induced by water ripples. One method of performing an objective validation of the

data, in a semi-automatic manner, is given comparing velocity measurements (in the x- and y- components) with the maximum and minimum admissible values. Velocity vectors that are outside of this range, are automatically rejected.

Data interpolation is necessary when the data validation phase has rejected vectors as inconsistent with the estimated velocity field. The missing vectors are then replaced by vectors obtained by spatial interpolation of the data.

Once the filtering and interpolation steps have been applied to the data obtained as output from the application of the cross-correlation algorithms, the mean surface velocity field can be calculated, considering each individual instantaneous surface velocity field.

3.4. Hydrometric station and critical issues

The S1 – AdB system consists of 125 hydrometric rods with manual field reading and 57 telemetry stations, which were recently installed in several rivers of the Sicilian region. According to the Agreement signed between DI and S1 – AdB, it was necessary to preliminarily identify 38 stations for which the reconstruction of the rating curves was planned. This choice was made in concert and synergy with the S1 – AdB, based on the information shared by S1 – AdB and taking into consideration only the telemetered stations. In particular, as can be seen from Figure 3.2, among the 57 telemetered stations, only 39 were active at the time the Agreement was signed, while the others were under maintenance. The 39 working stations were then preliminarily examined by means of on-site inspections in order to check for any criticalities.

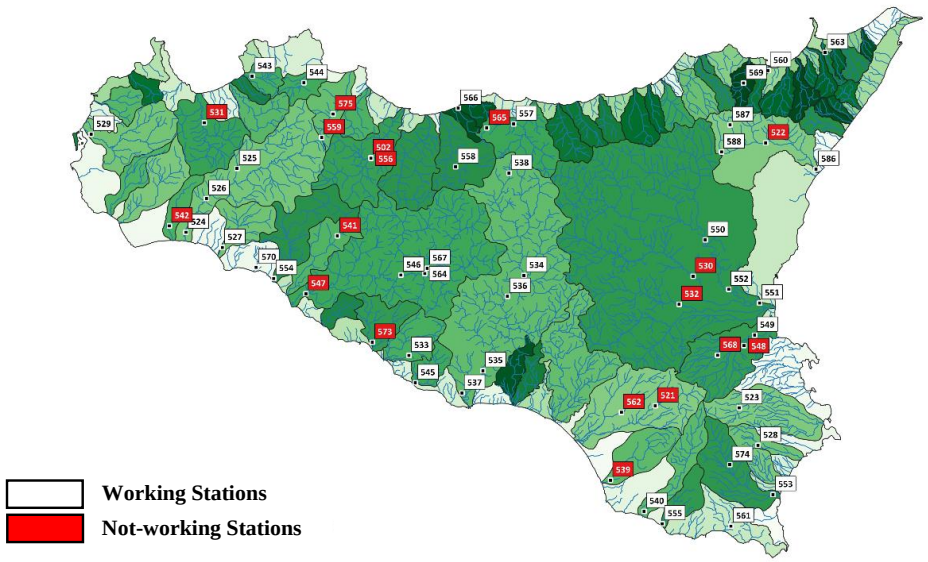

Figure 3.2 - Map of the S1 - AdB telemetering hydrometric stations with an indication of their operating status at the time the Agreement was signed.

Table 3.1 shows the complete list of stations declared to be operating at the beginning of the Agreement, and that were subject to preliminary inspection, with the correspondent date of the inspection. At the end of the inspections, the number of stations that were in operation was 26, which is considerably reduced from the 39 originally considered. Table 3.1 also shows the working status for each station.

Table 3.1 – List of hydrometric stations of the S1 – AdB subjected to technical inspection and declared operational at the time the Agreement was signed.

ID	Measurement gauge station	Date of inspection	Working status
544	Oreto a Parco	14/5/2019	V
524	Belice a Marinella	12/6/2019	V
525	Belice destro a Giacati Poggioreale	12/6/2019	V
526	Belice a Ponte Belice	12/6/2019	V
527	Carboj a Menfi	12/6/2019	V
554	Verdura alla Foce	12/6/2019	X

570	Vallone Portolana a Sovareto	12/6/2019	V
543	Nocella a Zucco	15/6/2019	X
534	Imera Meridionale a Capodarso	16/6/2019	V
536	Imera Meridionale a Ponte Besaro	16/6/2019	V
538	Imera Meridionale a Petralia	18/7/2019	X
557	Castelbuono a Pontevecchio	18/7/2019	V
558	Salito-Fondachello a Caltavuturo	18/7/2019	V
566	Roccella alla Foce	18/7/2019	V
549	San Leonardo a Lentini	22/8/2019	X
550	Simeto a Ponte Barca di Biancavilla	22/8/2019	X
551	Simeto a Catania	22/8/2019	V
552	Simeto a Ponte Giarretta	22/8/2019	V
553	Tellaro a Villa Tellaro	22/8/2019	X
540	Irminio a Plaja Grande	23/8/2019	V
555	Passo Gatta alla Foce	23/8/2019	V
533	Burraito a Villaggio la Loggia	3/9/2019	V
535	Imera Meridionale a Drasi	3/9/2019	V
537	Imera Meridionale a Stretto Licata	3/9/2019	V
545	Palma alla Foce	3/9/2019	V
546	Platani a Passofonduto	3/9/2019	V
564	Gallo d'oro a Fontanazza Bompensiere	3/9/2019	X
567	Salito a Raffe Sutera	3/9/2019	X
523	Anapo a San Nicola	13/9/2019	V
528	Cassibile a Manghisi	13/9/2019	V
561	Favara a Bufali Ispica	13/9/2019	X
574	Tellaro a Castelluccio	13/9/2019	V
586	Alcantara ad Alcantara	23/6/2020	X
587	Alcantara a San Giacomo	24/6/2020	V
588	Flascio a Ponte Flascio	24/6/2020	X
529	Chinisia-Birgi a Birgi	9/7/2020	V
560	Elicona a Falcone Vignazzi	9/7/2020	V
563	Floripotema a Passo Cattafi	9/7/2020	X
569	Timeto a Murmari	9/7/2020	X

As a result of the technical inspections, several critical issues emerged in several sections. These criticalities can be grouped into the following categories:

- excessive vegetation in the riverbed and/or on the banks;
- unsuitable location of the station along the river (absence of significant stage values) and/or unsuitable positioning of the telemetry sensor (e.g., installations on the floodplain and/or in a position that does not correspond to the passage of the water under ordinary flow conditions and/or in positions that do not guarantee sufficient safety standards for the acquisition of current measurements);
- other critical issues that emerged during the project.

The above mentioned first critical issue was found in several sections. In particular, the dense vegetation sometimes on the banks, sometimes in the riverbed, or in some cases on both sides, precluded not only direct access to the river, but also the use of any instrumentation to carry out the discharge measurements. The presence of vegetation can occlude the section, alter its roughness dynamically, and generally influence the reading of the hydrometric stage level and the usability of the rating curve. Sections that present this kind of issue are those where periodic cleaning activities would be necessary, with specific actions and appropriate means by qualified personnel.

The second kind of criticality refers to several situations: (i) an unsuitable location of the telemetered station along the river; (ii) an unsuitable positioning of the sensor; (iii) a position that does not guarantee sufficient safety conditions for the acquisition of current measurements. The first type of criticality is linked to the installation of the hydrometric sensor in sections that are not suitable for indirect flow monitoring from the stage measurements. These are sections that are dry for most of the year and in which the water levels are not sensitive to discharge variations. In such sections, the almost total absence of significant flows precludes the possibility of carrying out measurements for the definition of the rating curves. The second type of issue refers to stations in which the problems encountered could be resolved by simply moving the sensor.

Finally, there are some stations subject to criticalities that have arisen during the activities, such as significant changes in the geometry of the section as a result of reshaping or rearrangement of the riverbed and/or flood events, silting of

the area under the sensor and/or cover caused by vegetation, and inconsistency between the recorded water levels and the measured stage levels.

Critical issues not related to the measuring stations include the COVID-19 pandemic situation, which has imposed restrictions, limiting the possibility of carrying out measurement campaigns, especially during the winter periods characterized by the greatest discharge values in Sicilian rivers.

Chapter 4
Numerical analysis for LS-PIV optimization

4.1. Introduction

LS-PIV is a measurement technique and therefore it is always possible to define an error to be associated with the final measurement. Generally, the error expected after a measurement has been taken is as small as possible if the measurement activities have been conducted according to specific criteria, guidelines and, more generally, measurement standards. As the LS-PIV technique is of a new generation and is considered an innovative technique compared to those traditionally applied, it has no universally recognised standards. The application of the steps making up its characteristic workflow is carried out according to objective criteria obtained from field experience and the intensive activity of scientific research on optical methods.

Careful and considerable literature review on the subject has shown that errors in the estimation of surface velocity fields arising from the application of the LS-PIV technique are linked in the first instance to certain characteristic parameters and subsequently also to the settings chosen for the processing software. For example, the density of the tracer particles on the liquid surface is one of the factors most influencing the successful interpretation of particle movement. LS-PIV processing software is challenged whether the liquid surface is poorly seeded or over-seeded, leading to errors in the estimation of tracer pattern displacements by statistical algorithms. Another element that can influence the correct interpretation of surface velocity fields is the frame rate. Since the frame rate regulates the number of frames contained within the time unit, this parameter

is directly related to the deducible displacement of individual particles frame-by-frame. If the actual current velocities are too low, it may occur that the displacement of a single particle is smaller than the size of the pixels constituting the frames. In this circumstance it will therefore not be possible for the particle detection algorithm to understand the displacement of the tracer particle as there is a sub-pixel displacement problem, returning incorrect velocity vectors. Reducing the frame rate in these cases can reduce errors in estimation.

All these elements, together with the possibility of finding conditions in the open field that were far from ideal for the theoretical application of the LS-PIV technique, led to the reflection that careful preliminary analyses have to be carried out on certain fundamental parameters governing the technique. It was decided to carry out these preliminary studies from a numerical point of view, analysing the performance and the sensitivity of the most popular LS-PIV software on the main factors influencing the technique.

The numerical analysis took the form of the creation of a synthetic image generator, suitably coded in MATLAB environment, in order to produce synthetic video sequences with specific characteristics for both the tracer and the current on which it moves. The possibility of creating controlled flow conditions, of placing different tracer conditions on the virtual liquid surface, is the advantage of using numerical simulations.

All the synthetic image sequences were then analysed with one of the most famous and used open-source software based on LS-PIV theory: PIVlab (Thielicke and Stamhuis, 2014). The results arising from the software processing were finally evaluated from a statistical point of view, paying particular attention to the error in the estimation of the surface velocity fields.

4.2. Modelling framework

The numerical analyses for investigating the sensitivity and performance of the LS-PIV technique to certain peculiar parameters on which the technique depends were carried out by developing a modelling chain with three consecutive modules (Figure 4.1). The core of this chain is the PIVlab software, which is used for the application of statistical cross-correlation analysis. This module receives as

input image sequences that are generated appropriately by a previous module: the ISG (Image Sequence Generator). The outputs of PIVlab are instead reprocessed through a proper module for the analysis and the final visualization of the results, called RAV (Results Analysis and Visualization). The first (i.e., ISG) and last (i.e., RAV) modules were entirely coded in MATLAB environment, and subsequently integrated with PIVlab software, used directly by command lines to automate and customise the processing components to analysis needs.

With the aim of giving consistency to the analyses and adequately characterizing the results from a statistical point of view, several image sequences were produced with ISG module under different scenarios, leading to a wide number (i.e., 5200) of image sequences to be processed.

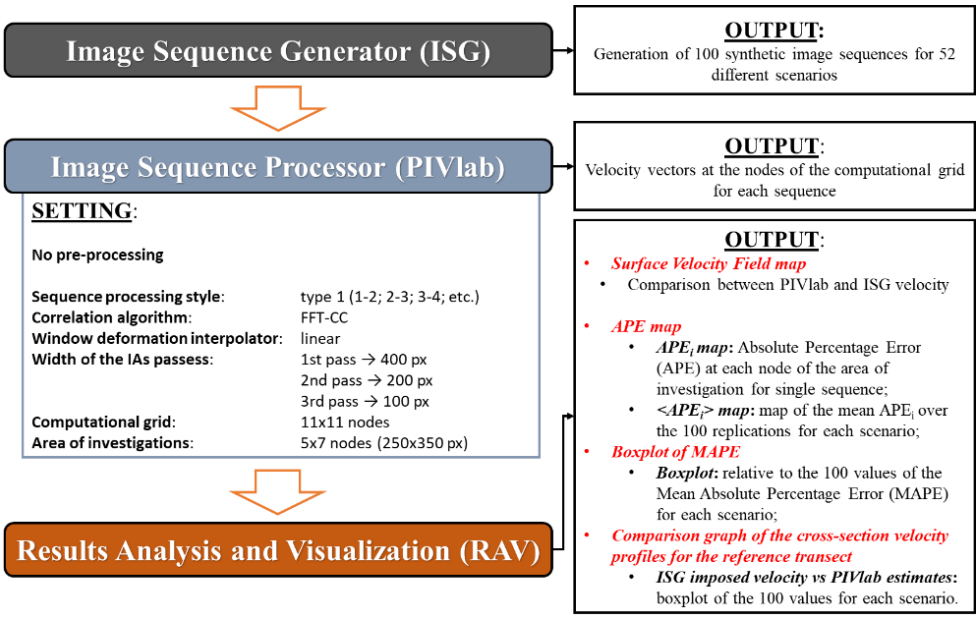

Figure 4.1 – Modelling chain implemented in MATLAB, including: (i) Image Sequence Generator (ISG); (ii) Image Sequence Processor (PIVlab); (iii) Results Analysis and Visualization (RAV). Settings and outputs of each module are reported.

4.2.1. ISG module

The frame sequence generator module (ISG) is able to generate a user-defined number of sequences and reproduces by default the liquid surface of a watercourse on which tracer is virtually dispersed. The advantage of having structured an ad-hoc module for sequence generator relates to the possibility of managing both flow conditions and the seeding of the liquid surface in a controlled manner.

In this respect, the floating tracer was dispersed under two different operating conditions: (i) ideal environment (ID), and (ii) semi-real environment (SR). In the first case, conditions have been reproduced that are difficult to observe in reality, as a perfectly white tracer moves against a completely black background. Similar conditions can only be achieved if intensive pre-processing is carried out on the recorded sequences. In the case of the semi-real environment, the background against which the tracer particles were forced to move was derived from the image of the surface of a real watercourse. In particular, all the pixels constituting the background of the synthetic images were filled with the intensity levels randomly sampled from the real image. In this way, the semi-real background presents characteristics similar to a real background, with the presence of intensity levels influenced by real environmental conditions, such as variable illumination during the recording of sequences, or the different incidence of the sunlight on the liquid surface. The image used in the semi-real environment is still representative of a watercourse in clean water conditions.

In terms of tracer dispersed virtually on the liquid surface, it is represented by circular disks perfectly white in the case of the ideal environment, while it is altered with white noise under semi-real conditions. In order to take into account the possibility in reality that tracer particles may have different sizes, sequences were generated considering two types of particles: constant size (CON) and variable diameter (VAR).

The CON condition is characterized by particles of a constant size of 10 pixels. This value is generally used for both laboratory and field applications (Dal Sasso et al., 2018; Pizarro et al., 2020; Tauro et al., 2016). Particles diameter takes on values between 2 and 20 pixels in the case of the VAR condition. These diameters are generated through a Gauss distribution with a mean of 10 pixels and standard deviation of 3 pixels.

In the two schemes ID and SR, the CON and VAR particles can be represented as perfectly white (ID case), or as disturbed by white noise (SR case; standard deviation of 0.05), simulating an external environmental disturbance.

Figure 4.2 shows an example of tracers for the possible schemes ID-CON, ID-VAR, SR-CON, and SR-VAR.

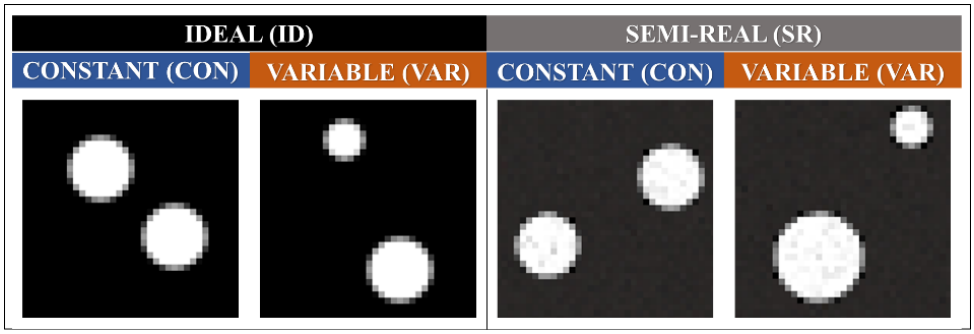

Figure 4.2 – Representation of the 4 possible schemes (ID-CON, ID-VAR, SR-CON, SR-VAR), obtained by combining the two different options for the tracer size (constant CON or variable VAR size) and the two environmental conditions (ideal ID and semi-real SR).

The dispersion of the tracer particles took place within a grid lattice representative of the liquid surface, with a background relative to the ID or SR cases, according to a Poisson distribution with parameter λ, i.e., the density of the tracer. A Poisson distribution is a discrete probability distribution that gives the probability of an event happening a certain number of times within a given interval of time or space. The unique parameter is λ and it represents the mean number of events. In the case of the tracer particles, having fixed the density value with which they must fill the grid lattice and knowing the size of the frames, the values of λ were obtained in terms of the average number of particles to be generated in each lattice. The particles generated were also excluded from overlapping during their movement in order to each retain their own characteristics of shape and size.

The tracer was finally forced to move by imposing a realistic and constant cross-sectional surface velocity profile at every point on the grid lattice. This profile reports normalized velocity values, so that velocity profiles can be obtained for different hydraulic conditions, simply by multiplying the profile by the

characteristic mean velocity of the current. The shape of the imposed velocity profile is typically parabolic, with a maximum value reached at the middle of the watercourse and with a reduction in velocity near the banks to take into account of the friction forces present in reality at the banks.

The imposed velocity profile was derived from the results of a measurement campaign carried out in a real river (Le Coz et al., 2008). The normalized curve was calculated by sampling field data up to half of the river, thus mirroring the profile obtained for the remaining part of the river around the axis of symmetry. The sampled velocity points were interpreted with different interpolation laws, but the most appropriate one (R^2=0.985) turned out to be the logarithmic function (Figure 4.3). This is known to characterize the behaviour of surface velocities with distance from the banks under undisturbed flow conditions (Plesinski et al., 2017). No disturbance effects on the velocity profile from turbulence were therefore considered, keeping the shape of the resulting curve uniform and constant.

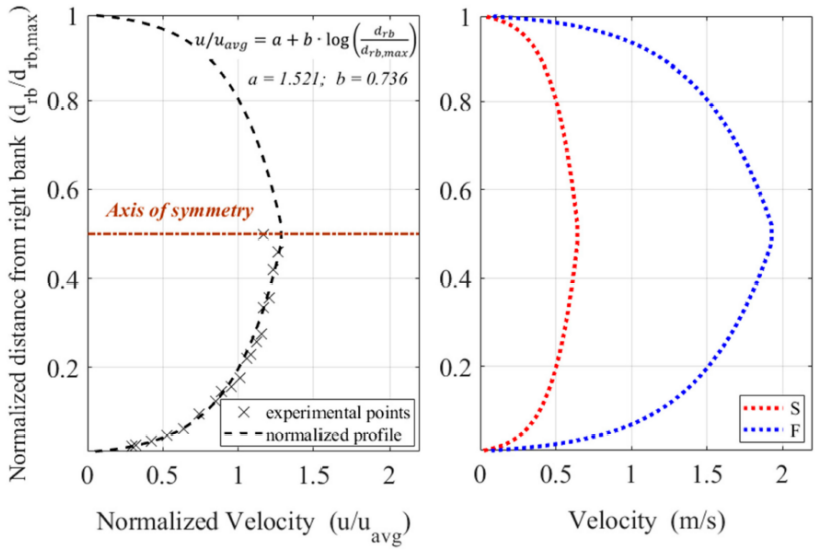

Figure 4.3 – On the left panel, the normalized cross-section velocity profile, with indication about the experimental points from (Le Coz et al., 2008), the curve fitting equation for half section with parameters (a=1.521 and b=0.736) and the axis of symmetry. On the right panel, slow (S) and fast (F) velocity profiles, obtained multiplying the normalized profile by the average velocity u_{avg} of 0.5 m/s and 1.5 m/s for the S- and F-profile, respectively. (Pumo et al., 2021)

The velocity profile was normalized considering the average velocity value u_{avg} and also normalizing the distance from the banks, in particular from the right bank ($d_{rb}/d_{rb,max}$). The "Slow" and "Fast" versions of the velocity profile have been calculated considering two different values for the average velocity: (i) 0.5 m/s for S-profile, and (ii) 1.5 m/s for the F-profile. In terms of pixels displacement per frame, the profiles obtained have average velocities of 42 px and 126 px, for the S and F cases respectively. The range of velocities assumed by the tracer particles therefore varies from a minimum of 32 pixels, in the S case near the banks, to approximately 161 pixels, in the F case in the centre of the watercourse.

All of the above elements were implemented within the ISG module with specific parameters (Figure 4.4). Sensitivity analyses were therefore performed on some of these parameters while keeping others constant over different scenarios. In all cases, the spatial resolution, set at 0.003 m/px, the frame size (i.e., 600px x 600px, i.e., 1.8m x 1.8m), the normalized velocity profile and finally the number of replications generated for each scenario considered were kept constant.

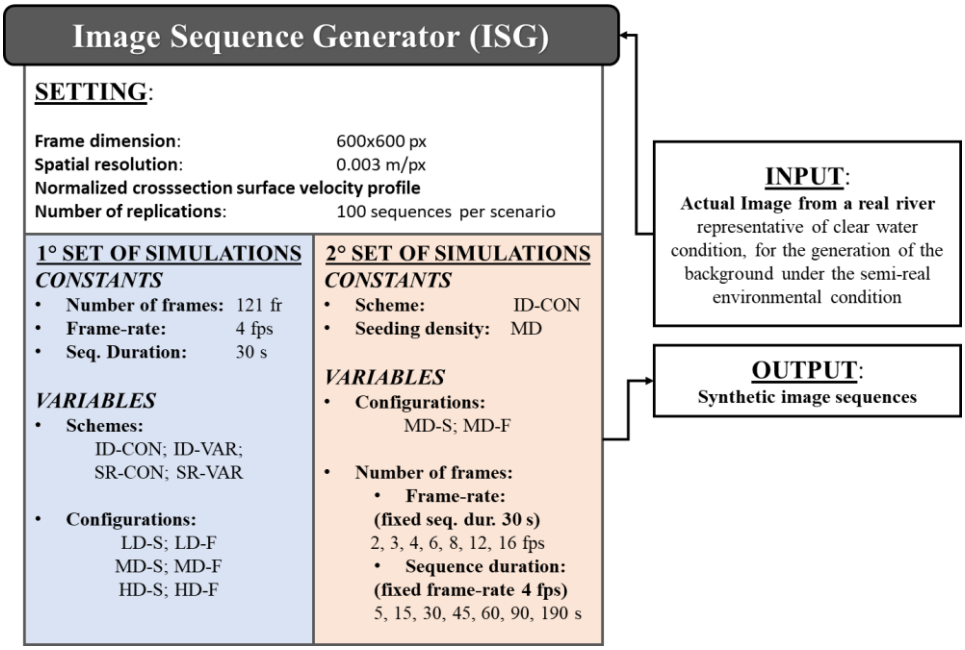

Figure 4.4 – Settings, input and output for the ISG. Parameters used for the generation of the various scenarios for the first and the second set of simulations are reported in the ISG setting box, distinguishing between constant and variable parameter.

By combining the two environmental conditions (i.e., ID and SR) with the two possibilities of generating tracer particles (i.e., CON and VAR), four different schemes were created: (i) ID-CON; (ii) ID-VAR; (iii) SR-CON; and (iv) SR-VAR.

Considering these schemes, analyses were conducted on a first set of simulations, creating sequences that had a fixed time duration and frame rate. Six different configurations obtained by combining different tracer density conditions (i.e., LD, low, MD, medium, and HD, high density) with the current regime on the free surface (i.e., S, slow, and F, fast velocity profiles, were considered for each scheme. Then, alternatively changing first the frame rate (keeping the duration fixed) and then the duration of the synthetic sequences (keeping the frame rate fixed), analyses were carried out on a second set of simulations, considering for it only the ID-CON configuration with a MD tracer density for both hydraulic conditions S and F.

All combinations developed for the first and second set of simulations led to the generation of 52 different scenarios (Table 4.1).

Table 1.1 – Parameters and configurations considered for generating the 52 different scenarios. The scenarios are obtained combining schemes (combination of environmental and tracer size conditions) and configurations (combination of seeding density and surface velocity profile). WN=white noise; px=pixel; ppp=particles per pixels; fps=frame per second.

ENVIRONM. CONDITION	Ideal		ID	*White uniform particles*			
				Black uniform background			
	Semi-real		SR	*White uniform+WN particles*			
				Real clear water background			
FLOW VEL. PROFILE	Slow		S	u_{avg}	*[m/s]*	0.5	
	Fast		F	u_{avg}	*[m/s]*	1.5	
TRACER SIZE	Constant		CON	D	*[px]*	10	
	Variable		VAR	D (mean)	*[px]*	10	
				SD (st. dev.)	*[px]*	3	
SEEDING DENSITY	Low		LD	λ	*[ppp]*	$6.4\ 10^{-5}$	
	Medium		MD	λ	*[ppp]*	$2.5\ 10^{-4}$	
	High		HD	λ	*[ppp]*	$1.3\ 10^{-3}$	
NUMBER OF PROCESSED FRAMES	*First set of simulations*			FR	*[fps]*	4	
				d	*[s]*	30	
	Second set of simulations	Fixed seq. dur. (30 s)		FR	*[fps]*	2-16	
		Fixed frame-rate (4 fps)		d	*[s]*	5-180	

PARAMETRIC SCENARIOS		**LD-S**	**LD-F**	**MD-S**	**MD-F**	**HD-S**	**HD-F**
	ID-CON	1	1	1, 2	1, 2	1	1
	ID-VAR	1	1	1	1	1	1
	SR-CON	1	1	1	1	1	1
	SR-VAR	1	1	1	1	1	1

The choice of tracer density values was made after studying other works in scientific literature about the same topic (Dal Sasso et al., 2018; Tauro and Grimaldi, 2017)

The parameter λ (mean seeding density per frame) of the Poisson distribution was set equal to $6.4\ 10^{-5}$ ppp for the LD-case, $2.5\ 10^{-5}$ ppp for the MD-case, and $1.3\ 10^{-3}$ ppp for the HD-case. In terms of particles created by the ISG module within each individual frame, the various density cases result in an average

number of disks respectively equal to 23, 91, and 459 units (LD, MD, and HD, Figure 4.5).

The two extreme conditions of particle density are to be understood as those below and above which optical processing software can go into crisis in estimating the surface velocity field. The LD case can be seen as the lower limit of the variability of the tracer density, below which the frames are not properly seeded, and the software cannot identify enough particles to trace. Some portion of the frame may also remain empty, leading to an incorrect estimation of the surface velocities in place. The HD case, on the other hand, is representative of an upper limit situation above which the phenomenon of particle aggregation can occur. Particle clustering increases the uncertainties in estimating surface velocities (Cierpka et al., 2013). The resulting velocity vectors are therefore not representative of the movement of the surface liquid particles, but of the agglomeration of tracer particles.

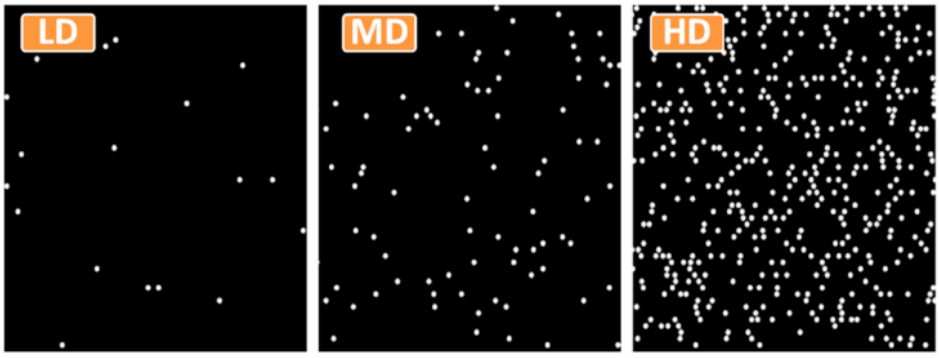

Figure 4.5 – A representative frame for the low (LD), medium (MD), and high (HD) seeding density for the scheme ID-CON. (Pumo et al., 2021)

Finally, for the first set of simulations, a constant frame rate of 4 fps and sequence duration equal to 30 seconds were set, with a total number of processed frames (n_{FR}) equal to 121 frames for each sequence. The second set of simulations was used to investigate the importance of the number of analysed frames. With this aim, first the sequence duration was fixed equal to 30 seconds, altering the frame rate (considering 2, 3, 4, 6, 8, 12, and 16 fps), and then, the frame rate was fixed equal to 4 fps, considering different sequence durations (5, 15, 30, 45, 60, 90, and

120 seconds), i.e., processing then a total number of frames ranging from 21 (for the 5-seconds sequence duration case) to 481 frames (for the 120-seconds one).

4.2.2. PIVlab module

The module represented by PIVlab is the one that accepts as input data the sequences synthetically generated in the previous module (ISG module). Since the images forming the sequences were generated with the aim of recreating specific features, no pre-processing operations have been applied, keeping the frames generated by the ISG module unmodified.

The synthetic frames were analysed using as the processing style the type 1 (i.e., 1-2; 2-3; 3-4; etc.), thus considering pairs of images with overlapping frames between one pair and the next one. This style of sequencing is certainly more time-consuming, but it is more efficient than type 2 (i.e., 1-2; 3-4; 5-6, etc.), where the same frame is not considered twice for two successive pairs of images.

However, processing times were in any case reduced by using the Fast Fourier Transform as a statistical cross-correlation algorithm, discarding the D-CC (Direct Cross-Correlation) algorithm. Three passes were set for FFT-CC algorithm, using linear interpolation option as window deformation interpolator. The width of the first pass IAs was chosen by imposing three criteria suggested by PIVlab developers:

- not lower than 50% of the minimum frame dimension;
- lower than minimum fame dimension;
- higher than two times the maximum presumable frame-by-frame particle displacement.

The condition to be satisfied considering the impositions set out above is that the particles have a displacement between successive frames that remains within the interrogation area in both frames. For the specific case of the generated sequences, considering (i) the square frame of 600x600 px, and (ii) the maximum frame-by-frame displacement of 161 pixels (F velocity profile), the width of first pass IA was set equal to 400 pixels. The dimensions of the subsequent interrogation areas at steps 2 and 3 were obtained by halving the IA at pass 1 by one (200x200 px) and two (100x100 px) times respectively.

The calculation grid resulting from the previous parametric set consists of 11 grid nodes in the two longitudinal and transverse directions, for a total of 121 grid nodes, positioned equally spaced at 50 pixels from each other and from the edges of the frames.

4.2.3. RAV module

The output results from the PIVlab processing module are represented by surface velocity fields, expressed as vector fields, computed node by node over the entire calculation grid. Vector fields define the input of the last module in the processing chain: the RAV (Results Analysis and Visualization) module. Through the RAV module, a statistical analysis has been conducted considering all sequences for fixed scenarios, obtaining descriptive statistical indexes.

For each sequence, the surface velocity field is represented in a simple way as a coloured "heat map", reporting the point velocity at any grid node. A matrix, reporting the Absolute Percentage Error, APE_i (i is referred to the generic i-th node), has been associated to each sequence. The values of APE_i is determined from the comparison at each computational grid node between the surface velocity estimated by PIVlab ($v_{PIVlab,i}$) and the velocity imposed in the ISG (u_i) (Eq. 4.1):

$$APE_i = \left|\frac{v_{PIVlab,i} - u_i}{u_i}\right| \% \qquad \text{(Eq. 4.1)}$$

Through the representation of the values assumed by the APE parameter, it was possible to identify the actual area of analysis of the results, discarding the portions of the frames in which the APE values were excessive.

Moreover, RAV module associates to each sequence an index, named MAPE (Mean Absolute Percentage Error), that is the mean of all the APE_i over the analyzed area (Eq. 4.2):

$$APE_i = \frac{1}{n}\sum_{i=1}^{n} APE_i = \frac{1}{n}\sum_{i=1}^{n} \left|\frac{v_{PIVlab,i} - u_i}{u_i}\right| \% \qquad \text{(Eq. 4.2)}$$

where n refers to the total number of computational nodes within the analysed area.

For each scenario, the script creates boxplots of all the MAPE values for the 100 corresponding realizations, with indications about the median, the interquartile range (IQR), the most extreme data points not considered outliers (whiskers) and the outliers (red marks). Moreover, it also generates maps reporting the node-by-node mean values of the APE_i over the 100 replications ($< APE_i >$). Finally, for a reference cross-section transect, the RAV module shows a comparison graph between the cross-section velocity profiles imposed by the ISG and that estimated by PIVlab; this last is displayed in the form of boxplots of the 100 surface velocity values estimated at each node of the transect for each replication of given scenario.

4.3. First set of simulations

The first set of simulations considered involved the analysis of a number of scenarios equal to 24, resulting from the combination of all the parameter configurations set out in the previous section. In particular, the duration of the synthetic sequences and the frame rate were kept constant, at 30 seconds and 4 fps respectively. Thus, for the two simulated environmental situations (ID and SR), 100 synthetic sequences were generated for each tracer density condition (LD, MD, and HD), always considering the two different types of tracer particles, under the two fixed flow regimes (S and F).

The total number of synthetic sequences generated, in order to make the analysis statistically robust, is 2400. Considering a number of frames of 121 per

sequence (30 seconds long at 4 fps), the number of frames generated by the ISG module was almost 300 thousand images. The schemes of the synthetic sequences properly generated are described in Figures 4.6 and Figure 4.7.

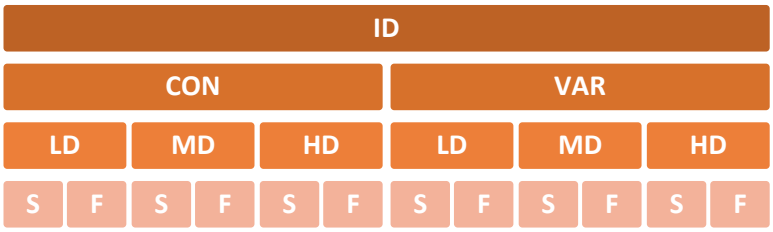

Figure 4.6 – Scheme of sequences generated from ideal environmental conditions.

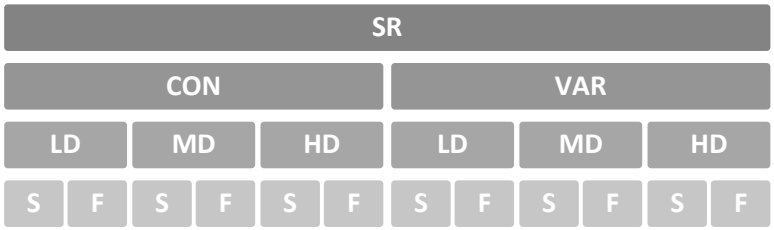

Figure 4.7 – Scheme of sequences generated from semi-real environmental conditions.

4.3.1. Border effects and the actual area of analysis

In the theoretical basis of the LS-PIV technique, it is known that problems can arise in the interpretation of particle movement at specific portions of frames. The reason for these interpretative difficulties on the part of the dedicated software lies in the phenomena of out-of-plane and in-plane motion. This is the sudden disappearance of a tracer particle that leaves the camera's field of view, or which, conversely, suddenly appears at any time during the recording. In these cases, the processing algorithms fail to consistently track the movement of the particles, giving an incorrect estimate to the resulting velocity vectors.

It is reasonable to assume that the portions of the frame affected by these problems are the border regions, where, in the direction of motion, the entrance and exit of the tracer are located, while in the direction crosswise to the motion, transverse velocity components can cause the tracer particles to suddenly exit or enter the field of view.

In the first phase of analysis of the first set of simulations, the frames were considered in their entirety. PIVlab software, with the IA size at the first pass equal to 400 px, then equal to half and ¼ in pass 2 and 3, generated a grid of 121 computational nodes: 11 in the flow direction (horizontal) and 11 in the orthogonal direction (vertical).

The results obtained from these preliminary analyses were examined in order to understand the extent of the problems at the frame boundaries and to select the area of the frame not significantly affected by the out-of-plane and in-plane effects.

Considering only the ID-CON scenario, in the S and F cases, for all tracer density conditions (LD, MD, and HD), Figure 4.8 shows the results in terms of $< APE_i >$ maps. Similar results were also obtained in the other configurations.

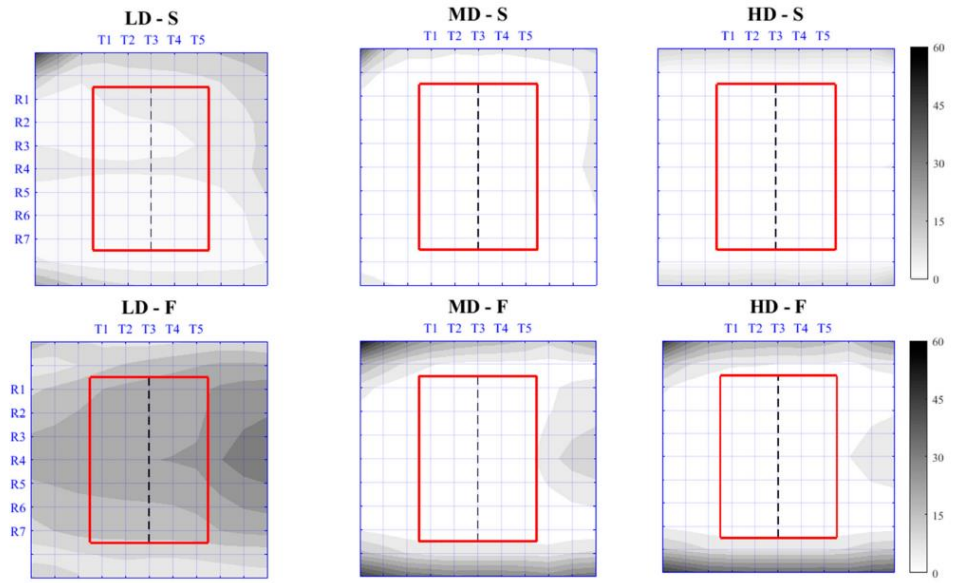

Figure 4.8 – Map of $< APE_i >$ for all the scenarios under ID-CON scheme. The six scenarios are characterized by different configurations, given by the combination of the three densities (LD, MD, and HD) with the two surface velocity profiles (S- and F-profile). $< APE_i >$ is the mean APE_i over the 100 replications per scenario at the generic node i. The central area of investigation (250x350 px) is highlighted by red contour, while the vertical black dashed line identifies the reference transect T3. R1, R2, …, R7 refer to the rows of the computational grid within the area of investigation, while T1, T2, …, T5 refer to the columns (cross-section transects). (Pumo et al., 2021)

As can be seen from the figure, the border effects are more visible in the higher velocity cases (F) than in the S flow condition. The reason for this behaviour is the high displacements that particles undergo in the case with an average velocity of 1.5 m/s (F case). There is a clear loss in the number of particles that can be tracked between pairs of frames. This behaviour is all the more exacerbated the fewer particles available for tracking.

Border effects are more concentrated in the particle input (left edge) and output (right edge) zones in the F cases, while in the S ones the banks (upper and lower edges) have the greatest uncertainties in surface velocity estimates. The case with the highest values of $< APE_i >$ is LD-F. Overall, the values of $< APE_i >$ decrease as the velocity decreases and the density of the tracer particles increases. The opposite case to LD-F is HD-S, which has the lowest values of $< APE_i >$. The

largest errors, in this case, are concentrated only on the banks of the virtual river, but still with values not exceeding 15%.

Analysing the $< APE_i >$ values, depicted in the figure, it is easy to see that, except for the LD-F and LD-S cases, the central area of the frames is characterized by very low $< APE_i >$ values, around 2-3%. This is the area (contoured with the red rectangle) to be defined as the region of interest (ROI) for the further analysis of the first set of simulations. The identified ROI consists of 5 central transects (from T1 to T5) each consisting of 7 computational nodes (from R1 to R7). The total number of computational grid nodes was thus reduced from 121 to 35, covering an area of 250x350 px.

Another element shown within the figure is transect T3 (black dashed line) on which comparisons were made between the imposed velocity profiles and those estimated using the LS-PIV technique. It is important to emphasize that, following the reduction of the analysis area, the imposed velocity profile is characterized by a higher average velocity than that which generated the imposed profile. Specifically, in the case of S flow condition, the average velocity is 0.59 m/s, instead of 0.5 m/s; while in the case of F flow condition, the average velocity is 1.76 m/s, instead of 1.5 m/s.

Analysing the specific cases S and F of the LD density condition, it can be seen that these have a quite different behaviour in terms of $< APE_i >$ compared to the other configurations. The reason for these results is to be found in the reduced seeded condition with which the sequences are generated. The PIVlab module encounters difficulties in maintaining the tracking of the particles due to both the reasons expressed before in terms of out-of-plane and in-plane effects, and the low number of particles available to be tracked in their movement.

However, for both LD-S and LD-F cases, the values of $< APE_i >$ within the ROI, although higher than the other two seeding density cases, remain in a range significantly lower than the $< APE_i >$ in the excluded border region. For the LD-S case, the mean value and the standard deviation of the $< APE_i >$ within the ROI are equal to 4.1% and 1.8%, respectively, while the corresponding values for the excluded border region are 8.6% and 7%, respectively.

4.3.2. Results of the sensitivity analysis: surface velocity fields

Once identified the region of interest (ROI) to which to restrict the analysis of the results obtained as output from the PIVlab module, they showed satisfactory accuracy in reproducing the velocity fields imposed with the ISG module. Considering the 100 replications of the same scenarios, again sufficient stability of results can be observed.

If the MAPE (Mean Absolute Percentage Error), whose mathematical formula was expressed earlier when presenting the characteristics of the RAV module, is taken as the performance index, it is possible to identify the best and worst cases among all configurations and realizations (Figure 4.9).

The best case (shown in the upper graph of the Figure 4.9) is identified in the case of the HD-S scenario, with a MAPE value below 0.6%. the surface velocity field is in this case well reproduced within the ROI, as the APE_i graph shows. In fact, the errors appear evenly distributed, with the highest value (up to 1.9%) in the central part of the virtual stream (i.e., the row of computational nodes R4). All other grid nodes in the ROI have an APE_i value of no more than 0.9%.

The worst case (shown in the lower graph of the Figure 4.9) is instead the LD-F scenario, with a MAPE value of around 35%. The surface velocity field estimated by PIVlab shows errors (in terms of APE_i) of even more than 40%, especially in the central part of the watercourse, with decreasing values approaching the banks.

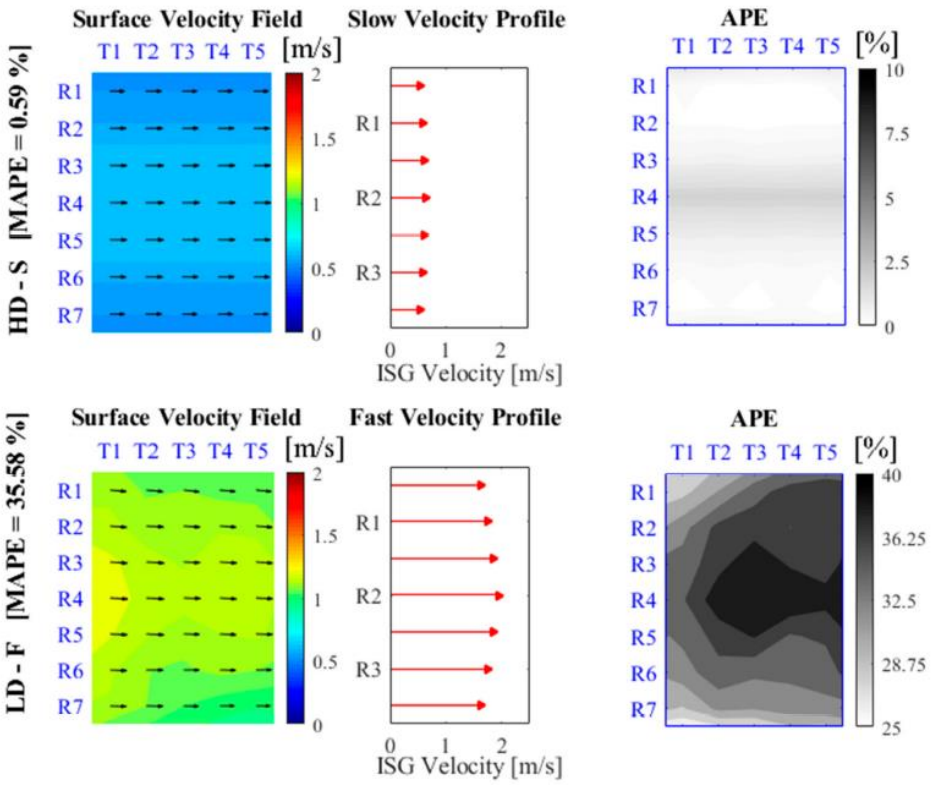

Figure 4.9 – The best (lowest MAPE) and the worst (highest MAPE) cases under the ID-CON scheme. Top graphs refer to the best case (HD-S configuration, MAPE=0.59%), while bottom graphs refer to the worst one (LD-F configuration, MAPE=35.58%). The indicator MAPE is the mean APE_i over the entire area of investigation. For each case, the surface velocity field estimated by PIVlab (left panel), the cross-section velocity profile imposed in the ISG (middle panel) and the map of APE_i (right panel), derived by RAV module after comparison between estimated and imposed velocities at each node, are reported. (Pumo et al., 2021)

The results provide an insight into the sensitivity of the PIVlab software to tracer density in relation to the flow conditions. A comparison between opposite conditions of LD and HD density is shown in Figure 4.10, considering the ID scenario with constant diameter particles (CON).

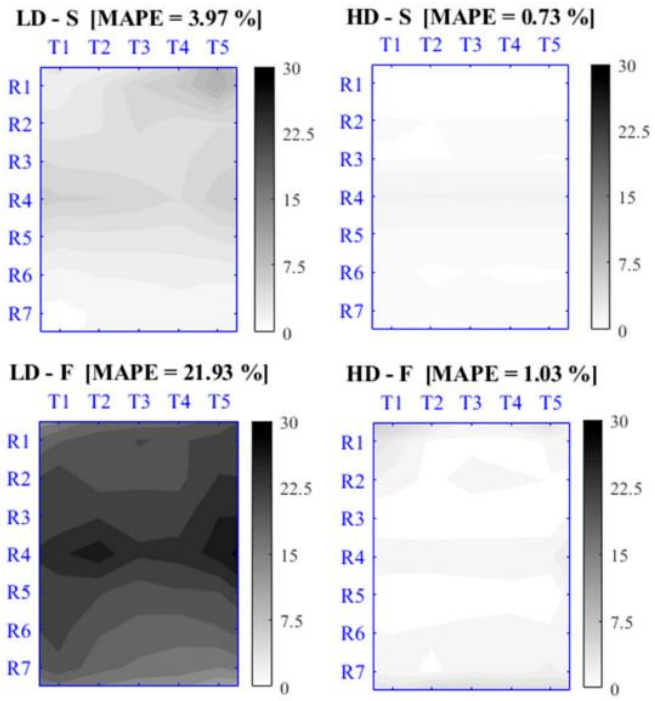

Figure 4.10 – Maps of APE_i for 4 representative cases (median case in terms of MAPE) of the scenarios under the ID-CON scheme, with low (LD – left graphs) and high (HD – right graphs) seeding density and slow (S – top graphs) and fast (F – bottom graphs) velocity profile. (Pumo et al., 2021)

The case with low tracer particle density has the highest errors, both in the case of flow S (MAPE equal to 3.97%) and F (MAPE equal to 21.93%). In particular, observing the graphs in Figure 4.10, the largest errors are found in the situation with low tracer material on the free surface (LD) and a high current velocity (F). With the same seeding conditions, the errors decrease as the flow velocity decreases, decreasing further as the density of the tracer particles increases. Arriving at the situation with high particle density, the best situation is obtained for the scenario with reduced velocity (HD-S; MAPE equal to 0.73%), rather than the one with higher velocity (HD-F; MAPE equal to 1.03%), although the errors in terms of MAPE remain around 1% in both cases.

Although not shown in the figure, the medium tracer density (MD) condition has errors comparable to those found for the HD condition. This means that increasing the presence of material to be traced on the free surface markedly alters the results from poor material conditions, but there is not the same amount of variation for higher density values.

The analysis of the influence of environmental recording conditions (ID and SR) and tracer size variability (CON and VAR) is shown in Figure 4.11. The representative case with medium tracer density (MD) was considered for each configuration, in both flow situations S and F. The error maps are for the replications with the median MAPE value among the 100 generated for each configuration.

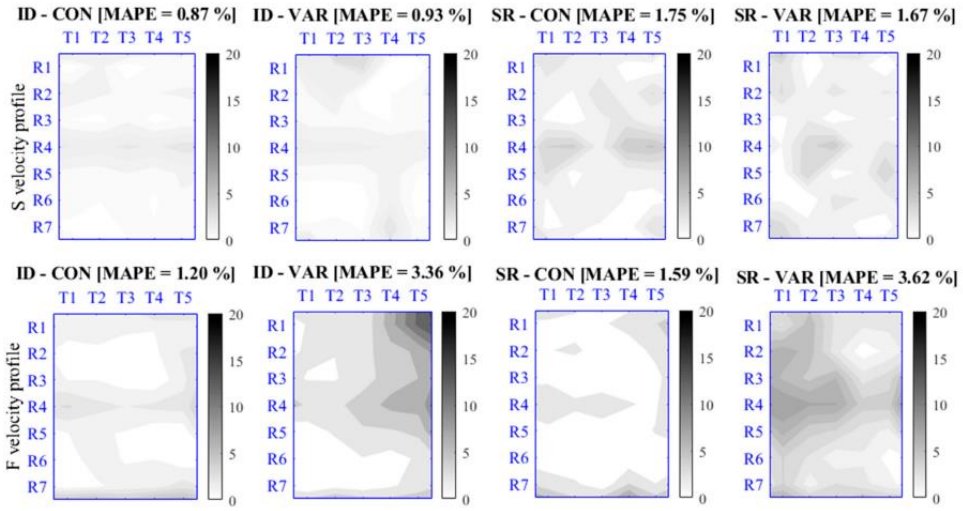

Figure 4.11 – Maps of APE_i for 8 representative cases (median case in terms of MAPE) of the scenarios with the MD seeding density for both slow (S – top graphs) and fast (F – bottom graphs) velocity profile, under all the 4 possible environmental condition-tracer size schemes, i.e., from the left to the right: ID-CON (ideal and constant size), ID-VAR (ideal and variable size), SR-CON (semi-real and constant size), SR-VAR (semi-real and variable size). (Pumo et al., 2021)

The introduction of noise effects relating both to the background against which the particles move, and to the particles themselves by varying their size and fouling them with white noise, deteriorates the results from PIVlab. The

deterioration of the accuracy of the results is higher considering the flow condition F. it is also important to note that the distribution of errors does not change much when moving from the ID scenario to the SR scenario, but there is a change in error patterns when moving from a configuration with constant particles (CON) to one with variable particle size (VAR).

a further analysis of the errors in PIVlab estimation of the surface velocity field considering different scenarios and realizations, is shown in Figure 4.12.

MAPE values calculated for each realization in each scenario and configuration, are represented in boxplot form in order to give a statistical interpretation to the results obtained in the first set of simulations.

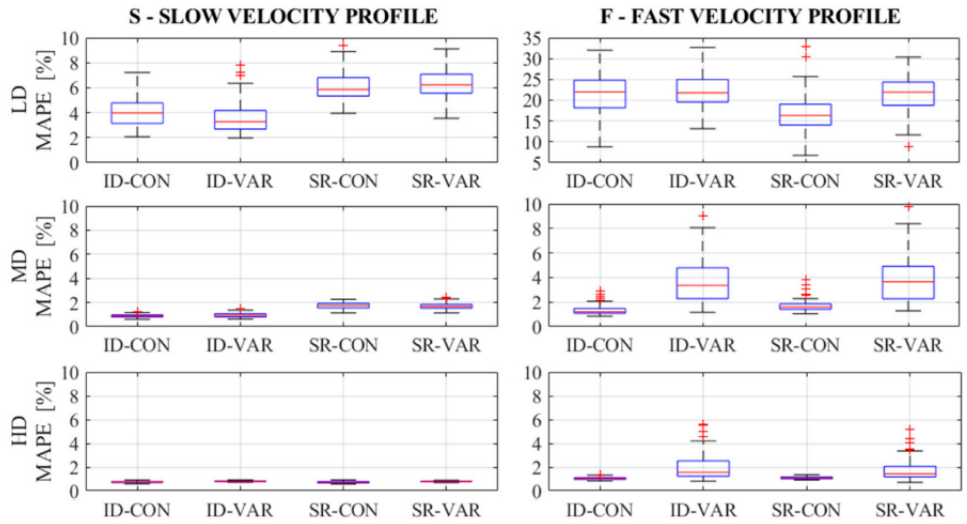

Figure 4.12 – Boxplots of MAPE for all the scenarios of the first set of simulations. Left graphs refer to the slow velocity case (S), while the right graphs to the fast (F) case. The low (LD), medium (MD), and high (HD) density scenarios are reported on the top, middle, and bottom graph, respectively. In each graph, all the 4 possible environmental condition-tracer size schemes are reported: ID-CON, ID-VAR, SR-CON, and SR-VAR. (Pumo et al., 2021)

Similar considerations can be derived from the figure as when analysing the previous plots:

- scenarios with slower velocity (S-case) are characterized by a better description of the surface velocity fields, with lower errors than the F-case scenarios;
- the increase in seeding density improves, in any case, the performance of the software by interpreting the frame-by-frame movement of particles more correctly;
- results are more sensitive to variations in tracer particle size (CON and VAR) than to different environmental conditions (ID and SR);
- LD-F scenario in all configurations is the most critical due mainly to the high displacement of particles between one frame and the next in relation to the width of the interrogation area;
- HD-S scenario is the one with the best surface velocity estimates, with very small MAPE interquartile ranges and high consistency of estimated velocity values with those imposed.

4.3.3. Results of the sensitivity analysis: surface velocity profiles

The results of the sensitivity analyses were also represented with reference to the velocity profiles relative to the central transect (T3) of the portion of the frame are used for the analyses (ROI).

In particular, Figure 4.13 shows a comparison between the velocities imposed in the ISG module during sequence generation and all velocity profiles estimated by the PIVlab module, considering the 100 realizations of each configuration. The graph refers to the ID-CON and ID-VAR scenarios, with similar curves behaviour for all the remaining scenarios.

The imposed velocities along T3 transect are shown as dashed lines (red for the F-case and blue for the S-case), while the estimated velocity profiles are shown as boxplots for each grid node contained along the transect. 100 velocity values are then available at each grid node, from which it is possible to obtain the value of the first and third quartile, the interquartile range, and the median.

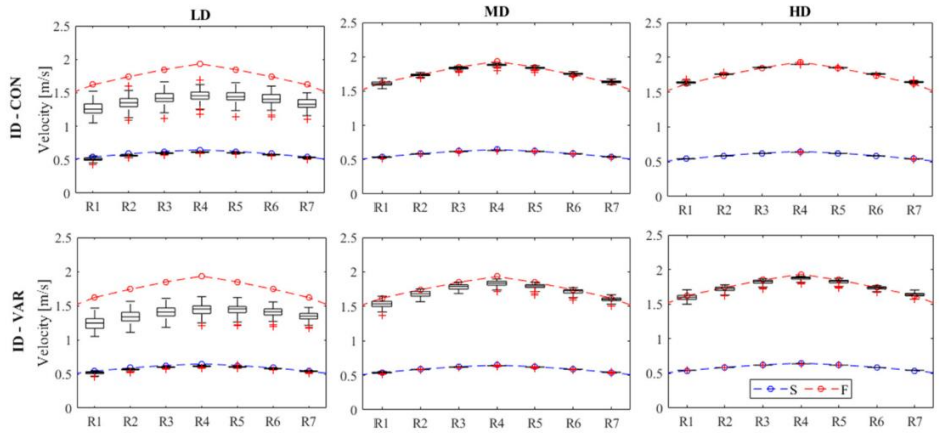

Figure 4.13 – Comparison between imposed (in the ISG) surface velocity profiles for the reference transect (cross-section T3) and the corresponding velocities estimated by PIVlab at each node of the same transect (from R1 to R7). The imposed profiles are reported by blue dashed curves for the slow (S) velocity cases and red dashed curves for the fast (F) velocity cases. The estimated velocities are reported in the form of boxplot of MAPE including the results of all the 100 replications per scenario. The three top graphs refer to the scheme ID-CON, while the bottom graphs to the scheme ID-VAR. For each scheme, the low (LD), medium (MD), and high (HD) density scenarios are reported on the left, middle, and right graph, respectively. (Pumo et al., 2021)

The comparison in Figure 4.13 confirms the high errors found for the LD-F scenario, both in the case of CON and VAR particles, with an overall underestimation of the estimated velocities. The percentage of error in the estimation of the mean velocity along the transect for the 100 ID-CON-LD-F sequences ranges from -9.1% to -36.6% (mean -21.8%). The results improve, for fixed conditions, if the flow velocity is lower, or by increasing the tracer density, in both cases CON and VAR.

The accuracy in reproducing the velocity profiles imposed by the ISG module becomes extremely high when the density of the tracer increases, up to the maximum values considered in the HD cases. The boxplots in these cases show very compact interquartile ranges, with very little variability in the results, observing for the ID-CON-HD-case (the best ones) an interquartile range of only 0.42%.

4.4. Second set of simulations

A final important and further sensitivity analysis was carried out by considering a second set of simulations.

Considering the ideal scenario (ID) with perfectly white, circular-shaped tracer particles (CON) dispersed on the liquid surface with medium density (MD), the sensitivity of PIVlab software to variation in the total number (n_{FR}) of frames constituting the video sequences was studied. The number of images n_{FR} is closely linked to two fundamental parameters:

- the frame rate (measured in fps), i.e., the number of frames contained in the unit of time (1 second);
- the video length (measured in seconds), i.e., the number of seconds constituting a recorded sequence.

In this respect, and with the aim of analysing the software's dependency on these parameters, 14 new scenarios were generated for both the S and F flow cases by alternately varying the two parameters. For each S and F condition, ISG module generated:

- 7 scenarios keeping the overall length of the video sequences constant (30 seconds) and varying their frame rate (from 2 to 16 fps);
- 7 scenarios keeping the frame rate constant (4 fps) and varying the overall length of the video sequence (from 5 to 120 seconds).

The ID-CON-MD-S/F scenarios with a frame rate of 4 fps and a duration of 30 seconds, already generated for the first set of simulations, are common to both new set of simulations. Table 4.2 details the characteristics of the newly generated scenarios.

Table 4.2 – Frame rate (FR), sequence duration (d), and total number of processed frames (n_{FR}) for each scenario of the second set of simulation. The configuration with FR=4 fps and d=30 s (highlighted in grey) is common for both first analysis, with fixed duration and variable frame rate, and second, with fixed frame rate and variable duration, and it also that considered for the first set of simulations.

FR [fps]	d [s]	n_{FR} [frames]
2	*30*	61
3	*30*	91
6	*30*	181
8	*30*	241
12	*30*	361
16	*30*	481
4	*30*	121
4	*5*	21
4	*15*	61
4	*45*	181
4	*60*	241
4	*90*	361
4	*120*	481

Similarly to the first set of simulations, 100 realizations of each scenario were generated in this analysis, in order to be able to apply a statistical analysis on a consistent dataset. Again, the MAPE was calculated for each replication as a performance indicator for the PIVlab software.

Figure 4.14 shows the MAPE behaviour as the frame rate and duration of the video change, in the two conditions S and F. the variation of the two parameters automatically results in a different number of frames n_{FR} constituting the sequences.

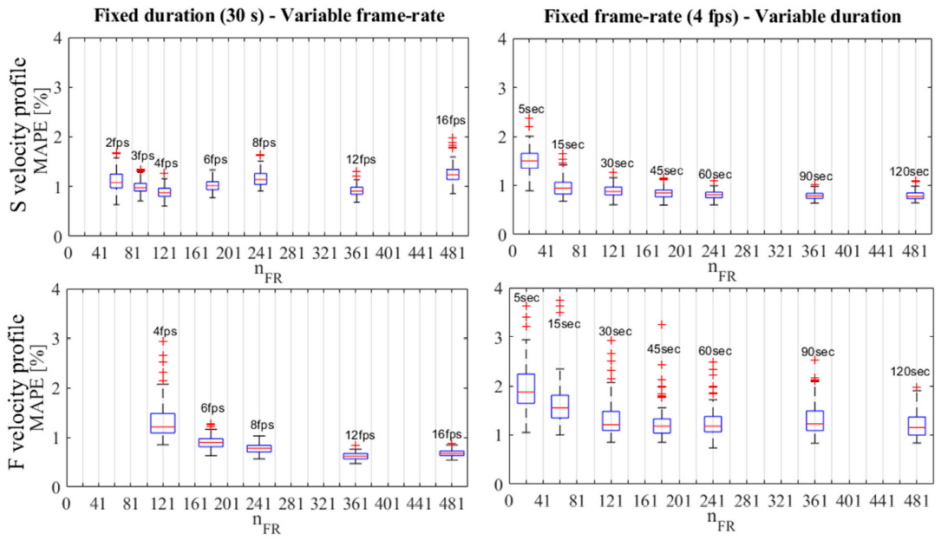

Figure 4.14 – Left panels refer to the analysis with fixed duration (d=30 s) and variable frame rate (whose values are reported as ticks above each box), while right panels refer to the analysis with fixed frame rate (FR=4 fps) and variable d (indicated by ticks above each box). Top panels refer to the S-velocity cases, while bottom panels to the F-cases. (Pumo et al., 2021)

Except for the case S with variable frame rate, in all other situations there is an increase in PIVlab performance as the number of frames of the sequences increases. This increase can be a consequence of either an increase in frame rate or an increase in durations.

Although they may appear to be two different aspects of the same problem, increasing the frame rate or duration acts on two different problems.

Changing the value of frames contained in 1 second (i.e., changing the frame rate) affects the software ability to track particles more effectively between one frame and the next one. Thus, if the velocity of particle displacement is high and the recording frame rate is small, increasing the number of frames in a second of recording allows for more efficient tracking of particles that would otherwise easily escape from the interrogation area or field of view. Conversely, if the recording frame rate is high, but the particle displacement velocity is low, a reduction in the frame rate allows the particle to have sufficient displacement per frame to be captured by the analysis algorithm.

Modifying the length of video sequences, and thus increasing or decreasing the number of frames to be analysed, allows the software to recreate surface velocity fields that consider a more complete phenomenology.

For the S cases (top-left graph), PIVlab performance improves with increasing frame rate up to 4 fps, while, for further frame rate increments, it reduces consistently. For instance, for the case with frame rate of 16 fps the median $MAPE$ increases of +1.36% with respect to the case with 4 fps.

In the F scenarios (bottom-left graph), the absence of boxplots for the lowest frame rates (2 and 3 fps) means that the displacements read frame-by-frame take on values greater than the size of the IA set at the first pass. For this reason, PIVlab is unable to produce results for these two situations, unless the IA value is modified.

4.5. Main outcomes

The analyses carried out and shown in this chapter have provided increased knowledge of optical techniques for monitoring flow in rivers. The results obtained provide important indications for the practical application of the LS-PIV technique. Although synthetic sequences have been studied mostly under ideal environmental and recording conditions, far from the real measurement campaigns conditions, some important considerations can be made.

First of all, the estimation error that generally occurs in the edge areas of the recorded frames was analysed. The highest errors are concentrated in the input and output regions of the field of view, and along the banks of the watercourse. For this reason, it is advisable to carry out analyses on a reduced portion of the frames, choosing a ROI of adequate size. The ROI must be sufficiently far from the tracer inlet and outlet areas, and sufficiently far from the banks, but not excessively so, in order to be able to analyse sufficient surface velocity variability along a river cross-section.

Another outcome of the analysis is that the main sources of error in the estimation of surface velocity fields using the LS-PIV technique is due to an inadequate tracer density on the liquid surface. Therefore, in those cases in which seeding phase is needed introducing manually the tracer material, it is necessary to

ensure a frame coverage with tracer of at least 2%, with reference to the ROI size. Considering real tracer particles of similar size to those considered in the analyses, a minimum of 30 tracer elements per m^2 is required.

Another consideration must be made regarding the choice of the total number of frames to be analysed using the LS-PIV technique. Taking into account not only the density of the tracer, but also the expected velocities at which tracer moves across the liquid surface, it is important to choose the most appropriate frame rate and video duration in order to best characterize the surface velocity fields. For this reason, the frame rate of the analysed sequences is not necessarily the same as the acquisition frame rate. It is possible to sample the frames of the recorded sequences according to the most appropriate frame rate and in any case in proportion to the actual flow velocities. For example, a flow with high velocities can be studied with a high frame rate, avoiding a possible loss of tracking particles. Vice versa, when particle movement is slow, a high frame rate may not be appropriate. Movement between two successive frames that are smaller than the pixels size may occur, so that the tracer particle appears almost still. The solution in these cases is to reduce the frame rate, i.e., increase the time interval between two successive frames and allow the tracer particles to travel a greater distance so that they can be more easily tracked.

Increasing the number of frames to be analysed, in this case by increasing the length of the recorded video, is equally important, especially when the tracer is present with low density on the liquid surface. In particular, increasing the number of images allows the software to estimate surface velocities for a longer time, with a higher probability to capture enough tracer dispersion to cover the entire ROI.

The aforementioned indications made possible to create operational guidelines for subsequent measurement campaigns in the open field and for the application of the LS-PIV technique on the real case studies of Chapter 5. However, it must be emphasized that all those indications relating to the density and distribution of the tracer on the liquid surface are very difficult to carry out optimally in the field. It may occur that even if seeding operations are performed in the best possible way, the flow conditions of the watercourse are such that they do not lead to an adequate distribution of the particles over the entire area of interest.

Chapter 5
Seeding analysis for LS-PIV optimization

5.1. Introduction

The numerical analyses carried out and previously shown in Chapter 4, showed that the LS-PIV technique is particularly sensitive to variations in the number of particles dispersed on the liquid surface, their size variability and, thus, their spatial distribution. Depending on the type of motion taking place and the velocity of the current, errors in the evaluation of the movement of the tracing material patterns by dedicated software can be particularly high.

The detection and tracking of tracer particle displacements between one frame and the next one are therefore highly influenced by the preliminary seeding activities of the river surface.

Although the seeding phase may seem marginal in the whole workflow of applying the LS-PIV technique, it is one of the most delicate phases. The correct introduction of tracer in terms of density and areal distribution ensures that the entire liquid surface can be interpreted by dedicated software. However, the activities that take place during the seeding phase are difficult to control precisely, especially if carried out manually and by several operators at the same time. In addition, external disturbance effects (e.g., turbulent hydraulic regime) often occur, such that even if the seeding phase is carried out optimally, the tracer particles undergo aggregation and dispersion phenomena that worsen the response of the optical software.

What can happen is that, once the video recording phase of the movement of the tracer on the river surface is complete, the resulting video cannot be used in its entirety to obtain an accurate final surface velocity field. Some portions of the video may be affected by an incorrect spatial distribution of the tracer or by a low tracer density, or both. Such portions worsen the results expected by the processing software and should therefore be removed from the original sequence.

The optimal condition is that the density of tracer is as constant as possible throughout the entire video sequence to be analysed and that the distribution of the particles is as uniform as possible over the entire frame (Pizarro et al., 2020a; Pizarro et al., 2020b; Dal Sasso et al., 2021).

Starting from the results obtained with the numerical analyses presented in Chapter 4 and analysing the problem of tracer density and distribution presented above, analyses were carried out considering real sequences recorded during specific measurement campaigns relating to the collaboration agreement mentioned in Chapter 3.

The aim of the analyses presented in this Chapter 5 and in the following paragraphs was to obtain an automatic procedure capable of automatically extracting the best sub-sequence of a recorded video to be processed with the LS-PIV technique using the PIVlab software (Thielicke and Stamhuis, 2014).

The automatic procedure was built, calibrated, and validated on several real case studies using measurements taken on several rivers in Sicily. The results of these analyses are shown in terms of the errors resulting from the comparison between the velocities estimated by the LS-PIV software and the velocities recorded by a traditional measuring instrument, i.e., an ADCP. These measurements were performed along specific transects and were used as reference measurements.

Preliminary analyses were carried out on the data collected by ADCP in order to calculate surface velocities, since the instrument used is not capable of measuring surface velocities but only depth velocities.

5.2. Case studies and traditional measurements

The application of the LS-PIV technique was conducted in six different rivers in Sicily, performing multiple measurements in some of them.

The rivers where the LS-PIV technique was applied were subjected to flow measurements using traditional techniques, so several acquisitions were made along specific measurement transects. The field case studies are shown in Figure 5.1, while in Table 5.1 some information about the date of measurement, measured discharge, wetted area and average velocity are reported.

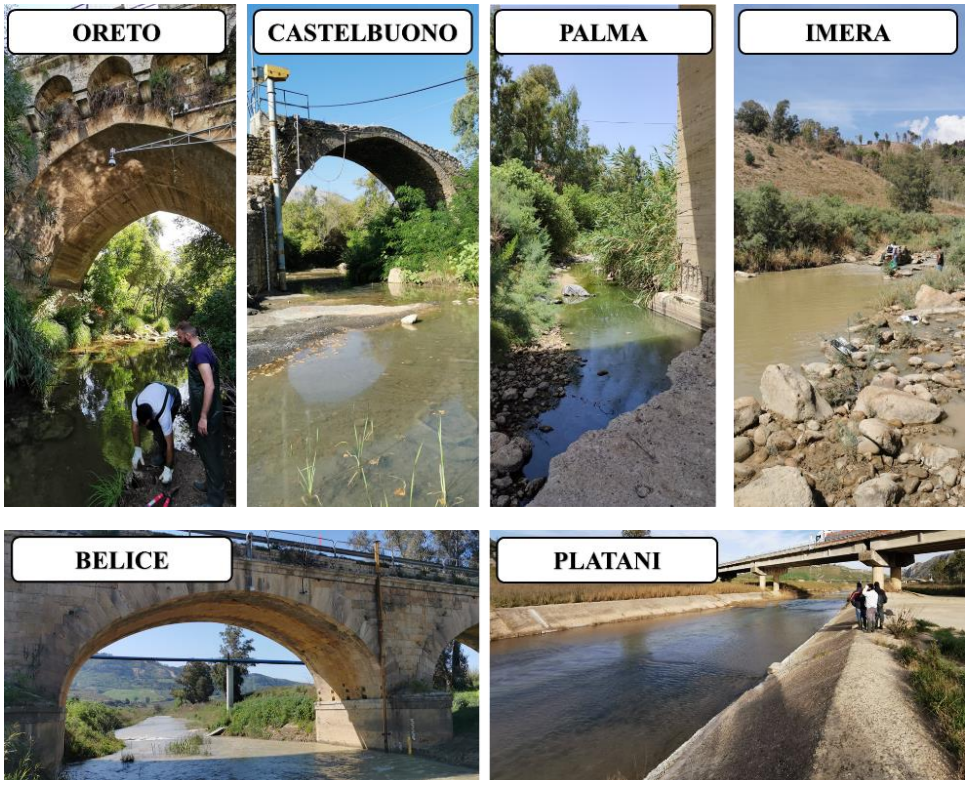

Figure 5.1 – Field case studies where LS-PIV and ADCP measurements were performed.

Table 5.1 - Discharge measurements obtained with ADCP for all the case studies.

River	Date	Q [m^3/s]	A [m^2]	Q/A [m/s]
ORETO	*07/02/2020*	0.230	2.95	0.08
	14/09/2020	0.150	1.92	0.07
	04/06/2021	0.228	2.90	0.08
PLATANI	*18/06/2020*	0.246	1.40	0.18
	08/09/2020	0.267	1.50	0.18
	07/05/2021	0.594	2.80	0.21
BELICE	*18/10/2021*	0.221	2.20	0.10
PALMA	*07/05/2021*	0.041	0.90	0.05
IMERA	*15/09/2020*	0.385	9.50	0.04
CASTELBUONO	*09/04/2021*	0.270	2.40	0.11

The LS-PIV technique was applied using wooden chips ranging between 2.5 and 4 centimetres in size. This tracer material was dispersed on the liquid surface of the rivers from the banks, throwing it in a continuous manner in order to achieve as even a distribution as possible. Video recording, which was carried out with a digital camera and/or drone (see Chapter 3), took place at an acquisition frame rate of 30 fps.

The images were taken from such a position that black and white markers, used as Ground Control Points (GCPs) for stabilization and orthorectification of the collected frames, were also clearly visible within the field of view. These pre-processing steps, which were not performed in previous numerical analyses because they were not necessary, are required in the case of real video recordings. Unlike the synthetic sequences, which are not affected by any distortion problems, nor by frame movements during the entire duration, the real sequences are affected by distortion problems related to the lens and the recording perspective, as well as characterized by movements of the field of view that cannot be attributed to the real movement of the tracer, but to external causes such wind, traffic, or the movements of the drone during hovering.

To validate the results obtained with the LS-PIV technique, and in any case for the purposes of the agreement between DI and S1-AdB, traditional measurements were performed during the measurement campaigns using an ADCP device. As is well known, an ADCP instrument measures the velocity of the stream through sound waves that are reflected from the bottom and suspended particles.

The water column is subdivided into cells and the velocities measured along the depth are associated with the centroids of each cell. However, there are portions of the transect along which the measurement is taken, whose velocities are not investigated. First of all, it is impossible to measure velocities close to the banks, as there are not the necessary depth conditions for the instrument to measure current velocities with sufficient reliability. Starting from the first and last water column sampled along the transect, it is possible to interpolate, usually linearly, the velocities for the left and right banks. Another part whose velocities are not investigated is that of the bottom. There is a portion of the cross-sectional area close to the bottom of the riverbed where side-lobe effects are recorded to such an extent that the velocities at that location are unreliable. Finally, it is impossible to measure the surface velocity of a watercourse with an ADCP instrument due to the need to immerse the sensor a few centimetres below the free surface and keep it in this position for the entire duration of the measurements.

Data collection, both velocity and bathymetry, can be performed with a PocketPC or laptop via Bluetooth using specific software, i.e., WinRiver II (v2.22). Two water velocity profiling mode (WM) are available in WinRiver II (see Chapter 3).

Benchmark discharge measurements with ADCP were performed considering the USGS guidelines and using a standard operating protocol divided into successive steps. The first step involves selecting the most suitable site for the measurements. The choice of the most suitable location for the measurement transects was made considering the suggestions made in the study by Rantz et al. (1982). In particular, the following factors must be taken into account:

- location, with the measuring section arranged in a straight branch of the watercourse, where the flow is uniform and as free of turbulent eddies as possible;
- shape, with the cross-section as regular as possible, without asymmetries, free of vegetation at the bottom;
- flow regime, with cases of turbulent regimes that should be avoided so as not to unduly reduce the reliability of velocity measurements.

The second step is to establish stable communication between the instrument and the computer through which to manage the data collection along the transects. There must be no more than 30 metres between the two devices, as the

communication established is via Bluetooth. It is also important to avoid having the instrument out of sight of the laptop, as the connection would easily be lost. The two devices must therefore watch each other continuously.

Once the most appropriate location of the measurement transect has been identified and a stable connection has been established between the instrument and the computer through which acquiring data, it is necessary to define the setup of the instrument's acquisition parameters (i.e., transducer depth, cell size, profiling mode, data storage folders). Operationally, the immersion depth of the sensor (i.e., transducer depth) was always chosen to be 5 centimetres, a value that prevented the sensor from leaking out of the water when handling the instrument between banks. The values to be associated with the remaining parameters are chosen based on the conditions under which the staff is operating at the time of discharge measurements. For example, the same measurement section can be investigated with two different profiling modes depending on the type of water regime in place. Similar considerations must be made regarding the size of the cells into which discretize the water column. The value to be associated with the parameter depends in these cases on the maximum water level expected on the measurement transect, bearing in mind the technical limit on the maximum depth that can be investigated (which in the case of the ADCP used for the analyses shown in this section is 2.1 metres).

Handling of the ADCP instrument is usually done between the two banks though the use of two ropes appropriately tied to the device. Two operators, positioned opposite each other on the banks, alternately pull on the ends of the ropes while trying to keep the instrument's dragging velocity lower than the water flow velocities. An alternative way of making measurement is to handle the instrument from a bridge, tying a single rope to the head of the instrument and dragging it from one side of the section to the opposite, keeping the dragging velocities always lower than the water velocities.

In any case, whatever the mode of instrument handling, the fundamental objectives of the activities are: (i) the acquisition of a conspicuous number of measurements; (ii) the acquisition of an even number of measurements to minimize directional measurements bias; and (iii) taking measurements for a sufficient exposure time (i.e., 720 seconds according to WMO standards).

The acquisition of discharge measurements is done through the use of WinRiverII software, where at the end of each measured transect a discharge value is graphically returned in a summary table (i.e., "Discharge Summary"). Together

with the discharge value, further information are shown (e.g., the wetted area, the length of the cross-section, the average velocity) and fundamental statistics (e.g., mean and standard deviation). The table is automatically updated if one or more transects are removed (or added) from the summary. The summary uses the Dynamic Residual Analysis (DRA) algorithm and provides a fast approach to error evaluation. The Relative Residual (RR) of a discharge is defined as Eq. 5.1:

$$RR = \frac{Q_i - Q_{mean}}{Q_{mean}} \% \quad \text{(Eq. 5.1)}$$

where Q_i is the i-th transect discharge, and Q_{mean} is the mean of n transect discharges. The residual control criterion is expressed as Eq. 5.2:

$$\max|RR| < MPRR \quad \text{(Eq. 5.2)}$$

where $MPRR$ is the Maximum Permissible Relative Residual and it depends on the number of acquired transects: the greater the number of transects, the greater the maximum permissible percentage error. The $MPRR$ value is 1.7% when only 2 transects are available; increases to 5% with 4 transects, 7.5% and 9.7% respectively with 6 and 8 transects, up to 19.6% with an amount of 20 recorded transects.

5.2.1. Evaluation of the surface velocity from ADCP data

The results of the analyses shown in this section are expressed in terms of errors derived from comparing surface velocity profiles estimated using LS-PIV technique with those obtained using traditional techniques and applying the operative protocol explained before (i.e., benchmark measurements).

However, the ADCP instrument, as widely explained, cannot measure water velocities in the most superficial part of a river. The WinRiverII software performs an extrapolation of the data from the first available data in terms of depth in order to be able to calculate the discharge resulting from the unmeasured surface portion.

Considering the raw velocity data collected by StreamPro, an approach similar to that reported in Le Coz et al. (2010) and Pearce et al. (2020) was adopted for the purposes of the analyses here shown. Specifically, velocities collected at different depths and for different transects were aggregated and represented within a normalized graph (Figure 5.2).

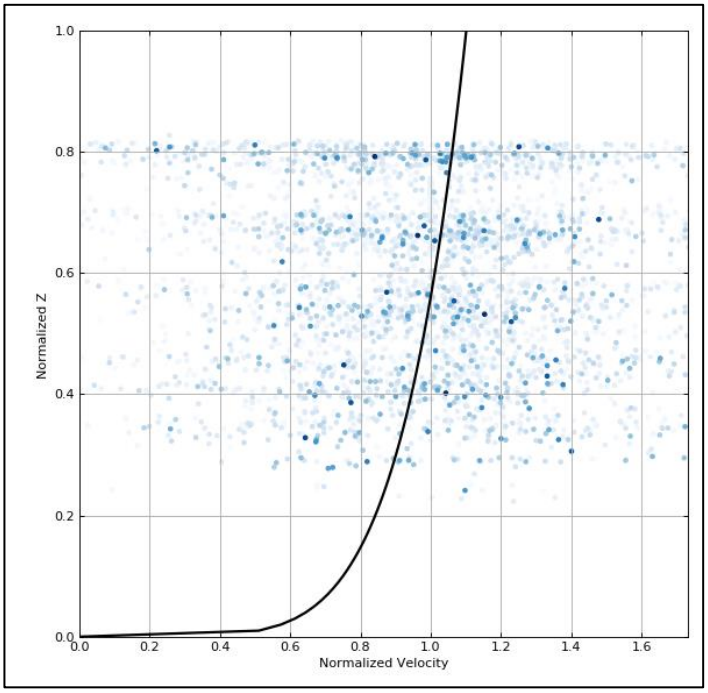

Figure 5.2 – Raw velocity data plotted on a normalized graph (Oreto 07/02/2020). The black solid line is representative of the best function fitting the data (i.e., a power law function).

As can be seen from Figure 5.2, the representative points of the normalized velocities are arranged in a specific and generally expected pattern. The best

function that fits the data is a typical power law, described in the specific case as follows (Eq. 5.3):

$$V_{norm} = \alpha Z_{norm}^{n} \quad \text{(Eq. 5.3)}$$

where V_{norm} is the normalized velocity obtained dividing the raw velocity data by the weighted mean of the values collected in each vertical and in each cell in which the vertical is divided; Z_{norm} is the normalized depth of each cell of a vertical, obtained dividing the cell depth by the maximum local depth; α is the coefficient of the power law; n is the exponent of the power law.

A widely accepted and used value is 1/6 and it is sufficiently suitable for many riverine contexts (Fukami et al., 2008; Le Coz et al., 2010, 2012; Muste et al., 2008; Rantz, 1982). However, it is observable that the shape of the curve interpolating the normalized velocity data can be modified in order to improve the interpretation of the data and obtain a more accurate description of the surface velocity profile. This results in identifying site-specific power law parameters, as the literature value often fails to adequately represent the velocity behaviour of a specific watercourse (Mueller, 2013). This happens because the standard value (i.e., 1/6) does not take into account the actual roughness of the riverbed, the possible presence of vegetation, or other features characteristic of the watercourse under analysis.

The site-specific approach was adopted in the performed analyses, obtaining exponent values for the power laws by appropriately interpreting the data from each specific field case study.

In the normalized graph, considering a normalized depth Z_{norm} equal to 1, i.e., placing on the free surface of the watercourse, it is possible to calculate the velocity value (normalized value) at the surface, which is then equal to the value assumed by the α coefficient of the fitting curve. Since the term of normalization for the velocity is the weighted mean of velocity values collected from the ADCP for each vertical, where the weights are given by the normalized depth of the depth cells, the surface velocity for each vertical of all the transects is easily evaluated. A cloud of surface velocity points is then resulting from the application of the explained approach (Figure 5.3).

In order to calculate the final surface velocity profile from ADCP, it is sufficient to resample the surface velocity data by considering a fixed step of lengths into which to divide the entire length of the reference transect. The profile velocities are then obtained as the average of the values falling within each length interval (Figure 5.3).

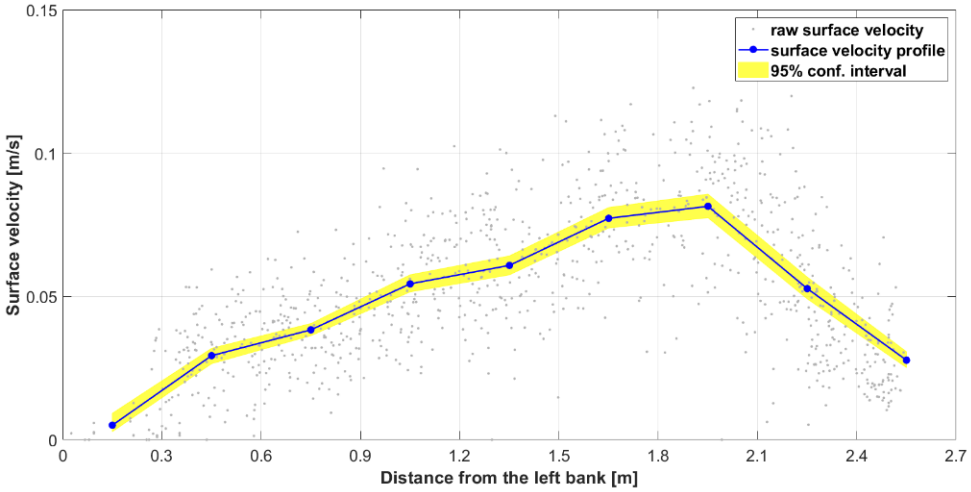

Figure 5.3 – Surface velocity data obtained from ADCP raw velocity data (grey points) for the case of Palma river. Surface velocity profile obtained resampled surface velocity data from ADCP (blue line).

5.3. Data preparation, processing and post-processing

The automatic procedure structured for the analyses and for finding the best video sub-sequence to be analysed by LS-PIV technique, needs as input data the original sequence properly stabilized, orthorectified and graphically enhanced.

As the first step, images of the original sequences were extracted considering the initial acquisition frame rate of 30 Hz (i.e., 30 frames per second). Unlike the numerical analyses reported in Chapter 4, the sequences of frames were

appropriately stabilized by exploiting the capabilities of the KLT-IV software (Perks, 2020). The software has an easy-to-use Graphical User Interface and allows calculation of the discharge of a river from videos acquired from fixed locations or mobile platforms (i.e., UAVs). For this purpose, the software uses the Good Features to Track (GFTT) algorithm (Shi and Tomasi, 1994) for the detection of the tracer particles, and the pyramidal Kanade Lucas Tomasi tracking scheme (Lucas and Kanade, 1981; Tomasi and Kanade, 1991) for subsequent track. Software and algorithms contained within have been optimized for LS-PTV analysis, but generally KLT-IV is high-performing in stabilizing images, also minimizing the computational time for this task. A stabilization module is provided with the software, able to account for and fix camera movements through the application of projective or similarity transformations. Considering a "dynamic" orientation of the cameras used in the field campaigns, since they could be affected by unwanted shifts, and the possibility to have the black and white markers not always clearly visible along the entire recorded sequences, the "GCPs & Stabilization" option was chosen. Frames were then stabilized relative to the first frame to account for movements (Perks, 2020).

An orthorectification activity was applied to transform images from pixel scale to metric one and establish how distance between pixels relate to real-world distances. The orthorectification step has been applied using instead FUDAA-LSPIV software (Le Coz et al., 2014). It offers two different options for orthorectify images:

- scaling, when images are not distorted by perspective effects;
- complete orthorectification, when images are distorted by perspective effects.

The latter option was used to apply metric scale to stabilized frames, easily identifying a number of GCPs in a reference image and inputting the correspondent coordinates, previously obtained from DEMs. The total number of GCPs to use for the orthorectification depends on what kind of image to orthorectify. Frames acquired from a considerable height with the use of a drone can be orthorectified using at least 4 not aligned GCPs (2D orthorectification), assuming that the z-coordinate of each GCP is approximately equal to the z-coordinate of the water table (Jolley et al., 2021). At least 6 not aligned GCPs (3D orthorectification) are needed for frames heavily affected by perspective. Frames acquired from a fixed location, e.g., from a bridge, generally show a strong perspective component due to the non-orthogonality to the water table of the field of view.

Since the application of the stabilization phase of the frames, they have undergone a basic graphic enhancement, which was the greyscale transformation of coloured images. The characteristic digital numbers (DNs) of the images thus have a range of variability between 0 (black) and 255 (white).

(a)

(b)

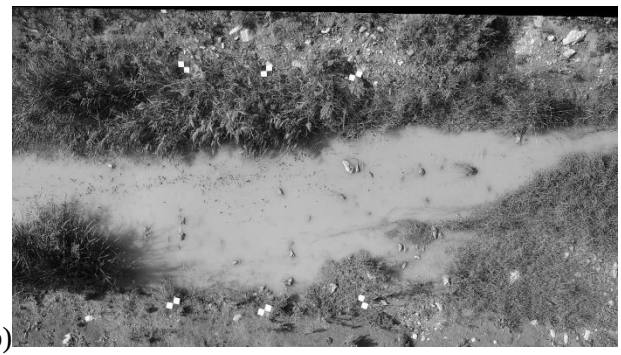

(c)

Figure 5.4 – Example of pre-processed frame (Belice river): original image (a), grey-scaled and stabilized image (b), image after orthorectification process (c).

An important point to note is that all sequences obtained from the application of LS-PIV technique to field case studies were downgraded in terms of frame rate value, halving the original one. Following the indications found in Chapter 4, the reason for this choice lies in the intent to avoid a sub-pixel displacement of tracer particles within the scene captured between successive frames. By estimating the velocity of the current and knowing the spatial resolution of the images (previously obtained during orthorectification step), it was possible to estimate the expected displacement in terms of pixels per frame. This value was found to be locally smaller than the size of a single pixel, such that any particles assuming those displacements would appear stationary in the evaluation of the displacement maps. The reduction of the frame rate from 30 to 15 Hz (15 images in one second), ensured that the movement of tracer particles could be tracked more effectively.

The processing phase of the video sequences identified by the suitably structured automatic procedure and for the objectives of the analyses, is also described in this section.

In particular, PIVlab software (Thielicke and Stamhuis, 2014) was also used in these analyses. This allowed an assessment of the surface velocity of the current using the FFT-CC (Fast Fourier Transform Cross-Correlation) algorithm. In all the case studies frames were processed with the same processing style, i.e., 1-2, 2-3, 3-4, etc. A total number of 3 passes were set, using linear interpolation option as window deformation interpolator. The size of the first Interrogation Area (IA) was decided using the suggested criteria of PIVlab developers (Pumo et al., 2021), so the width of the first pass IAs was set equal to 32 px. The widths of the second and third passes were calculated halving twice the previous value, obtaining areas with size, respectively, of 16x16 px, and 8x8 px.

The final step involved the application of the post-processing phase, through which velocity vectors evaluated in an erroneous way were appropriately discarded and replaced by spatially interpolated values.

The filtering algorithm used for the purposes of the post-processing step is the Standard Deviation Test (SDT). SDT method was applied globally calculating the mean and standard deviation of the velocity fields. Velocity vectors differing a number of times (n) the standard deviation from the mean value were rejected and replaced with a Not a Number (NaN) value. The most effective and efficient value for n was 2 (Eq. 5.4 and Eq. 5.5).

$$V = V \pm 2\,\sigma \quad \text{(Eq. 5.4)}$$

$$V(V < V_{min} | V > V_{max}) = NaN \quad \text{(Eq. 5.5)}$$

The filtering procedure generally led to missing data in the resulting velocity fields, thus a final interpolation of NaN data was applied to fill the gaps and make velocity fields continuous.

5.4. Procedure for the identification of the optimal sequence to process

The basic assumption in the application of optical techniques in general is that tracer particles move in solidarity with liquid surface particles. Consequently, tracer density and distribution are key aspects when the objectives are to reconstruct surface velocity fields. A low tracer density may not result in a correct representation of surface velocity fields, just as a high density would lead to incorrect estimates of velocity vectors due to the phenomenon of particle aggregation. Similarly, incorrectly distributed tracer particles on the liquid surface would leave incorrectly sampled portions of the velocity field, leading to an underestimation or overestimation of velocities. By homogeneously distributing the tracer, errors are certainly minimized.

As mentioned in the previous sections, the seeding phase is very complicated to manage optimally in the field, due to various environmental factors or related to the hydraulic regime of the river. For example, the presence of main currents could lead to a concentration of the tracer on only a portion of the liquid surface, just as the presence of vegetation in the riverbed could leave parts of the areas of interest unsampled. As a consequence, the seeding density and tracer distribution do not generally remain constant throughout the recording phase, creating portions of video sequences that are not fully usable for the calculation of surface velocity fields.

The automatic structured methodology is able to overcome the problems arising from the use of an entire (not fully suitable) video sequence, avoiding

calculating surface velocity fields that are not representative of the effective velocities in place.

The methodology requires stabilized, orthorectified and greyscale rendered original sequences as input data. Nevertheless, through the procedure is applied a further marked graphic enhancement activity. The aim is to extremize the contrast between the background and the tracer particles, much more than what a greyscale transformation can do, making the latter perfectly white and the first perfectly black. This purpose is achieved with the use of the background subtraction technique.

Getting a video of the liquid surface, even of few seconds, prior to the seeding activities, it is possible to obtain an image that is representative of the background across with the tracer particles move during the recording phase. The pre-seeding sequences must undergo the same pre-processing activities as the sequences characterized by the presence of tracer.

By then analysing the pre-seeding sequences, an average image background, obtained averaging the DN values of luminance assumed by the pixels in the entire greyscale video sequence, is evaluated. Once the background image is available, it is subtracted, pixel-by-pixel, from each frame of the post-seeding sequence, obtaining new frames in which the background of the scene is markedly darker than the tracer.

As the last step in this further pre-processing activities, a binarization algorithm is applied in order to obtain Boolean maps. The binary images show pixels with tracer particles assuming value for DN equal to 1 (white) and background pixels that have DN equal to 0 (black).

The key assumption for the background subtraction algorithm to be applied is that the background is not profoundly different from that captured in the post-seeding sequences. It is important that the lighting conditions and field of view of the camera remain the same between the pre- and post-seeding phase.

Binarization of frames is essential since it is through this that an index closely related to the density of tracer on the liquid surface can be calculated. By identifying a region of interest and masking everything that is not related to the watercourse and the movement of the tracer particles, it is possible to calculate frame-by-frame the Instantaneous Seeding Density (ISD) parameter. It is given by

the total number of pixels representative of the tracer particles (DN=1) in a frame, n_{tracer}, over the total number of pixels within the ROI, n_{ROI} (Eq. 5.6).

$$ISD_i = \frac{n_{tracer}}{n_{ROI}} \quad i = 1,2,\dots,N_{frames} \qquad \text{(Eq. 5.6)}$$

ISD index is non-dimensional and can assume values ranging from 0 to 1.

The ISD index is a reliable proxy for the actual instantaneous density of the tracer, despite the fact that binary frames are affected by elements with DN=1 that are not exactly tracer particles, but simply pixels with high luminance levels. The incorrect interpretation of pixels as tracer particles does not however heavily influence the reliability of the parameter, describing well the frame-by-frame variability of the density, even dimensionless, of the tracer.

The proposed methodology divides the original video into all possible sub-sequences and, using a moving window, extracts those sub-sequences starting from a minimum size of 30 seconds to a maximum sub-sequence duration of 2 minutes, with a 30-seconds step. Sub-sequence extraction time shift (i.e., moving window shift) was set equal to 2 seconds, or 45 frames considering the operating frame rate of 15 Hz. The choice of this value for the extraction time lag is justified by the intention not to extract successive identical video sequences, which would return redundant results. Each single sub-sequence is identified by an ID denoting the location of the initial frame within the entire video sequence from which sub-sequences are extracted.

At this point of analysis, the procedure evaluates for each sub-sequence four synthetic parameters linked to the seeding density and tracer distribution:

- the average value of ISD (ISD_{avg});
- the standard deviation of ISD (ISD_{std});
- the Seeding Distribution index (SD);
- the Undersampling Coverage index (UC).

An explanation of each individual index is necessary to understand how the procedure takes into account the density and distribution conditions of the tracer present on the liquid surface.

The first two parameters, derived from ISD index, express the seeding density levels and how constant they remain over the total extracted sub-sequences. The last two indexes give instead information about tracer dispersion over the ROI.

More specifically, ISD_{avg} is evaluated calculating the average of the values assumed from ISD for each frame constituting each sub-sequence; ISD_{std} is defined as the standard deviation of the frame-by-frame ISD values within each sub-sequence.

SD index is derived first computing pixel-by-pixel the relative frequency, f_P, of the tracer (DN=1) over each sub-sequence, then evaluating the average value, $< f >$, over the ROI. This latter represents the ideal value of f_P under the conditions of perfectly uniform spatial distribution of the tracer. SD index is then calculated as Root Mean Square Error ($RMSE$) of the differences between f_P and $< f >$ over the ROI.

UC parameter is instead calculated as the percentage of pixels within the ROI that are under-sampled. The classification of well- or under-sampled pixels is achieved considering an empirical fixed threshold (i.e., 1%) of the total number of frames of the sub-sequence. A pixel is classified as under-sampled if the sum of DN it assumes over the duration of each sub-sequence is minor to the prefixed threshold for the same sub-sequence.

Figure 5.5 shows a boxplot graph representing the variability of the 4 indexes in each field case study, regardless of the size of the sub-sequences.

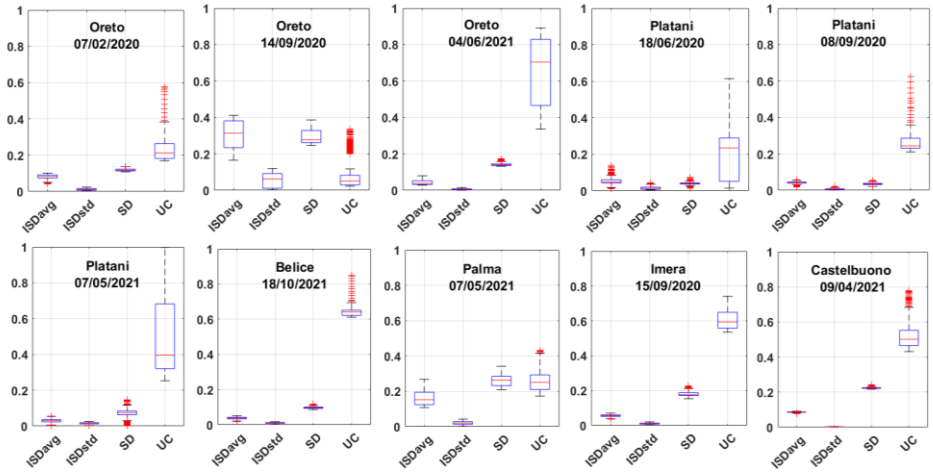

Figure 5.5 – Boxplots of the values assumed by the indexes in all sub-sequences of each case study.

It is possible to notice that the index with the greatest variability is that related to the degree of sampling of the free surface by the tracer material. This means that there are some case studies in which the original video sequences are characterized by a marked nonuniformity in the distribution of the tracer. Regarding the ISD_{avg} index, it is maintained with rather little variability, indicative of a density that tends not to vary excessively during the video recording phase.

Once the indexes have been calculated for all extracted sub-sequences, the procedure calculates an overall index, GI (Global Index), which summarizes the tracer density and distribution characteristics specified by each of the 4 aforementioned indexes. The global index is obtained as linear combination of the 4 indexes (Eq. 5.7):

$$GI = \beta_1 \, ISD_{avg} + \beta_2 \, ISD_{std} + \beta_3 \, SD + \beta_4 \, UC \qquad \text{(Eq. 5.7)}$$

The coefficients [β_1, β_2, β_3, and β_4] of the linear combination were appropriately calibrated by applying multiple linear regression considering all case

studies together. In the multiple linear regression, the values assumed by the 4 indexes in all cases were taken as independent variables. The response variable was represented by the Root Mean Square Error (RMSE) of the errors arising from the comparison of surface velocity profiles obtained with PIVlab and ADCP (benchmark measurements) (Eq. 5.8). More specifically, the calibration phase of the global index coefficients has been performed using the jack-knife approach. This is a resampling method introduced by Quenouille (1949) and named by Tukey (1958). Adopting the leave-one-out strategy, all the possible set of values for the coefficients have been derived using a multiple linear regression analysis, excluding a case study each time. The final set of coefficients is thus evaluated averaging the values obtained from each possible jack-knife combination (Eq. 5.9).

$$RMSE = \beta_{1_i} ISD_{avg} + \beta_{2_i} ISD_{std} + \beta_{3_i} SD + \beta_{4_i} UC \qquad \text{(Eq. 5.8)}$$

$$\beta_k = \frac{1}{n_{comb}} \sum_i^{n_{comb}} \beta_{k_i} \qquad \text{(Eq. 5.9)}$$

where i is the i-th jack-knife combination, k is the generic β-coefficient, and n_{comb} is the total number of jack-knife combinations.

The representation of GI as a function of all possible sub-sequences extracted from the original video, allows the deterministic identification of the best video sub-sequence to process with PIVlab. In particular, the minimum value for GI identifies the best sub-sequence, unlike the maximum one that denotes the worst one.

The estimated set of coefficients (Tab. 5.2) was then applied to all field case studies to test the ability of the procedure to identify the best sub-sequence to be analyzed with the PIVlab software.

Table 5.2 – β-coefficients obtained with the multiple linear regression and adopting the jack-knife approach and the leave-one-out strategy.

β_1	β_2	β_3	β_4
0.69	***-0.27***	**-0.50**	**0.21**

Figure 5.6 shows the results obtained for each case study, comparing the surface velocity profile arising from the processing of the best identified sub-sequence, and the benchmark surface velocity profile calculated from ADCP raw data. For all the charts of the figure, in the x-axis is reported the progressive distance from the left bank, while in the y-axis the surface velocity values are shown. The grey lines represent all the surface velocity profiles obtained from the processing of all the sub-sequences extracted for each field case study. In this way, it is possible to notice how variable could be the response from the software considering different portions of the original recorded video. The variation of the curves is minimized for those cases in which the seeding density and distribution are optimal for the entire video; while a high variability is recorded for those videos in which the seeding parameters are highly variable from one part to another of the original sequence. This characteristic is evident in the case of: Oreto river (14/09/2020 and 04/06/2021), Platani river (07/05/2021), Imera river (15/09/2020), and Castelbuono river (09/04/2021). It is also notable for Oreto river (14/09/2020) and Imera river (15/09/2020) the presence of some surface velocity profiles that not well represent the actual benchmark velocity behaviour. Looking at the original sequences for the aforementioned field case studies, it is evident how parts of the liquid surface remain continuously not sampled by the tracer for several seconds. This reflects on the software's ability to correctly interpret the velocity field for those parts of the domain in which there is a lack of tracer, leading to, as in the mentioned cases, an overestimation of the surface velocity field. In Figure 5.6 are also shown the surface velocity profiles (blue dashed lines) obtained from the ADCP, together with the 95% confidence bands (yellow bands), calculated applying a bootstrap resampling approach to the raw ADCP data.

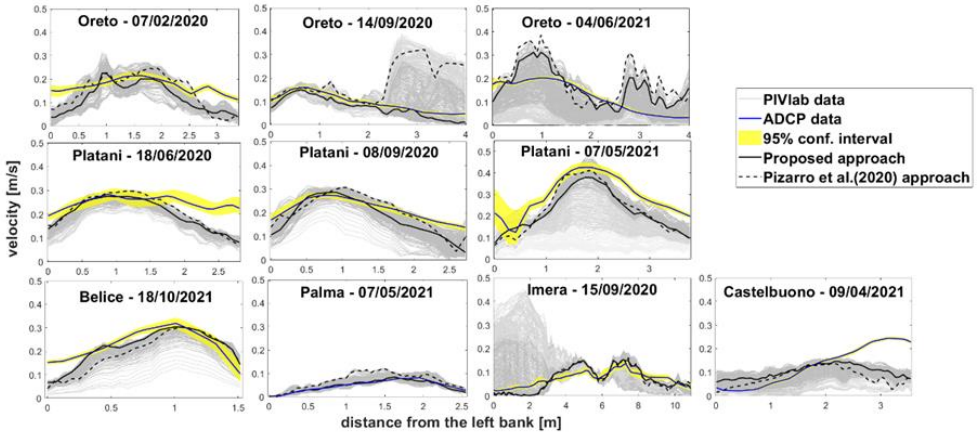

Figure 5.6 – Comparison between surface velocity profiles obtained by the ADCP (blue dashed line) and the PIVlab (grey solid lines). In the graph are underlined with black solid line the surface velocity profile of the best sub-sequence obtained with the proposed work, instead the surface velocity profile of the best sub-sequence detected by existing methodology is reported with the dashed black line. In the graph are also shown the 95% confidence bands for the benchmark profiles (yellow bands).

Figure 5.6 shows in addition the results (dashed black lines) arising by the application of an existing methodology for the detection of the best sub-sequence within a recorded video. More specifically, Pizarro et al. (2020) introduce a descriptor of the seeding characteristics called Seeding Distribution Index (SDI). This index is obtained considering frame-by-frame the ratio between the level of distribution of the tracer and the seeding density. The SDI formula presents also coefficients evaluated through the analysis of numerical case studies, both for the LS-PIV and LS-PTV approaches. Applications to real case studies are also reported by Pizarro et al. (2021), showing a systematically reduction of the error in the evaluation of the surface velocity field by optical software. Figure 5.6 shows that the response from the existing approach and the proposed procedure are in good agreement, providing best sub-sequences resulting in a good description of the benchmark velocity profile. However, some case studies have larger errors with the existing methodology. For example, for the second measurement (14/09/2020) of the Oreto river, the SDI approach returns a sub-sequence whose surface velocity profile is far from the best software response; unlike the proposed procedure that is able to detect a sub-sequence with a surface velocity profile really close to the benchmark behaviour. Similar results are obtained for the Palma river

(07/05/2021), for which the SDI approach results in a surface velocity profile that is not in the best match with the ADCP benchmark, although in this case study the variability of the software's response is very small, not leading to high errors. The proposed procedure provides, anyway, a sub-sequence that matches almost perfectly the benchmark velocity profile.

Table 5.3 shows the Global Index values through which it was possible to extract the best sub-sequence for each case study, with the corresponding $RMSE$ evaluated comparing the surface velocity profiles arising from the processing of the identified best sub-sequences and the benchmark surface velocity profile from ADCP. In the table is also shown the duration of the sub-sequences extracted with the proposed procedure.

Table 5.3 – Global Index values through which best sub-sequences were obtained; RMSE values comparing surface velocity profile from ADCP and that arising from the processing of the best sub-sequences; duration of the extracted best sub-sequences.

River	Date	GI [-]	RMSE [-]	Duration [s]
ORETO	*07/02/2020*	0.03	0.06	120
	14/09/2020	0	0.02	90
	04/06/2021	0.04	0.07	60
PLATANI	*18/06/2020*	0.02	0.07	120
	08/09/2020	0.05	0.05	120
	07/05/2021	0.03	0.08	120
BELICE	*18/10/2021*	0.10	0.04	60
PALMA	*07/05/2021*	0.01	0.01	120
IMERA	*15/09/2020*	0.06	0.03	60
CASTELBUONO	*09/04/2021*	0.04	0.08	120

The Table 5.3 shows a good agreement of the obtained results related to the benchmark velocity profile from ADCP. $RMSE$ assumes low values for all the field case studies, and this is also notable in the previous Figure 5.6 where the PIVlab best velocity profiles follow well the benchmark ADCP ones. Analysing the duration of the best sub-sequences extracted by the proposed procedure, it can be seen that most frequent duration is the longest one, i.e., 120 seconds. This is representative of the fact that the longer the processed video, the better the representation of the surface velocity field through the tracer. In this case, the extracted videos are not only longer enough, but they have also the best seeding conditions for providing the better results in terms of surface velocity evaluation.

5.5. Main outcomes

The experience acquired in applying the LS-PIV technique to real cases during the measurement campaigns discussed in Chapter 3, provided the basis for the analyses shown in this chapter.

Performing the LS-PIV technique in the open field and on real rivers highlights several critical issues compared to the ideal and numerical applications seen in Chapter 4.

In all the field case studies a seeding phase was carried out by manually introducing tracer material. This was due to the absence of tracer particles on the liquid surface of the watercourses. These seeding activities were performed taking into account the considerations made on the basis of the results obtained in Chapter 4. However, the environmental conditions in which the seeding activities took place, the light conditions, as well as the hydraulic regimes, made difficult the attempt to make the liquid surface traceable in an optimal manner. The areal distribution of the tracer was the most sensitive parameter, followed by the seeding density.

The result of the influence of these factors was video sequences in which tracer density and distribution did not remain constant throughout the entire registration.

The use of recorded raw sequences results in the evaluation of surface velocity fields with errors due to portions of the videos being poor in terms of tracer density, or with an inadequate distribution over the entire region of analysis, or both. It is therefore not convenient to perform an analysis with optical software by considering the videos in their entirety, but rather to focus on analysing a smaller portion of them, taking proper account of seeding parameters.

The proposed procedure allows the automatic extraction of the portion of the raw video with the best seeding conditions. They were summarized through 4 indexes representative of the density and areal distribution of the particles. A synthetic global index, that takes into account all 4 previous metrics, allows the identification of the sub-sequence that would return the best results in terms of estimation of surface velocities.

Such a procedure allows to immediately obtain the best results with the available sequences, accounting for the real conditions of seeding of the liquid surface. The procedure is a useful tool for all those cases in which, although the seeding activities have been performed in an optimal way, there have been external disturbing causes and therefore worsened the sampling of the velocities of the liquid surface.

Chapter 6
The influence of hydraulic turbulence on the LS-PIV technique

6.1. Introduction

One aspect that needs to be taken into account in the application of optical techniques, both for LS-PIV and LS-PTV, is that currentmetric behaviour of the stream is derived by making the free surface traceable. Each individual tracer particle is therefore responsible for describing the velocity of the liquid particles that carry it in the downstream movement of the river. The conjoint motion of the water particles is a basic assumption of the innovative techniques, which must always be verified in order not to obtain erroneous results in estimating surface velocities.

There are several situations for which the motion of the particles fails to adequately represent the motion of the liquid surface of the river. As was shown both in Chapter 4, with numerical analyses, and in Chapter 5, with real case studies, the density of the tracer is a fundamental parameter in order to be able to describe the surface velocity. Increasing the density of the tracer material is not sufficient, however, since it is necessary that this tracer be uniformly distributed over the entire surface.

The reduced presence of tracer can leave some portion of the area under analysis not optimally sampled, so software used to process recorded images struggles to interpret the field of frame-by-frame displacements for those areas where there is a marked absence of tracer. The same problem arises when considering an opposite situation. If a high amount of tracer material is available, it

tends to aggregate and form unique patterns that poorly describe the behaviour of the liquid surface.

Aggregates of tracer particles will then move across the river surface with a different dynamic than that which characterizes the movement of the underlying liquid particles. The phenomenon of aggregation is therefore something to be avoided, similarly to the sparse presence of tracer.

Particle aggregation is a phenomenon that is mostly dependent on poor distribution of tracer on the river by the operators in charge. The spreading of tracer at regular time intervals by personnel minimizes the probability of aggregation, and a spatially distributed, rather than localized, launch incentivizes a more uniform distribution over the surface. However, there are other reasons why a particle aggregation may be recorded and often these reasons are to be found in the type of current under analysis.

If it is considered a uniform flow, it is likely that the particles will move without any propensity for aggregation, unless its density is so high that the spaces between particles are so small that one particle can exert a pull effect on the adjacent ones. If it is considered a non-stationary motion, that is one with characteristics that vary in space and time, the velocity field in a certain instant will be different from the velocity field in the next one. In these cases, the flows are called fully turbulent, and the hydraulic turbulence play a key role in the probability of aggregation of the tracer particles.

The study of turbulence has always been a challenging topic for the scientific community, especially for scientists working on river dynamics. Turbulence phenomena influence the morphology of rivers, as well as erosion and the transport of solid material downstream.

The aim of this Chapter is to provide future perspectives in the LS-PIV techniques taking into account the turbulence phenomenon. In the next section the turbulent motion for free surface currents, such as rivers, is reported.

6.2. Turbulent motion in natural watercourses

In general, the phenomenon of turbulence has two aspects: inertial and dissipative. A high presence of kinetic energy in the current causes the development of secondary motions which are responsible for the velocity fluctuations typical of turbulent motion. At the same time, the phenomenon is dissipative since all the kinetic energy produced is dissipated as heat by the viscous forces.

Considering the Reynolds number, physically defined as the ratio between inertia and viscous forces, this assumes a very high value in the case of ordinary turbulence: 10^5 or 10^6. These values therefore reveal that the forces of inertia are preponderant in a turbulent flow with respect to the viscous forces. However, this characteristic is verified for the average motion of the current. At this order of the phenomenon the inertia forces overwhelm the viscous forces, and the dissipation of energy is particularly low.

However, the turbulence scales have a wide range of values starting from the size of the average motion, passing through smaller and smaller quantities. The forces of inertia remain the most present up to a so-called dissipative scale, where the viscous forces acquire greater importance. At this scale, the Reynolds number is equal to unity, the viscous forces become important, and the kinetic energy produced by the turbulence is dissipated into heat.

The transition from the inertial to the dissipative scale occurs gradually and according to a phenomenon called “energy cascade” (Figure 6.1). At the basis of this phenomenon is the instability of large vortices (eddies) that fragment into smaller and smaller structures, producing the cascade of energy from large to small scales. The first eddies that are created are the large ones, which acquire their energy from the average motion. These eddies, due to phenomena of destabilization and fragmentation, break up into vortices of lower dimensions, whose energy derives from the eddies of immediately higher sizes. The destabilization and fragmentation process stops when all the energy is dissipated due to the viscosity.

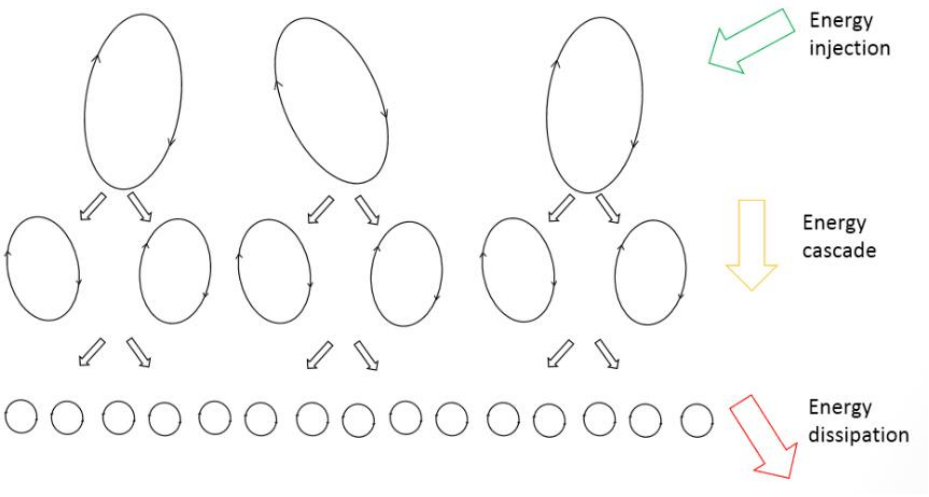

Figure 6.1 – Energy cascade scheme, showing disintegration of eddies into successive smaller eddies until energy dissipation occurs. (http://simscale.com)

The fundamental laws that can model any flow, turbulent flow included, are the Navier-Stokes equations. However, for the turbulent flows, due to the very high values of the Reynolds number, the resolution of the Navier-Stokes equation is really challenging and unstable (Chandler et al., 2012).

This problem is partially solved thanks to the use of the Reynolds-Averaged Navier-Stokes Equations (RANS). The basic principle is to consider the flow as the sum of the mean flow and the turbulent flow. Average velocity can be calculated as (Eq. 6.1):

$$U_i = \lim_{T\to\infty} \frac{1}{T} \int_0^T u \, dt \qquad \text{(Eq. 6.1)}$$

The velocity can be decomposed as Eq. 6.2:

$$u_i = U_i + u_i' \qquad \text{(Eq. 6.2)}$$

where U is the mean velocity, u' is the turbulent flow velocity, T is the averaging time-scale, which must be small enough to have a good approximation of the problem, but also sufficiently higher than the turbulence time-scale (Figure 6.2).

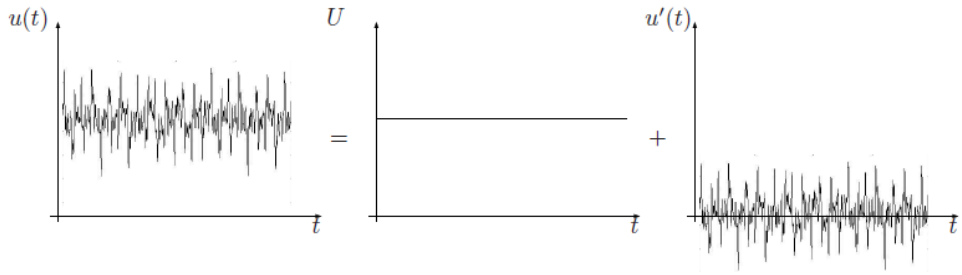

Figure 6.2 – Velocity decomposition in the case of turbulent flow. (http://manchestercfd.co.uk)

Substituting the previous equations into the Navier-Stokes equations, it is possible to obtain a quantity called "Reynolds stress" which represents the effect of turbulence in the average flow. This term is unknown and needs to be modelled.

6.3. Numerical modelling of turbulence

As explained in the previous sections, the typical mechanism of turbulence phenomena is the energy cascade from the largest to the finest structures, up to the so-called Kolmogorov scale (i.e., the smallest possible structures in the energy transfer process) (Leonard, 1975).

In some situations of turbulence, the existing range in terms of turbulent structures that can be generated is enormous. In this case it is necessary to understand at what level to stop the description and resolution of the phenomenon. There are therefore different calculation methodologies that are based on which motion scales to calculate and which to model.

The most obvious technique is to not make a "cut" inside the energy cascade, solving practically all the motion scales. This technique is known as Direct Numerical Simulation (DNS) and is the one characterized by a very high

computational burden not only for the quantity of motions to be reproduced, but also for the very high number of elements that should make up the computing domain. Moreover, it is necessary to simulate reduced time intervals in order to be able to grasp the peculiar characteristics of the phenomenon that is reproducing. The numerical simulations must be carried out for a sufficient long time to allow the evaluation of the statistics of the largest turbulent structures.

Generally, DNS simulations can be applied considering geometries, thus limiting the number of computational nodes. If geometric complexities are introduced, DNS simulations become limiting even for the modern super computers available.

An opposite approach to direct numerical simulation (DNS) is that which involves the use of RANS equations, thus parameterizing the "Reynolds stress" factor. The most used models for the resolution of Reynolds stress term are those labelled as K-ε (Goudsmit et al., 2002). In these models, the turbulent kinetic energy K and its dissipation rate ε are used to create, through dimensional considerations, a scale of length (Eq. 6.3) and time (Eq. 6.4):

$$l = \frac{K^{\frac{3}{2}}}{\varepsilon} \qquad \text{(Eq. 6.3)}$$

$$\mathrm{T} = \frac{K}{\varepsilon} \qquad \text{(Eq. 6.4)}$$

with these quantities a turbulent viscosity can be written as Eq. 6.5:

$$\upsilon_{\mathrm{T}} = C_{\upsilon}\frac{l^2}{\mathrm{T}} = C_{\upsilon}\frac{K^2}{\varepsilon} \qquad \text{(Eq. 6.5)}$$

where C_{υ} is a constant empirically determined.

Modelling turbulence according to the RANS rules means explicitly simulating only the average component, or at most the slowly variable component, of a flow, while all fluctuations are modelled as turbulence.

A third type of approach, intermediate between DNS and RANS, is the Large Eddy Simulation (LES) technique (Piomelli and Chasnov, 1996; Piomelli, 1999), in which all the larger structures (defined as “eddies”), but already in the inertial range, are explicitly simulated with a dense grid, while the smaller scales of motion of the grid (or sub-grid scales) are parametrized with a model. LES technique allows good reliability with lower computational costs than those of the DNS approach.

6.4. A first approach to the study of the influence in the LS-PIV technique

Since natural watercourses are mostly characterized by turbulent motions, the modelling of this phenomenon and the study of its influence on the LS-PIV technique are essential. For these purposes a numerical approach was chosen, making also use of a hydraulic simulation model.

The idea behind these analyses was to recreate first, through the hydraulic model, a virtual open channel within which to generate a three-dimensional turbulent water movement. From the results of the hydraulic model, it was possible to obtain the surface turbulent velocity fields. By virtually disseminating the tracer (with known characteristics), the aim was to verify the accuracy and performance with which the LS-PIV technique estimated the velocity field by analysing the motion of tracer particles (Figure 6.3).

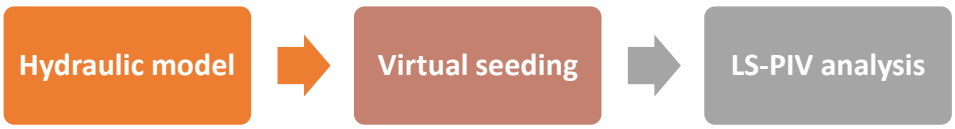

Figure 6.3 – Workflow of the modelling chain structured for the analyses.

In summary, the reported analyses represent a development of what was analysed and reported in Chapter 4, considering the turbulence factor that was not

considered previously. The analyses were also necessary in view of what could be observed experimentally in the open field with the measurement activities mentioned in Chapter 5.

A description of the analyses carried out is given in the next sections, keeping in mind that those obtained represent only preliminary results. The topic of turbulence is particularly complex, and the tools necessary for its modelling require in-depth and timely parametrization. The topic is therefore framed within a work with potential future developments.

6.4.1. Hydraulic model

The first part of the structured workflow for conducting analyses on the turbulence phenomenon related to LS-PIV techniques, is related to the hydraulic model. Through the hydraulic model, it was possible to create a virtual domain in which to reproduce turbulent flow conditions in a controlled manner.

The first step was therefore to frame the type of problem and understand how it is generally handled in computational fluid dynamics (CFD). In particular, analyses were carried out considering open channel theory. An open channel flow is defined as a flowing liquid with a free surface open to the atmosphere. In open channel theory it is assumed that the pressure at the free surface is constant and equal to the atmospheric pressure.

The software used for hydraulic model determination, and which has presented several advantages in its use, including a highly user-friendly and intuitive GUI (Graphical User Interface), is ANSYS Fluent by ANSIS, Inc (Matsson, 2022). ANSYS Fluent is a computer program for modelling fluid flow, heat transfer, and chemical reactions in complex geometries. The software is written in C computer language, and it is a particularly flexible solution for modelling simple and complex phenomena.

ANSYS Fluent can be defined as a Finite Volume Solver (FVS) whose numerical algorithm consists of the following steps:

- integration of the governing equations of fluid flow over all the (finite) control volumes of the domain;

- discretization – conversion of resulting integral equations into a system of algebraic equations;
- solution of the algebraic equations by an iterative method.

Within the software there are modules for generating computational domain (Figure 6.4), subsequent subdivision of the domains into computational cells by means of a computational mesh (Figure 6.5), and finally for the launching of simulations with the possibility of customizing all the values of typical parameters of the conditions to be imposed.

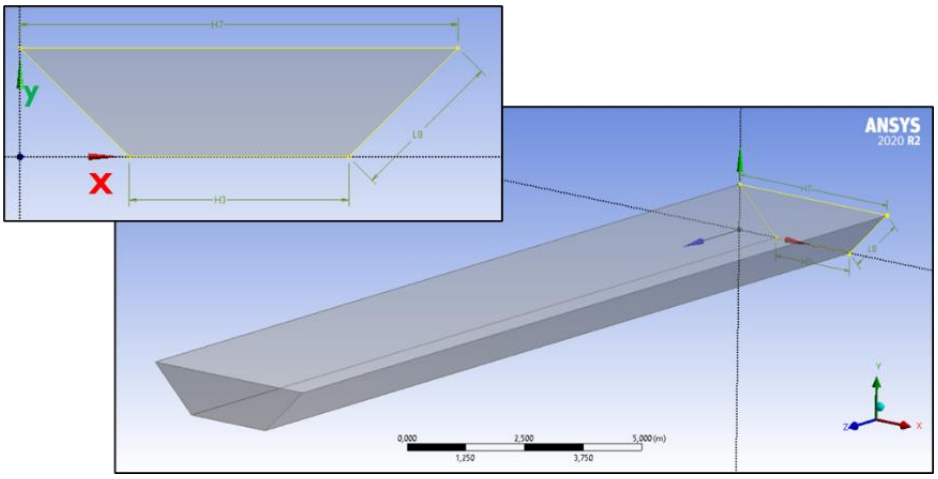

Figure 6.4 – Creation of a geometry with the proper module of the ANSYS software.

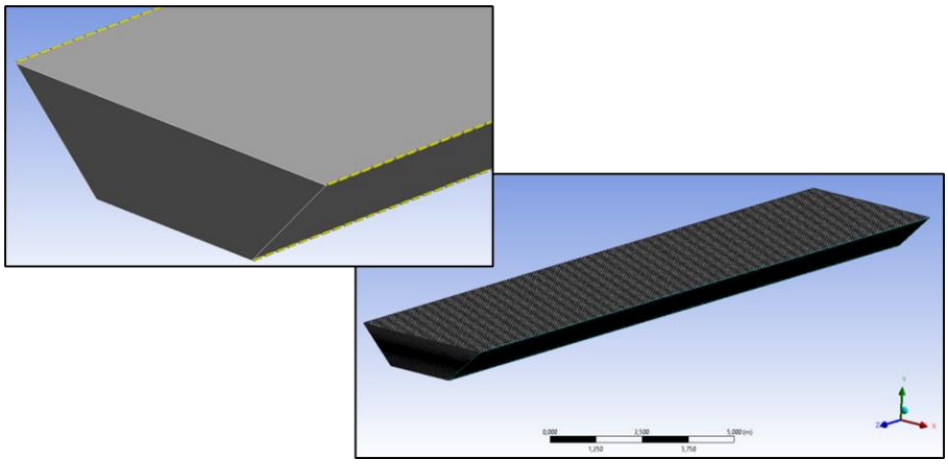

Figure 6.5 – Meshing the domain with the proper module of the ANSYS software.

In open channel flow theory, it is assumed that two different phases coexist: water and air. Since there is a contact surface between the two fluids, the main problem, when simulations of this type are initiated, is how to properly track the position of the free surface during a simulation.

The most appropriate model for describing the behaviour of two fluids cohabiting a single domain, as well as the one used in the analyses shown in this chapter, is the Volume of Fluid (VOF) model. The VOF method is a fixed-grid tracking method that reconstructs the position of the interface between water and air through the information arising from the volume fraction of the fluid.

The basic idea of the VOF method is to define a liquid fraction variable f. If f in a cell is equal to 1, the cell is completely in liquid phase, if f is equal to zero, the cell is empty. The case in which f has a value between 0 and 1, the cell is containing the interface (Figure 6.6). It is possible to define also a fraction variable for the air, such that if there is a liquid volume fraction equal to 1 in the cell, the air volume fraction is 0. It is then possible to define the volume fraction as the fraction of cell volume occupied by a specific phase (air or water in the open channel cases).

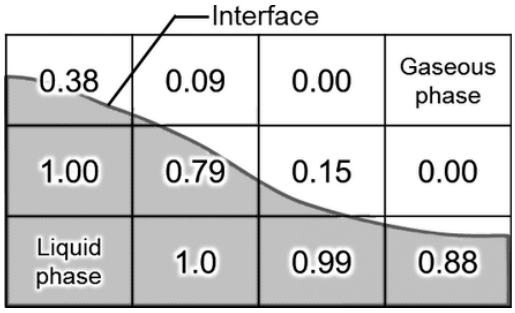

Figure 6.6 – Scheme of the VOF model. (Ogino, 2018)

The VOF model is properly implemented in ANSYS Fluent, introducing a variable for each phases' volume fraction (α_q). Navier-Stokes equations, the liquid mass conservation equation, as well as pressure and viscosity formulation will then all be expressed as a function of the volume fraction of the phase being referred to.

Open channel flow problems require a very specific set of initial and boundary conditions that, if incorrectly chosen, could produce unphysical results.

One of the most important initial conditions is related to the water volume fraction. It is necessary to set at unit value the volume fraction of the portion of the domain occupied by the water. Is this requirement is not satisfied, the water will simply enter the domain from the inlet and cascade to the bottom creating instabilities.

Regarding the boundary conditions, it is possible to use different option for the top, inlet, and outlet parts of a domain. Generally, pressure conditions are applied at inlet and outlet. In the first case, and in similar way for the outlet, the user must specify:

- the bottom height;
- the free-surface height;
- the velocity of the liquid phase (water).

These quantities allow to calculate the total pressure p_0 at inlet (Eq. 6.6), which can be broken into two parts: the dynamic pressure q (Eq. 6.7) and the static pressure p_s (Eq. 6.8):

$$p_0 = q + p_s \quad \text{(Eq. 6.6)}$$

$$q = \frac{\rho - \rho_0}{2} V^2 \quad \text{(Eq. 6.7)}$$

$$p_s = (\rho - \rho_0)|\vec{g}|\left(\left(g \cdot \vec{b}\right) + y_{local}\right) \quad \text{(Eq. 6.8)}$$

where

ρ	density of the mixture in a cell
ρ_0	reference density (density of the lightest fluid)
V	velocity magnitude
$\vec{g}$	gravity vector
$\vec{b}$	position vector of the centroid of a cell with respect to a reference location
y_{local}	vertical distance from the free surface to the reference location

Once the boundary and initial conditions have been set, the appropriate settings for starting the simulation can be chosen. Within the software, it is possible to model the effects of open channel flow through the definition of gravity acceleration. The flow of an open channel is usually governed by the force of gravity and inertia.

For the purposes of the analyses presented in this chapter, and always keeping in mind that what is reported represents a first approach to the problem of turbulence related to the LS-PIV technique, a virtual channel of simple shape, characterized by water and air confined in two different portions of the domain, was created (Figure 6.7).

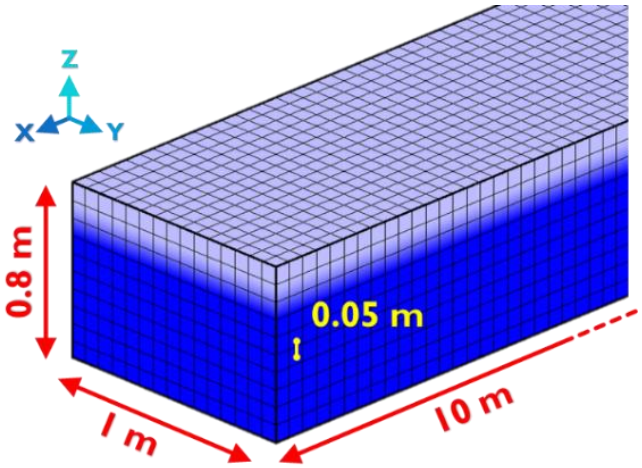

Figure 6.7 – Virtual domain created for the analyses, properly meshed with the module of ANSYS software.

As can be seen from the figure, the channel has a rectangular cross-section; the entire volume was evenly divided into 200 cells in the x-direction, 20 cells in the y-direction, and in 16 cells in the z-direction, with the volume of individual cells being 0.5x0.5x0.5 m^3.

When choosing settings about the setup of the simulations, Large Eddy Simulation (LES) was chosen as the technique for modelling turbulence. The reason for this choice lies in the desire to resolve the larger, macroscopic turbulent eddies, while modelling the small ones.

This choice stems from the experimental observation of how tracer particles undergo the greatest displacements from the coarsest turbulent vortices, which are then the ones that lead the particles to aggregate with each other. Considering that the observation times for the phenomenon of particle motion on the free surface are on the order of a few minutes, it is not convenient to carry out the resolution of turbulent eddies at smaller scales.

In order to verify the performance of the LS-PIV technique, two different simulations were carried out considering two flow conditions for the simulated stream, one with reduced velocity and equal to 0.5 m/s, and the other one with higher velocity and equal to 1.5 m/s. The hydraulic model results were returned in

3 dimensions, so being interested in understanding only what was happening along the free surface, the results were extracted for a plane coincident with the free surface within the computational domain (Figure 6.8).

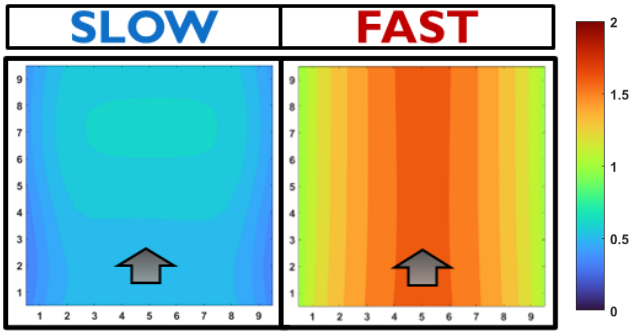

Figure 6.8 - Imposed surface velocity fields for the two flow regime (slow=0.5 m/s, fast=1.5 m/s).

6.4.2. Seeding phase and processing

Similarly to what was done in the analyses in Chapter 4, a virtual seeding step was again performed by distributing tracer particles of known characteristics on the liquid surface of the virtual watercourse.

Imaging ideal conditions, a circular shape was chosen for the particles considered for seeding, with disks of constant size equal to 2 centimetres, which were made to move against an ideal perfectly black background. Two different tracer density conditions were considered in order to also analyse the influence of this parameter in the presence of the turbulence phenomenon (Figure 6.9).

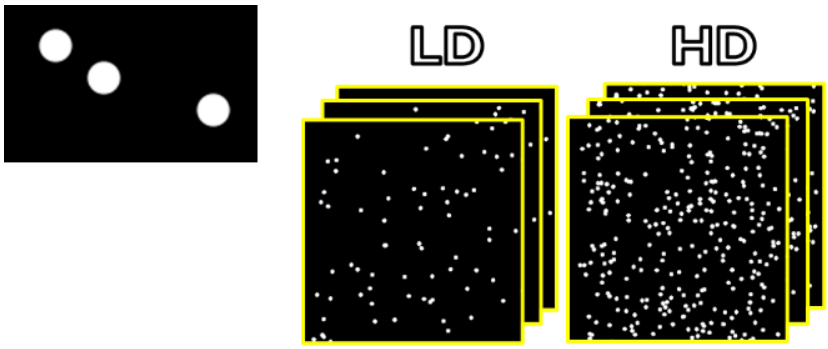

Figure 6.9 – Tracer particles considered for the virtual seeding phase.

Two sequences of about 1 minute each were then created with a frame rate of 8 Hz (8 frames per second) for a total of about 240 frames for each sequence.

Sequences were not subjected to any pre-processing activities, while PIVlab software was again used for the statistical processing step. A sequence style of type 1 (i.e., 1-2; 2-3; 3-4; etc.) was used, applying the FFT-CC algorithm with an Interrogation Area at the first pass of 400 pixels.

6.4.3. Preliminary results

The results obtained with the procedure explained above, appear promising in that the PIVlab software returned estimated surface velocity fields not very different from those imposed with the hydraulic model.

In Figure 6.10 are shown the results arising from the application of PIVlab processing.

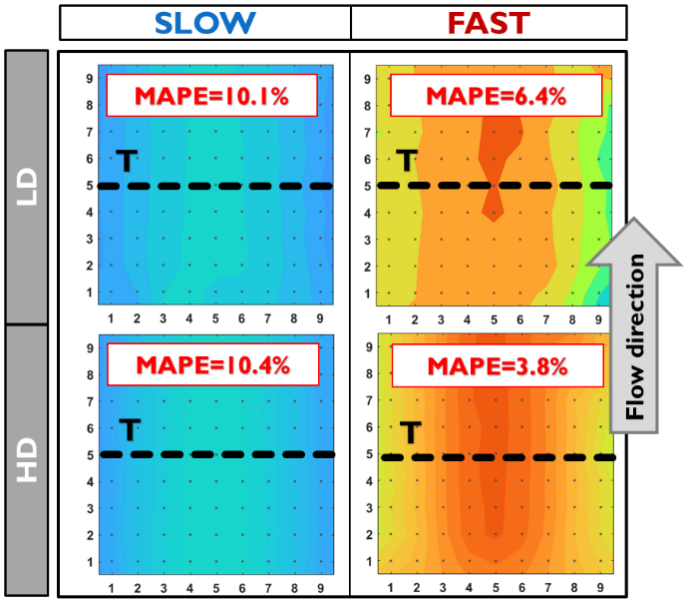

Figure 6.10 – Assessed surface velocity fields. MAPE error is reported for each analysed configuration.

Figure 6.10 also shows the error, expressed in terms of MAPE, in the estimation of the average surface velocity, compared to that imposed with the hydraulic model. It is important to note that the error is reduced as the velocity of movement of the particles on the liquid surface increases with the same density conditions. Minimal error is achieved by increasing the tracer density for the case with high velocity. There is no substantial change in performance by increasing the density in the case with reduced velocity. Indeed, the performance in the case of high density and low velocity is worse than in the case of low density. This behaviour can be explained by the reduced capacity of the PIVlab software to interpret the movement of particles between successive frames when the number of particles is excessively high.

Figure 6.10 also shows the position of a transect (T) along which comparisons have been made in terms of surface velocity profiles, shown in Figure 6.11 instead.

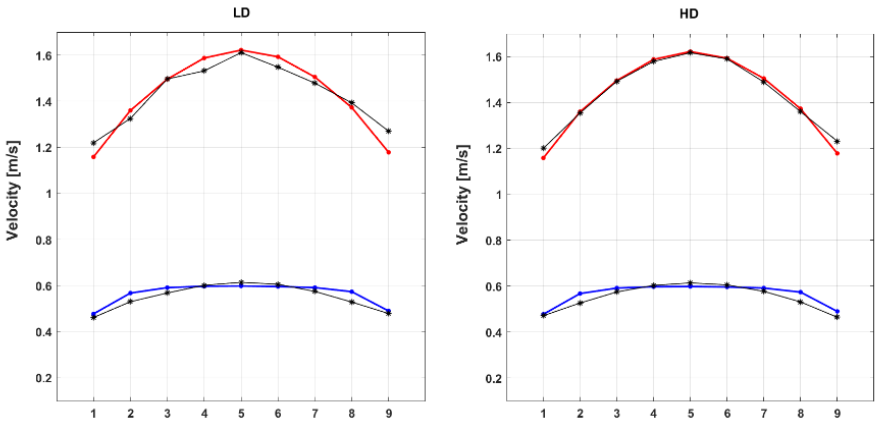

Figure 6.11 – Comparison between imposed and assessed velocity profiles along transect T.

Figure 6.11 shows how the highest errors tend to be concentrated in all cases along the banks of the virtual channel. This is an expected behaviour as it has already been observed in Chapter 4 how the PIVlab software has difficulty in tracking particles that are located along the banks due to out-of-plane and in-plane phenomena. The maximum local error found in terms of MAPE is equal to 7.8%, located at node 8 of the case at low density and low velocity; while the lowest error, located at computational node 3 of the low density and high velocity case, is equal to 0.1%.

The best fitting between velocities estimated with PIVlab and velocities imposed by the hydraulic model in the case of high density and high velocity is confirmed. The worst reproduction of the velocity profile is instead given by both the high and low velocity cases of the low-density configuration.

Although the choices made to complete the analyses reported were rather simplistic due to the incomplete knowledge of the problem, the results obtained are particularly promising. PIVlab software and therefore the LS-PIV technique shows to be able to estimate the surface velocities of a watercourse even in turbulent conditions.

However, it is necessary to underline that the turbulence generated within the computational domain is not actually the one observed in the open field. No turbulent eddies were generated, simulating a movement of water with trajectories

that deviated slightly from the direction they would have had in stationary conditions.

These are analyses in which a first approach to the problem of turbulence has been applied. It is possible to imagine alternative applications that are decidedly more complex than the one carried out. For example, it would be necessary to generate a computational domain with a more complicated geometries, thus introducing additional factors of turbulence production.

6.5. Main outcomes

The analyses carried out and shown in this chapter seek to investigate the influence of the hydraulic turbulence phenomenon within the process of estimating the surface velocity field using optical techniques.

The phenomenology of turbulence is a key factor to be taken into account during the application of the LS-PIV technique, especially considering the implications that this phenomenon has toward the tracer, either artificially introduced or natural one. In particular, the behaviour of tracer particles depends on the presence of secondary currents and eddies, which are the most macroscopic representation of turbulence within liquid current.

Although proficient seeding operations can be carried out, thus in the best possible way, the presence of turbulent effects can result in the generation of particle patterns that are difficult for optical software to interpret in their movement. Turbulence may incentivize the phenomenon of coalescence, generating aggregates of tracer particles whose movement may not be representative of surface water particles. This would generate erroneous surface velocity fields inconsistent with the actual regime of the river motion. Turbulence can also lead to an overdispersion of the tracer, leaving portions of the liquid surface unsampled. The creation of these areas where there is a lack of tracer leads equally to the generation of erroneous surface velocity fields.

Since turbulent phenomena are very complex to study in any field of sciences, the turbulent problem was approached from a numerical point of view. Numerical analyses, with the use in this case of hydraulic models typical of

computational fluid dynamics, allow for maximum flexibility in handling the parameters and characteristics of the problems to be studied.

With the advantages already pointed out in Chapter 4 in adopting numerical analysis, the study of turbulence was performed first by generating a computational domain, then simulating the turbulent motion of a water current, and finally applying seeding step for the final optical analysis. The results emphasized that optical techniques, specifically the LS-PIV technique, can reproduce the surface behaviour of a watercourse with sufficient accuracy, despite turbulent motion. Since the analyses performed represented a first approach to the turbulence-optical analysis problem, turbulent phenomena generated during simulations are not fully developed.

The simulations performed were an initial extension of the study conducted in Chapter 4, where the turbulence effects were neglected as not the main subject of the analyses.

The possibility of generating any turbulence conditions, in computational domains of any geometry, by managing seeding operations in a controlled manner, makes this first attempt at analysis promising and prone to future developments.

Future research needs

The results arising from the analysis carried out and shown within this thesis work, the evidence shows the ability of LS-PIV, and more generally of optical methods all, to be a valuable support to traditional measurement techniques. Furthermore, characteristics of non-intrusiveness, cost-effectiveness, and simplicity of application, allow the LS-PIV technique to obtain discharge information even under limiting conditions for traditional instruments, thus representing a viable alternative to the classical approach.

However, the analyses conducted so far and what has been reported in the scientific literature highlight some as-yet-undiscovered aspects that may also heavily influence the performance of the optical techniques.

In this regard, hydrologists and agencies responsible for managing discharge measurements and monitoring of watercourses must direct their efforts to obtain unique references and guidelines in order to be able to apply the workflow of optical techniques as uniformly as possible in any area of the world. The lack of universally recognized protocols for the proper application of LS-PIV and LS-PTV techniques, is one of the weakness points due to which there has not been a marked replacement of the traditional approach with these innovative methods in recent years. There are numerous papers, however, that report targeted analyses for increasing the performance of the technique, pointing out possible practical procedures to be implemented in the open field and achieve the desired improvements. It is therefore possible to retrieve practical guidelines for proper optical analysis; what is lacking is the organicity of such guidelines of application with specific and recognized standards.

As shown in both Chapter 4 and Chapter 5, there are some fundamental aspects of the LS-PIV technique that need special attention. On all those occasions when the tracer must be introduced manually, but also when it is naturally present on the liquid surface, the density and areal distribution of the particles assume a role of significant importance. Research efforts have been focused in recent years

in this direction, trying to understand how considering a proper amount of tracer and proper dispersion of particles within the recording video area. Therefore, it is necessary to continue to thoroughly investigate aspects related to the seeding characteristics of the free surface, striving for optimal results even when the amount of tracer present and its distribution deviate from optimal values.

Deviation from the best values of seeding parameters is often due to the presence of hydraulic turbulence, which is typical of natural flows. All rivers, at different levels of magnitude, are affected by hydraulic turbulence, causing the presence of eddies and secondary currents that cause a unpredictable change in the positions of the tracer particles leasing them to aggregate or over-disperse.

The effects of the turbulence on the LS-PIV technique and on all optical techniques in general, are still weakly investigated today. Simplifying assumptions are often affecting the analyses to return results that do not effectively account for the phenomenology of turbulence, in all its major aspects.

Regarding the application of the LS-PIV technique with surface tracer dispersion, turbulence has important implications not only for particle density and distribution, but also in the final stages of discharge assessment from surface velocity fields. Knowing the area of a cross-section of a river and having calculated the average surface velocity with LS-PIV technique along the same section, there is the problem of how to define the functional relationship between this surface velocity and the depth-averaged velocity along the vertical. Such velocity ratio is assumed to be constant and equal to 0.85, but this value may differ considerably depending on the environmental and hydraulic regime conditions in place. The possible presence of vegetation on the bottom and banks of the river, the geometry of the cross-sections, and the planimetric shape of the current all contribute to changing the value of the velocity ratio, as observed during the analyses reported in Chapter 5.

Other aspects that can be investigated in future analyses are related to the type of used tracers for seeding the free surface. The analysis on tracer could highlight the existence of specific materials to be used under specific environmental and hydraulic conditions. There could be also the possibility of investigating specific tracers for specific video recording devices, being able to make use of advanced recording tools, such as thermal or infrared cameras.

Another aspect that should be carefully analysed is the importance of using UAV platforms for video recording of tracer movement on the liquid surface. This

kind of approach has several pros including: (i) monitoring the watercourse with sufficient safe distance, (ii) possibility of recording with camera orthogonal to the liquid surface (with consequent reduction of perspective distortions), (iii) choice of flight height with possibility of varying the spatial resolution of the images. However, the use of drones must be carried out by specialized and appropriately skilled personnel; moreover, the use of UAVs devices is limited in case of bad weather conditions (e.g., strong wind, intense precipitation, etc.).

Conclusions

Careful rivers monitoring through flow measurement is crucial for managing the resources of a specific area. Rivers can also flood so that the measurements of water levels within watercourses play an important role in the protection of the population and of all existing structures in the territory.

The need to monitor the hydraulic regime of rivers has recently increased due to the impact of climate change on the processes of the hydrological cycle. The total volume of water that crosses the natural and artificial channels depends on the hydrological processes controlled by the geology, geomorphology, and climate of the area under analysis, as well as on the impact of human activities.

The flow discharge in open channels is usually estimated by measuring the elevation of the liquid surface (stage) referred to a zero-reference level, linking this measurement to the discharge through empirical relations. Stage-discharge relations are curves that allow the assessment of flows once the water levels are known and represent a centuries-old tool used to monitor the discharge of watercourses. The stage-discharge curves are obtained by carrying out numerous simultaneous measurements of discharge and water level, but these are often not accurate in the minima and maxima values. If in the case of measurement of water levels, no specific problems are encountered, as hydrometric rods are used suitably anchored to the banks of the rivers and easily accessible even at a safe distance from the flow, the same does not happen for the measurement of the discharge.

The volume flowing through a cross-section of a channel in the unit of time is historically measured indirectly through instruments such as current meters (mechanical or electromagnetic). Numerous limitations are detected in the use of these devices, although they have been used for years in order to obtain stage-discharge curves all over the world. The main limiting factor is that operators, who must be highly specialized, have to dive into the water. This is possible only for specific flow conditions, i.e., those for which it is not risky for the operators to carry out flow measurements. The flood conditions are therefore those for which

current meter measurements are never made, considering the risk that exists for personnel and the difficulties in accessing rivers.

The limitations of current meters have been partially overcame by the use of devices that use sound waves and the Doppler effect principle: the ADCPs. In this case the personnel carrying out the flow measurement does not need to immerse themselves inside the river, as they can also move the instrument from a bridge or safely from the banks. However, although it has been possible to extend the range of measured discharges far beyond the capabilities of current meters, the ADCPs can be used in a limited manner in flood conditions. The high velocities and high turbulence of the current make it difficult to move the instrument with concrete risks of damaging the device or even losing it in the current.

Considering the lower part of the stage-discharge curves, both the current meters and the ADCPs show technical limits in the measurement of small discharges. In both cases there are often not enough water levels to use the instruments. In the case of current meters, a minimum water level must be checked to immerse the sensor, while in the case of ADCPs, a minimum water column height must be ensured so the sensor can adequately receive the echoes of the sound impulses.

The extensive literature review conducted on the state of the art of discharge and stage measurements and the study of stage-discharge curve, highlighted the strong need to identify new technologies for obtaining flow measurements in conditions where traditional tools fail.

The techniques that are most suitable for overcoming the difficulties mentioned above and in the first part of the thesis are based on the processing of recorded images showing the movement of a tracer in motion, suitably dispersed on the surface of the rivers. These techniques are indicated as optical techniques and among these the most famous are the LS-PIV (Large-Scale Particle Image Velocimetry) and the LS-PTV (Large-Scale Particle Tracking Velocimetry). The thesis work was focused more on the analysis of the performances deriving from the application of the LS-PIV technique, which adopts a Eulerian approach of analysis.

This technique, if applied with the appropriate precautions, allows to identify ample margins for improvement in the monitoring and measurement phases of the flow discharges of a watercourse. Being a non-intrusive technique, it allows the mapping of the surface velocity field of an area of the river under

analysis without the immersion of personnel or tools. The only elements necessary for the application of the technique are the tracing material for making liquid surface traceable, a video recording device (e.g., digital camera), and a software (generally free and open source) for the statistical processing of the recorded sequences.

The technique is therefore easy to apply, inexpensive, and safe for those who perform the measurements.

Since the analysis of the images can be carried out in any flow conditions, from normal flow to flood or small flow conditions, the technique allows to easily calculate points of the stage-discharge relationship that are not easily obtainable from traditional tools.

However, since the LS-PIV techniques is innovative in the panorama of methods that can be used for river flow monitoring, it lacks universally recognized guidelines and standards for its application. The research activity conducted and shown in Chapters 4, 5 and 6, is directly linked to the need to increase knowledge about optical techniques, obtaining useful information to be applied in an optimal way. All the analyses performed, also provide useful insights for consolidating operational protocols for the use of the LS-PIV technique in practical, full-field applications.

Under the latter aspect, the field activities framed within a collaboration agreement between the University of Palermo and the Hydrographic Authority of Sicily, represented an opportunity for the open field application of the LS-PIV, being able to verify through real experience the actual criticalities in the use and application of the technique.

Considering the numerical study performed and shown in Chapter 4, many factors related to the real conditions of river flow have been neglected. The created scenarios (also for the most realistic SR-VAR cases) could be rather far from real scenarios. Nevertheless, the creation of controlled conditions by a numerical approach has the advantage to conduct sensitivity analyses on specific factors of interest, minimizing the effects of external disturbances.

Coherently with other works similarly conducted on the other optical technique, the LS-PTV, attention has been focused on some factors which are easily control during field surveys. Then, the numerical approach provides useful recommendations for an appropriate choice in terms of seeding density, frame rate,

and duration of the video-sequence depending on the presumable local flow and environmental conditions.

Several main insights can be obtained from the analyses of Chapter 4.

Particular attention should be paid to the choice of an appropriate tracer concentration: low seeding densities produce large errors in numerical simulations, while a sufficiently high seeding density of particles ensures satisfying performance of LS-PIV. This suggests an operative criterion for choosing the proper seeding density in field campaigns, in which additional seeding particles could be artificially introduced to improve accuracy of LS-PIV measurements in the case of scarce presence of natural tracers.

An important performance improvement can be obtained increasing the duration of the processed video sequence. This is a well-known strategy to compensate problems related to low seeding density, especially when flow velocity is rather low. Longer durations also imply an increase of computational costs, and, in real cases, the occurrences of possible environmental disturbances over the video sequence.

The choice of the frame rate for the processed sequence should be made with extreme care and according to the local flow conditions. The selected frame rate should optimize the frame-by-frame tracer displacements. The frame rate with respect to the typical image acquisition frame rate (i.e., 24/30 fps) should be considerably reduced for very slow flows in order to avoid excessively small displacements, while, for very fast flows, it should be increased to limit the frame-by-frame displacements.

The numerical approach provides a useful tool also for studying the border effect in optical techniques, which is an aspect scarcely investigated in the past. The analyses have confirmed the importance in removing the contour region of the frame, where the error is one order of magnitude higher than in the central part.

Since the core of the optical approach is the ability of the software to find statistically the most probable displacement of tracer between two frames, all the possible pre-processing operations can help the cross-correlation algorithms to improve the detection frame-by-frame of the tracer displacement. The proposed methodology, shown in Chapter 5, responds to the need to process only a portion of the entire video recorded in the field, and in particular the best part.

The parameters that most influence the results expected from optical software, from the very beginning of the characteristic workflow of the techniques, are those related to the density of the tracer and its distribution. Difficulties in controlling the seeding phases in the field may result in videos where the tracer is not well dispersed or introduce in insufficient quantities to characterize the velocity domain.

The analysed methodology, considering the characteristics of the tracer, both temporally and spatially, succeeds in extracting the best video sub-sequence to process with the optical software. The proposed methodology has been calibrated and tested on several real case studies, giving robust results, also comparable with existing methodologies, that use different approach. In this case, it has been proved that the proposed approach can extends the existing methods giving a valid alternative, and more physical based solutions. The identification of the best sub-sequences provided significant improvements in the reconstruction of the surface velocity profile along a transect, minimizing the errors with respect to the benchmark data.

Finally, the results shown in Chapter 6, although deriving from preliminary analyses, show how optical techniques, specifically the LS-PIV technique, can integrate or replace traditional techniques for measuring and monitoring rivers flow in limiting conditions.

The optical techniques applied to river flow monitoring are not costly, they have great versatility of use, are not intrusive and can easily complement, or even replace, traditional measurement techniques. The joint use of traditional methods and optical techniques would make it possible to achieve two main goals: the possibility of carrying out measurements even in prohibitive conditions for traditional techniques (e.g., flood situations or in the presence of excessively low water levels), and the opportunity to use measurements from optical techniques in order to validate the flow rating curves.

It is possible to conclude by stating that optical techniques have shown, both from the point of view of numerical studies and from field applications, wide margins for improvements. Constant technological development will make it possible to further improve the performance of techniques, being able to exploit increasingly high-performance devices at low costs.

References

Acreman, M. (2001). Ethical aspects of water and ecosystems. Water Policy, 3(3), 257-265.

Adrian, R. J. (2005). Twenty years of particle image velocimetry. Experiments in fluids, 39(2), 159-169.

Adrian, R. J., & Westerweel, J. (2011). Particle image velocimetry (No. 30). Cambridge university press.

Alexander, B. F., & Ng, K. C. (1991). Elimination of systematic error in subpixel accuracy centroid estimation [also Letter 34 (11) 3347-3348 (Nov1995)]. Optical engineering, 30(9), 1320-1331.

Al-Khudhairy, D. H. A., Leemhuis, C., Hoffmann, V., Shepherd, I. M., Calaon, R., Thompson, J. R., ... & Papadimos, D. (2002). Monitoring wetland ditch water levels using Landsat TM and ground-based measurements. Photogrammetric Engineering and Remote Sensing, 68(8), 809-818.

Alsdorf, D., Melack, I., Dunne, T., Mertes, L., Hess, L. & Smith, L. (2000) Interferometric radar measurements of water level changes on the Amazon flood plain. Nature 404, 174–177.

Ancey, C., Davison, A. C., Böhm, T., Jodeau, M., & Frey, P. (2008). Entrainment and motion of coarse particles in a shallow water stream down a steep slope. Journal of Fluid Mechanics, 595, 83-114.

Angarita-Jaimes, D. A., Ormsby, M. P., Chennaoui, M., Angarita-Jaimes, N. C., Towers, C. E., Jones, A. C., & Towers, D. P. (2008). Optically efficient fluorescent tracers for multi-constituent PIV. Experiments in fluids, 45(4), 623-631.

Aronica, G., Corrao, C., Amengual, A., Alonso, S., & Romero, R. (2005, April). Water resources evaluation under climatic trend effects in Mediterranean catchments. In Geophys. Res. Abstr (Vol. 7, p. 04091).

Ashmore, P., & Sauks, E. (2006). Prediction of discharge from water surface width in a braided river with implications for at-a-station hydraulic geometry. Water Resources Research, 42(3).

Baffaut, C., Sadler, E. J., & Ghidey, F. (2015). Long-term agroecosystem research in the Central Mississippi River Basin: Goodwater Creek Experimental Watershed flow data. Journal of Environmental Quality, 44(1), 18-27.

Bailey, J. F., & Ray, H. A. (1966). Definition of stage-discharge relation in natural channels by step-backwater analysis (p. 24). US Government Printing Office.

Bandini, F., Frias, M. C., Liu, J., Simkus, K., Karagkiolidou, S., & Bauer-Gottwein, P. (2021). Measuring River Surface Velocity with Doppler Radar and Particle Image Velocimetry (PIV) Using Unmanned Aerial Systems (UASs).

Bandini, F., Olesen, D., Jakobsen, J., Kittel, C. M. M., Wang, S., Garcia, M., & Bauer-Gottwein, P. (2018). Bathymetry observations of inland water bodies using a tethered single-beam sonar controlled by an unmanned aerial vehicle. Hydrology and Earth System Sciences, 22(8), 4165-4181.

Barrow, C. J. (1998). River basin development planning and management: a critical review. World development, 26(1), 171-186.

Batra, N., Islam, S., Venturini, V., Bisht, G., & Jiang, L. E. (2006). Estimation and comparison of evapotranspiration from MODIS and AVHRR sensors for clear sky days over the Southern Great Plains. Remote Sensing of Environment, 103(1), 1-15.

Becchi I., Anselmo V., Saccardo I. e Pinelli P.F. (1994) Manuale per il monitoraggio idrografico, U.O. 1.31 G.N.D.C.I., ENEL –CRIS

Bhattacharya, B., & Solomatine, D. P. (2000, July). Application of artificial neural network in stage-discharge relationship. In Proc. 4th International Conference on Hydroinformatics, Iowa City, USA (pp. 1-7).

Birk, S., & Ecke, F. (2014). The potential of remote sensing in ecological status assessment of coloured lakes using aquatic plants. Ecological indicators, 46, 398-406.

Birkett, C. (1998) Contribution of the TOPEX NASA radar altimeter to the global monitoring of large rivers and wetlands. Water Resour. Res. 34,1223–1239.

Bjerklie, D. M., Moller, D., Smith, L. C., & Dingman, S. L. (2005). Estimating discharge in rivers using remotely sensed hydraulic information. Journal of hydrology, 309(1-4), 191-209.

Bodo, B. (2001) Flow rates of selected world rivers. http://dss.ucar.edu/dataset/ds552.0.

Bolognesi, M., Farina, G., Alvisi, S., Franchini, M., Pellegrinelli, A., & Russo, P. (2017). Measurement of surface velocity in open channels using a lightweight remotely piloted aircraft system. Geomatics, Natural Hazards and Risk, 8(1), 73-86.

Bonacci, O., & Andrić, I. (2015). Karst spring catchment: an example from Dinaric karst. Environmental Earth Sciences, 74(7), 6211-6223.

Bos MG (1976) Discharge measurement structures. Publication 20 International Institute for Land Reclamation and Improvement (ILRI), Wageningen

Bosbach, J., Kühn, M., & Wagner, C. (2009). Large scale particle image velocimetry with helium filled soap bubbles. Experiments in fluids, 46(3), 539-547.

Botter, G., Milan, E., Bertuzzo, E., Zanardo, S., Marani, M., & Rinaldo, A. (2009). Inferences from catchment-scale tracer circulation experiments. Journal of Hydrology, 369(3-4), 368-380.

Brakenridge, G. R., Knox, J. C., Paylor, E. D., & Magilligan, F. J. (1994). Radar remote sensing aids study of the great flood of 1993. Eos, Transactions American Geophysical Union, 75(45), 521-527.

Brakenridge, G. R., Nghiem, S. V., Anderson, E., & Chien, S. (2005). Space-based measurement of river runoff. Eos, Transactions American Geophysical Union, 86(19), 185-188.

Brakenridge, G. R., Tracy, B. T., & Knox, J. C. (1998). Orbital SAR remote sensing of a river flood wave. International journal of remote sensing, 19(7), 1439-1445.

Brossard, C., Monnier, J. C., Barricau, P., Vandernoot, F. X., Le Sant, Y., Champagnat, F., & Le Besnerais, G. (2009). Principles and applications of particle image velocimetry. Aerospace Lab, (1), p-1.

Caldwell, L. (2019). Mobile Instructional Particle Image Velocimetry for STEM Outreach and Undergraduate Fluid Mechanics Education.

Calkins, D., & Dunne, T. (1970). A salt tracing method for measuring channel velocities in small mountain streams. Journal of Hydrology, 11(4), 379-392.

Calmant, S., & Seyler, F. (2006). Continental surface waters from satellite altimetry. Comptes Rendus Geoscience, 338(14-15), 1113-1122.

Cao, L., Weitbrecht, V., Li, D., & Detert, M. (2018). Feature tracking velocimetry applied to airborne measurement data from Murg creek. In E3S Web of Conferences (Vol. 40, p. 05030). EDP Sciences.

Carrel, M., Detert, M., Peña-Haro, S., & Lüethi, B. (2019). Evaluation of the DischargeApp: A smartphone application for discharge measurements. HydroSenSoft 2019, Madrid, Spain.

Cerqueira, R. F. L., Paladino, E. E., Ynumaru, B. K., & Maliska, C. R. (2018). Image processing techniques for the measurement of two-phase bubbly pipe flows using particle image and tracking velocimetry (PIV/PTV). Chemical Engineering Science, 189, 1-23.

Chandler, G. J., Juniper, M. P., Nichols, J. W., & Schmid, P. J. (2012). Adjoint algorithms for the Navier–Stokes equations in the low Mach number limit. Journal of Computational Physics, 231(4), 1900-1916.

Charonko, J. J., & Vlachos, P. P. (2013). Estimation of uncertainty bounds for individual particle image velocimetry measurements from cross-correlation peak ratio. Measurement Science and Technology, 24(6), 065301.

Chaudhry, M. H. (2008). Open-channel flow (Vol. 523). New York: Springer.

Chauhan, M. S., Kumar, V., Dikshit, P. K. S., & Dwivedi, S. B. (2014). Comparison of discharge data using ADCP and current meter. Int J Adv Earth Sci, 3(2), 81-86.

Chen, B., Zhang, X., Tao, J., Wu, J., Wang, J., Shi, P., ... & Yu, C. (2014). The impact of climate change and anthropogenic activities on alpine grassland over the Qinghai-Tibet Plateau. Agricultural and Forest Meteorology, 189, 11-18.

Cheng, H. D., & Shi, X. J. (2004). A simple and effective histogram equalization approach to image enhancement. Digital signal processing, 14(2), 158-170.

Christensen, K. T., & Scarano, F. (2015). Uncertainty quantification in particle image velocimetry. Measurement Science and Technology, 26(7), 070201.

Cierpka, C., Lütke, B., & Kähler, C. J. (2013). Higher order multi-frame particle tracking velocimetry. Experiments in Fluids, 54(5), 1-12.

Clarke, R. T. (1999). Uncertainty in the estimation of mean annual flood due to rating-curve indefinition. Journal of Hydrology, 222(1-4), 185-190.

Coe, M. T., & Birkett, C. M. (2004). Calculation of river discharge and prediction of lake height from satellite radar altimetry: Example for the Lake Chad basin. Water Resources Research, 40(10).

Comina, C., Lasagna, M., De Luca, D. A., & Sambuelli, L. (2014). Geophysical methods to support correct water sampling locations for salt dilution gauging. Hydrology and Earth System Sciences, 18(8), 3195-3203.

Corbett, D. M. (1943). Stream-gaging procedure. US Department of the Interior.

Costa, J. E., Cheng, R. T., Haeni, F. P., Melcher, N., Spicer, K. R., Hayes, E., ... & Barrick, D. (2006). Use of radars to monitor stream discharge by noncontact methods. Water Resources Research, 42(7).

Costa, J. E., Spicer, K. R., Cheng, R. T., Haeni, F. P., Melcher, N. B., Thurman, E. M., ... & Keller, W. C. (2000). Measuring stream discharge by non-contact methods: A proof-of-concept experiment. Geophysical Research Letters, 27(4), 553-556.

Creutin, J. D., Muste, M., Bradley, A. A., Kim, S. C., & Kruger, A. (2003). River gauging using PIV techniques: a proof of concept experiment on the Iowa River. Journal of Hydrology, 277(3-4), 182-194.

Cristianini, N., & Shawe-Taylor, J. (2000). An introduction to support vector machines and other kernel-based learning methods. Cambridge university press.

Dal Sasso, S. F., Pizarro, A., & Manfreda, S. (2020). Metrics for the quantification of seeding characteristics to enhance image velocimetry performance in rivers. Remote Sensing, 12(11), 1789.

Dal Sasso, S. F., Pizarro, A., & Manfreda, S. (2021). Recent Advancements and Perspectives in UAS-Based Image Velocimetry. Drones, 5(3), 81.

Dal Sasso, S. F., Pizarro, A., Pearce, S., Maddock, I., & Manfreda, S. (2021). Increasing LSPIV performances by exploiting the seeding distribution index at different spatial scales. Journal of Hydrology, 598, 126438.

Dal Sasso, S. F., Pizarro, A., Samela, C., Mita, L., & Manfreda, S. (2018). Exploring the optimal experimental setup for surface flow velocity measurements using PTV. Environmental Monitoring and Assessment, 190(8), 1-14.

Dawdy, D. W. (1961) Depth-discharge relation of alluvial streams; discontinuous rating curves. Water-supply Paper 1498-C.

de Baar, J. H., Percin, M., Dwight, R. P., van Oudheusden, B. W., & Bijl, H. (2014). Kriging regression of PIV data using a local error estimate. Experiments in fluids, 55(1), 1-13.

Deka, P., & Chandramouli, V. (2003). A fuzzy neural network model for deriving the river stage—discharge relationship. Hydrological sciences journal, 48(2), 197-209.

Dellenback, P. A., Macharivilakathu, J., & Pierce, S. R. (2000). Contrast-enhancement techniques for particle-image velocimetry. Applied optics, 39(32), 5978-5990.

Detert, M. (2021). How to avoid and correct biased riverine surface image velocimetry. Water Resources Research, 57(2), e2020WR027833.

Detert, M., & Weitbrecht, V. (2015). A low-cost airborne velocimetry system: proof of concept. Journal of Hydraulic Research, 53(4), 532-539.

Detert, M., Johnson, E. D., & Weitbrecht, V. (2017). Proof-of-concept for low-cost and non-contact synoptic airborne river flow measurements. International Journal of Remote Sensing, 38(8-10), 2780-2807.

Di Baldassarre, G., & Montanari, A. (2009). Uncertainty in river discharge observations: a quantitative analysis. Hydrology and Earth System Sciences, 13(6), 913-921.

Dingman, S. L. (2015). Physical hydrology. Waveland press.

Dobson, D. W., Holland, K. T., & Calantoni, J. (2014). Fast, large-scale, particle image velocimetry-based estimations of river surface velocity. Computers & Geosciences, 70, 35-43.

Dramais, G., Le Coz, J., Camenen, B., & Hauet, A. (2011). Advantages of a mobile LSPIV method for measuring flood discharges and improving stage–discharge curves. Journal of Hydro-Environment Research, 5(4), 301-312.

Duncan, J., Dabiri, D., Hove, J., & Gharib, M. (2010). Universal outlier detection for particle image velocimetry (PIV) and particle tracking velocimetry (PTV) data. Measurement Science and Technology, 21(5), 057002.

Dunkerley, D. L. (2003). An optical tachometer for short-path measurement of flow speeds in shallow overland flows: improved alternative to dye timing. Earth Surface Processes and Landforms: The Journal of the British Geomorphological Research Group, 28(7), 777-786.

Durst, F., Miloievic, D., & Schönung, B. (1984). Eulerian and Lagrangian predictions of particulate two-phase flows: a numerical study. Applied Mathematical Modelling, 8(2), 101-115.

Egusa, T., Ohte, N., Oda, T., & Suzuki, M. (2013). Relationship between catchment scale and the spatial variability of stream discharge and chemistry in a catchment with multiple geologies. Hydrological Research Letters, 7(2), 12-17.

Eltner, A., Bertalan, L., Grundmann, J., Perks, M. T., & Lotsari, E. (2021). Hydro-morphological mapping of river reaches using videos captured with UAS. Earth Surface Processes and Landforms, 46(14), 2773-2787.

Eltner, A., Elias, M., Sardemann, H., & Spieler, D. (2018). Automatic image-based water stage measurement for long-term observations in ungauged catchments. Water Resources Research, 54(12), 10-362.

Emiroglu, M. E., Agaccioglu, H., & Kaya, N. (2011). Discharging capacity of rectangular side weirs in straight open channels. Flow Measurement and Instrumentation, 22(4), 319-330.

Fekete, B. M., & Vörösmarty, C. J. (2007). The current status of global river discharge monitoring and potential new technologies complementing traditional discharge measurements. IAHS publ, 309, 129-136.

Flener, C., Wang, Y., Laamanen, L., Kasvi, E., Vesakoski, J. M., & Alho, P. (2015). Empirical modeling of spatial 3d flow characteristics using a remote-controlled ADCP system: monitoring a spring flood. Water, 7(1), 217-247.

Flury, M., & Wai, N. N. (2003). Dyes as tracers for vadose zone hydrology. Reviews of Geophysics, 41(1).

Fujita, I. (2017). Discharge measurements of snowmelt flood by space-time image velocimetry during the night using far-infrared camera. Water, 9(4), 269.

Fujita, I., & Kunita, Y. (2011). Application of aerial LSPIV to the 2002 flood of the Yodo River using a helicopter mounted high density video camera. Journal of Hydro-environment Research, 5(4), 323-331.

Fujita, I., Muste, M., & Kruger, A. (1998). Large-scale particle image velocimetry for flow analysis in hydraulic engineering applications. Journal of hydraulic Research, 36(3), 397-414.

Fujita, I., Muto, Y., Shimazu, Y., Tsubaki, R., & Aya, S. (2004). Velocity measurements around non-submerged and submerged spur dykes by means of Large-Scale image velocimetry. Journal of hydroscience and hydraulic engineering, 22(1), 51-61.

Fujita, I., Watanabe, H., & Tsubaki, R. (2007). Development of a non-intrusive and efficient flow monitoring technique: The space-time image velocimetry (STIV). International Journal of River Basin Management, 5(2), 105-114.

Fukami, K., Fukagata, K., & Taira, K. (2019). Super-resolution reconstruction of turbulent flows with machine learning. Journal of Fluid Mechanics, 870, 106-120.

Fulton, J., & Ostrowski, J. (2008). Measuring real-time streamflow using emerging technologies: Radar, hydroacoustics, and the probability concept. Journal of Hydrology, 357(1-2), 1-10.

Ghodsian, M. (2003). Supercritical flow over a rectangular side weir. Canadian Journal of Civil Engineering, 30(3), 596-600.

Gollin, D., Brevis, W., Bowman, E. T., & Shepley, P. (2017). Performance of PIV and PTV for granular flow measurements. Granular Matter, 19(3), 1-16.

Gonzalez, C. A., & Chanson, H. (2008). Turbulence manipulation in air–water flows on a stepped chute: An experimental study. European Journal of Mechanics-B/Fluids, 27(4), 388-408.

Gordon, N. D., McMahon, T. A., Finlayson, B. L., Gippel, C. J., & Nathan, R. J. (2004). Stream hydrology: an introduction for ecologists. John Wiley and Sons.

Goudsmit, G. H., Burchard, H., Peeters, F., & Wüest, A. (2002). Application of k-ϵ turbulence models to enclosed basins: The role of internal seiches. Journal of Geophysical Research: Oceans, 107(C12), 23-1.

Greve, F. W., & Zucrow, M. J. (1925). MEASUREMENT OF PIPE FLOW BY THE COÖRDINATE METHOD. Journal (American Water Works Association), 13(3), 306-311.

Guizar-Sicairos, M., & Fienup, J. R. (2008). Direct image reconstruction from a Fourier intensity pattern using HERALDO. Optics letters, 33(22), 2668-2670.

Hain, R., Buchmann, N. A., & Cierpka, C. (2016). On the possibility of using mobile phone cameras for quantitative flow visualization. In 18th International Symposium on Applications of Laser Techniques to Fluid Mechanics (Lisbon).

Hamilton, A. S., & Moore, R. D. (2012). Quantifying uncertainty in streamflow records. Canadian Water Resources Journal/Revue canadienne des ressources hydriques, 37(1), 3-21.

Haritashya, U. K., Singh, P., Kumar, N., & Gupta, R. P. (2006). Suspended sediment from the Gangotri Glacier: Quantification, variability and associations with discharge and air temperature. Journal of Hydrology, 321(1-4), 116-130.

Harmel, R. D., Smith, D. R., King, K. W., & Slade, R. M. (2009). Estimating storm discharge and water quality data uncertainty: a software tool for monitoring and modeling applications. Environmental Modelling & Software, 24(7), 832-842.

Harpold, A. A., Mostaghimi, S., Vlachos, P. P., Brannan, K., & Dillaha, T. (2006). Stream discharge measurement using a large-scale particle image velocimetry (LSPIV) prototype. Transactions of the ASABE, 49(6), 1791-1805.

Harrelson, C. C. (1994). Stream channel reference sites: an illustrated guide to field technique (Vol. 245). US Department of Agriculture, Forest Service, Rocky Mountain Forest and Range Experiment Station.

Hart, D. P. (2000). PIV error correction. Experiments in fluids, 29(1), 13-22.

Harwell, G. R., & Asquith, W. H. (2011). Annual peak streamflow and ancillary data for small watersheds in central and western Texas. US Department of the Interior, US Geological Survey.

Hassan, M. A., & Bradley, D. N. (2017). Geomorphic controls on tracer particle dispersion in gravel-bed rivers. Gravel-Bed Rivers: Process and Disasters, 167.

Hassan, M. A., & Ergenzinger, P. (2003). Use of tracers in fluvial geomorphologie. GM Kondolf et H. Piégay (Eds), Tools in Fluvial Geomorphologie.

Hauer, F. R., & Lamberti, G. A. (Eds.). (2017). Methods in stream ecology: Volume 1: Ecosystem structure. Academic Press.

Hauet, A., Creutin, J. D., & Belleudy, P. (2008). Sensitivity study of large-scale particle image velocimetry measurement of river discharge using numerical simulation. Journal of Hydrology, 349(1-2), 178-190.

Hauet, A., Kruger, A., Krajewski, W. F., Bradley, A., Muste, M., Creutin, J. D., & Wilson, M. (2008). Experimental system for real-time discharge estimation using an image-based method. Journal of Hydrologic Engineering, 13(2), 105-110.

Herschy R. W. (1995) Streamflow Measurement, Chapman & Hall, Second Edition

Herschy, R. W. (2008). Streamflow measurement. CRC press.

Hess, L. L., Melack, J. M., Filoso, S., & Wang, Y. (1995). Delineation of inundated area and vegetation along the Amazon floodplain with the SIR-C synthetic aperture radar. IEEE transactions on geoscience and remote sensing, 33(4), 896-904.

Higham, J. E., & Brevis, W. (2019). When, what and how image transformation techniques should be used to reduce error in Particle Image Velocimetry data?. Flow Measurement and Instrumentation, 66, 79-85.

Hilgersom, K. P., & Luxemburg, W. M. J. (2012). How image processing facilitates the rising bubble technique for discharge measurement. Hydrology and Earth System Sciences, 16(2), 345-356.

Hirt, C. W., Amsden, A. A., & Cook, J. L. (1974). An arbitrary Lagrangian-Eulerian computing method for all flow speeds. Journal of computational physics, 14(3), 227-253.

Holecek, J. and Vocel, J., (1965). Measurement of time of travel in the Volynka Experimental Basin. In: Representative and experimental areas, IAHS Symposium of Budapest, 28 September–1 October 1965. Wallingford, UK: IAHS Press, IAHS Publ. 61, 299–310

Horritt, M. S., & Bates, P. D. (2002). Evaluation of 1D and 2D numerical models for predicting river flood inundation. Journal of hydrology, 268(1-4), 87-99.

Hubbard, E. F. (1982). Measurement of time of travel and dispersion in streams by dye tracing. US Department of the Interior, Geological Survey.

Hudson, J. A. (2004). The impact of sediment on open channel flow measurement in selected UK experimental basins. Flow Measurement and Instrumentation, 15(1), 49-58.

Hudson, J. D. (1993). The effect of a wavy boundary on turbulent flow. University of Illinois at Urbana-Champaign.

Hudson, N. (1993). Field measurement of soil erosion and runoff (Vol. 68). Food & Agriculture Org..

Huntington, K. W., Blythe, A. E., & Hodges, K. V. (2006). Climate change and Late Pliocene acceleration of erosion in the Himalaya. Earth and Planetary Science Letters, 252(1-2), 107-118.

Immerzeel, W. W., Droogers, P., De Jong, S. M., & Bierkens, M. F. P. (2009). Large-scale monitoring of snow cover and runoff simulation in Himalayan river basins using remote sensing. Remote sensing of Environment, 113(1), 40-49.

Jin, S., Huang, P., Park, J., Yoo, J. Y., & Breuer, K. S. (2004). Near-surface velocimetry using evanescent wave illumination. Experiments in fluids, 37(6), 825-833.

Jodeau, M., Hauet, A., Paquier, A., Le Coz, J., & Dramais, G. (2008). Application and evaluation of LS-PIV technique for the monitoring of river surface velocities in high flow conditions. Flow Measurement and Instrumentation, 19(2), 117-127.

John, P. H. (1978). Discharge measurement in lower order streams. Internationale Revue der gesamten Hydrobiologie und Hydrographie, 63(6), 731-755.

Johnson, D., & Pattiaratchi, C. (2004). Transient rip currents and nearshore circulation on a swell-dominated beach. Journal of Geophysical Research: Oceans, 109(C2).

Jolley, M. J., Russell, A. J., Quinn, P. F., & Perks, M. T. (2021). Considerations When Applying Large-Scale PIV and PTV for Determining River Flow Velocity. Frontiers in Water.

Jones, B. E. (1916). A method of correcting river discharge for a changing stage (No. 375-E). US Geological Survey.

Kääb, A., Altena, B., & Mascaro, J. (2019). River-ice and water velocities using the Planet optical cubesat constellation. Hydrology and Earth System Sciences, 23(10), 4233-4247.

Kähler, C. J., Astarita, T., Vlachos, P. P., Sakakibara, J., Hain, R., Discetti, S., ... & Cierpka, C. (2016). Main results of the 4th International PIV Challenge. Experiments in Fluids, 57(6), 1-71.

Kähler, C. J., Scharnowski, S., & Cierpka, C. (2012). On the uncertainty of digital PIV and PTV near walls. Experiments in fluids, 52(6), 1641-1656.

Keane, R. D., & Adrian, R. J. (1992). Theory of cross-correlation analysis of PIV images. Applied scientific research, 49(3), 191-215.

Kennedy, E. J. (1984). Discharge ratings at gaging stations. Department of the Interior, US Geological Survey.

Kim, J., Kim, D., Son, G., & Kim, S. (2015). Accuracy analysis of velocity and water depth measurement in the straight channel using ADCP. Journal of Korea Water Resources Association, 48(5), 367-377.

Kim, Y., Muste, M., Hauet, A., Krajewski, W. F., Kruger, A., & Bradley, A. (2008). Stream discharge using mobile large-scale particle image velocimetry: A proof of concept. Water Resources Research, 44(9).

Kinzel, P. J., & Legleiter, C. J. (2019). sUAS-based remote sensing of river discharge using thermal particle image velocimetry and bathymetric lidar. Remote Sensing, 11(19), 2317.

Koblinsky, C. J., Clarke, R. T., Brenner, A. C., & Frey, H. (1993). Measurement of river level variations with satellite altimetry (Vol. 29, No. 6, pp. 1839-1848).

Kouraev, A. V., Zakharova, E. A., Samain, O., Mognard, N. M., & Cazenave, A. (2004). Ob'river discharge from TOPEX/Poseidon satellite altimetry (1992–2002). Remote sensing of environment, 93(1-2), 238-245.

Kumar, A. (2011). Stage-discharge relationship. Encyclopedia of Snow, Ice and Glaciers. Encyclopedia of Earth Sciences Series, edited by: Singh, V., Singh, P., and Haritashya, U., Springer, Dordrecht, https://doi. org/10.1007/978-90-481-2642-2_537.

Landreth, C. C., & Adrian, R. J. (1988). Measurement and refinement of velocity data using high image density analysis in particle image velocimetry. In 4th International Symposium on Applications of Laser Anemometry to Fluid Mechanics (pp. 6-14).

Le Coz, J., Camenen, B., Peyrard, X., & Dramais, G. (2012). Uncertainty in open-channel discharges measured with the velocity–area method. Flow Measurement and Instrumentation, 26, 18-29.

Le Coz, J., Hauet, A., Pierrefeu, G., Dramais, G., & Camenen, B. (2010). Performance of image-based velocimetry (LSPIV) applied to flash-flood discharge measurements in Mediterranean rivers. Journal of hydrology, 394(1-2), 42-52.

Le Coz, J., Jodeau, M., Hauet, A., Marchand, B., & Le Boursicaud, R. (2014, September). Image-based velocity and discharge measurements in field and laboratory river engineering studies using the free FUDAA-LSPIV software.

In Proceedings of the international conference on fluvial hydraulics, River Flow (Vol. 3, No. 09, pp. 2014-05).

Le Coz, J., Pierrefeu, G., & Paquier, A. (2008). Evaluation of river discharges monitored by a fixed side-looking Doppler profiler. Water Resources Research, 44(4).

Lee, K., Ho, H. C., Marian, M., & Wu, C. H. (2014). Uncertainty in open channel discharge measurements acquired with StreamPro ADCP. Journal of hydrology, 509, 101-114.

Leibundgut, C., Maloszewski, P., & Külls, C. (2009). Tracers in hydrology (p. 432). Chichester: Wiley-Blackwell.

Leon, J. G., Calmant, S., Seyler, F., Bonnet, M. P., Cauhopé, M., Frappart, F., ... & Fraizy, P. (2006). Rating curves and estimation of average water depth at the upper Negro River based on satellite altimeter data and modeled discharges. Journal of hydrology, 328(3-4), 481-496.

Leonard, A. (1975). Energy cascade in large-eddy simulations of turbulent fluid flows. In Advances in geophysics (Vol. 18, pp. 237-248). Elsevier.

Lindken, R., Rossi, M., Große, S., & Westerweel, J. (2009). Micro-particle image velocimetry (μPIV): recent developments, applications, and guidelines. Lab on a Chip, 9(17), 2551-2567.

Liu, S. D., Zhou, Z. Y., Zou, R. P., Pinson, D., & Yu, A. B. (2014). Flow characteristics and discharge rate of ellipsoidal particles in a flat bottom hopper. Powder technology, 253, 70-79.

Liu, W. C., Lu, C. H., & Huang, W. C. (2021). Large-scale particle image velocimetry to measure streamflow from videos recorded from unmanned aerial vehicle and fixed imaging system. Remote Sensing, 13(14), 2661.

Ljubičić, R., Strelnikova, D., Perks, M. T., Eltner, A., Peña-Haro, S., Pizarro, A., ... & Manfreda, S. (2021). A comparison of tools and techniques for stabilising UAS imagery for surface flow observations. Adv. River Basin Monit.

Lloyd, P. M., Stansby, P. K., & Ball, D. J. (1995). Unsteady surface-velocity field measurement using particle tracking velocimetry. Journal of Hydraulic Research, 33(4), 519-534.

Lourenco, L. M. (1993). Velocity bias technique for particle image velocimetry measurements of high-speed flows. Applied optics, 32(12), 2159-2162.

Lourenco, L., & Krothapalli, A. (1995). On the accuracy of velocity and vorticity measurements with PIV. Experiments in fluids, 18(6), 421-428.

Lowe, D. G. (1999, September). Object recognition from local scale-invariant features. In Proceedings of the seventh IEEE international conference on computer vision (Vol. 2, pp. 1150-1157). Ieee.

Lu, Y., & Lueck, R. G. (1999). Using a broadband ADCP in a tidal channel. Part II: Turbulence. Journal of Atmospheric and Oceanic Technology, 16(11), 1568-1579.

Lucas, B. D., & Kanade, T. (1981). An iterative image registration technique with an application to stereo vision (Vol. 81, pp. 674-679).

Lyon, S. W., Desilets, S. L., & Troch, P. A. (2008). Characterizing the response of a catchment to an extreme rainfall event using hydrometric and isotopic data. Water Resources Research, 44(6).

Malepati, H. (2010). Digital media processing: DSP algorithms using C. Newnes.

Manfreda, S. (2018). On the derivation of flow rating curves in data-scarce environments. Journal of Hydrology, 562, 151-154.

Manfreda, S., McCabe, M. F., Miller, P. E., Lucas, R., Pajuelo Madrigal, V., Mallinis, G., ... & Toth, B. (2018). On the use of unmanned aerial systems for environmental monitoring. Remote sensing, 10(4), 641.

Martin, E. (2006). Measuring water flow in surface irrigation ditches and gated pipe.

Martin, J. E. (2009). Particle image velocimetry study of density current fronts. University of Illinois at Urbana-Champaign.

Masullo, A., & Theunissen, R. (2016, July). Improvement of PIV dynamic range in the presence of velocity gradients using multiple correlation peak analysis and self-adaptive windows. In The International Symposia on Applications of Laser Techniques to Fluid Mechanics.

Mata, L. J., & Budhooram, J. (2007). Complementarity between mitigation and adaptation: the water sector. Mitigation and Adaptation Strategies for Global Change, 12(5), 799-807.

Matgen, P., Schumann, G., Henry, J. B., Hoffmann, L., & Pfister, L. (2007). Integration of SAR-derived river inundation areas, high-precision topographic data and a river flow model toward near real-time flood management. International Journal of Applied Earth Observation and Geoinformation, 9(3), 247-263.

Matsson, J. E. (2022). An Introduction to ANSYS Fluent 2022. Sdc Publications.

Meselhe, E. A., Peeva, T., & Muste, M. (2004). Large scale particle image velocimetry for low velocity and shallow water flows. Journal of Hydraulic Engineering, 130(9), 937-940.

Mingkhwan, E., & Khawsuk, W. (2017, January). Digital image stabilization technique for fixed camera on small size drone. In 2017 Third Asian Conference on Defence Technology (ACDT) (pp. 12-19). IEEE.

Moramarco, T., Barbetta, S., & Tarpanelli, A. (2017). From surface flow velocity measurements to discharge assessment by the entropy theory. Water, 9(2), 120.

Moran, D., & Dann, S. (2008). The economic value of water use: implications for implementing the water framework directive in Scotland. Journal of environmental Management, 87(3), 484-496.

Mosley, M.P., McKerchar, A.I., (1993). Streamflow. In: Maidment, D.R. (Editor-in-Chief) Handbook of Hydrology. McGraw-Hill, chapter 8

Mueller, D. (2013). Roland v. Davis, 302 P. 3d 91 (Mont. 2013). Water Law Review, 17(1), 197.

Mueller, D. S., Wagner, C. R., Rehmel, M. S., Oberg, K. A., & Rainville, F. (2009). Measuring discharge with acoustic Doppler current profilers from a moving boat (p. 72). Reston, Virginia (EUA): US Department of the Interior, US Geological Survey.

Muja, M., & Lowe, D. G. (2012, May). Fast matching of binary features. In 2012 Ninth conference on computer and robot vision (pp. 404-410). IEEE.

Muste, M., Fujita, I., & Hauet, A. (2008). Large-scale particle image velocimetry for measurements in riverine environments. Water resources research, 44(4).

Muste, M., Yu, K., & Spasojevic, M. (2004). Practical aspects of ADCP data use for quantification of mean river flow characteristics; part I: moving-vessel measurements. Flow measurement and instrumentation, 15(1), 1-16.

Mutz, M., Kalbus, E., & Meinecke, S. (2007). Effect of instream wood on vertical water flux in low-energy sand bed flume experiments. Water Resources Research, 43(10).

Naithani, A. K., Nainwal, H. C., Sati, K. K., & Prasad, C. (2001). Geomorphological evidences of retreat of the Gangotri glacier and its characteristics. Current Science, 87-94.

Najafi, M. R., Moradkhani, H., & Piechota, T. C. (2012). Ensemble streamflow prediction: climate signal weighting methods vs. climate forecast system reanalysis. Journal of Hydrology, 442, 105-116.

Nobach, H., & Honkanen, M. (2005). Two-dimensional Gaussian regression for sub-pixel displacement estimation in particle image velocimetry or particle position estimation in particle tracking velocimetry. Experiments in fluids, 38(4), 511-515.

Oberg, K., & Mueller, D. S. (2007). Validation of streamflow measurements made with acoustic Doppler current profilers. Journal of hydraulic Engineering, 133(12), 1421-1432.

Ogino, Y., Hirata, Y., Kihana, S., & Nitta, N. (2018). Numerical simulation of free-flight transfer by a 3D metal transfer model. QJ Jpn. Weld. Soc, 36(1), 94-103.

Overton, I. C. (2005). Modelling floodplain inundation on a regulated river: integrating GIS, remote sensing and hydrological models. River research and applications, 21(9), 991-1001.

Papa, F., Prigent, C., & Rossow, W. B. (2007). Ob'River flood inundations from satellite observations: A relationship with winter snow parameters and river runoff. Journal of Geophysical Research: Atmospheres, 112(D18).

Parodi, U., & Ferraris, L. (2004). Influence of stage discharge relationship on the annual maximum discharge statistics. Natural Hazards, 31(3), 603-611.

Pasley R., Snider D., Lee O.P., Riekert E.G. (1972) Stage-discharge relationships, NEH National Engineering Handbook, Section 4 Hydrology, Chapter 14.

Patalano, A., García, C. M., & Rodríguez, A. (2017). Rectification of Image Velocity Results (RIVeR): A simple and user-friendly toolbox for large scale water surface Particle Image Velocimetry (PIV) and Particle Tracking Velocimetry (PTV). Computers & Geosciences, 109, 323-330.

Pearce, S., Ljubičić, R., Peña-Haro, S., Perks, M., Tauro, F., Pizarro, A., ... & Manfreda, S. (2020). An evaluation of image velocimetry techniques under low flow conditions and high seeding densities using unmanned aerial systems. Remote Sensing, 12(2), 232.

Pedocchi, F., Martin, J. E., & García, M. H. (2008). Inexpensive fluorescent particles for large-scale experiments using particle image velocimetry. Experiments in Fluids, 45(1), 183-186.

Pelletier, P. M. (1988). Uncertainties in the single determination of river discharge: a literature review. Canadian Journal of Civil Engineering, 15(5), 834-850.

Perks, M. T. (2020). KLT-IV v1. 0: Image velocimetry software for use with fixed and mobile platforms. Geoscientific Model Development, 13(12), 6111-6130.

Perks, M. T., Dal Sasso, S. F., Hauet, A., Jamieson, E., Le Coz, J., Pearce, S., ... & Manfreda, S. (2020). Towards harmonisation of image velocimetry techniques for river surface velocity observations. Earth System Science Data, 12(3), 1545-1559.

Perks, M. T., Russell, A. J., & Large, A. R. (2016). Advances in flash flood monitoring using unmanned aerial vehicles (UAVs). Hydrology and Earth System Sciences, 20(10), 4005-4015.

Peterson, M., & Cromwell, C. F. (1993). Measuring irrigation water in a ditch stream or reservoir. University of Missouri Extension G, 1681.

Pfeffer, M. J., & Wagenet, L. P. (2007). Volunteer environmental monitoring, knowledge creation and citizen–scientist interaction. Sage handbook on environment and society. SAGE Publications, Los Angeles, 235-249.

Pilgrim, D. H. (1966). Radioactive tracing of storm runoff on a small catchment: II. Discussion of results. Journal of Hydrology, 4, 306-326.

Pilgrim, D. H. (1975). Travel times and nonlinearity of flood runoff from tracer measurements on a small watershed. Water Resources Research, 12(3), 487-496.

Piomelli, U. (1999). Large-eddy simulation: achievements and challenges. Progress in aerospace sciences, 35(4), 335-362.

Piomelli, U., & Chasnov, J. R. (1996). Large-eddy simulations: theory and applications. In Turbulence and transition modelling (pp. 269-336). Springer, Dordrecht.

Pizarro, A., Dal Sasso, S. F., & Manfreda, S. (2020a). Refining image-velocimetry performances for streamflow monitoring: Seeding metrics to errors minimization. Hydrological Processes, 34(25), 5167-5175.

Pizarro, A., Dal Sasso, S. F., Perks, M. T., & Manfreda, S. (2020b). Identifying the optimal spatial distribution of tracers for optical sensing of stream surface flow. Hydrology and Earth System Sciences, 24(11), 5173-5185.

Planchon, O., Silvera, N., Gimenez, R., Favis-Mortlock, D., Wainwright, J., Bissonnais, Y. L., & Govers, G. (2005). An automated salt-tracing gauge for flow-velocity measurement. Earth Surface Processes and Landforms, 30(7), 833-844.

Plant, W. J., & Keller, W. C. (1990). Evidence of Bragg scattering in microwave Doppler spectra of sea return. Journal of Geophysical Research: Oceans, 95(C9), 16299-16310.

Plesinski, K., & Radecki-Pawlik, A. (2017). Block Ramps A Field Example. In Open Channel Hydraulics, River Hydraulic Structures and Fluvial Geomorphology (pp. 82-97). CRC Press.

Podlinski, J., Kocik, M., Dors, M., Metel, E., & Mizeraczyk, J. (2007, March). Flow patterns measurements with PIV laser method. In 14th International

School on Quantum Electronics: Laser Physics and Applications (Vol. 6604, pp. 273-277). SPIE.

Prandtl, L. (1904). Über Flussigkeitsbewegung bei sehr kleiner Reibung. Verhandl. III, Internat. Math.-Kong., Heidelberg, Teubner, Leipzig, 1904, 484-491.

Prandtl, L. (1927). The generation of vortices in fluids of small viscosity. The Aeronautical Journal, 31(200), 718-741.

Prasad, A. K. (2000). Stereoscopic particle image velocimetry. Experiments in fluids, 29(2), 103-116.

Price, J. F. (2006). Lagrangian and eulerian representations of fluid flow: Kinematics and the equations of motion (pp. 1-99). MIT OpenCourseWare.

Pumo, D., Alongi, F., Ciraolo, G., & Noto, L. V. (2021). Optical methods for river monitoring: A simulation-based approach to explore optimal experimental setup for LSPIV. Water, 13(3), 247.

Pun, C. S., Susanto, A., & Dabiri, D. (2007). Mode-ratio bootstrapping method for PIV outlier correction. Measurement Science and Technology, 18(11), 3511.

Raffel, M., Willert, C. E., Scarano, F., Kähler, C. J., Wereley, S. T., & Kompenhans, J. (2018). Applications: Volumetric Flow Measurements. In Particle Image Velocimetry (pp. 597-632). Springer, Cham.

Raffel, M., Willert, C. E., Scarano, F., Kähler, C. J., Wereley, S. T., & Kompenhans, J. (2018). PIV uncertainty and measurement accuracy. In Particle Image Velocimetry (pp. 203-241). Springer, Cham.

Raffel, M., Willert, C., Wereley, S., & Kompenhans, J. (2007). Particle image velocimetry. Experimental fluid mechanics. Springer, Berlin. doi, 10(1007), 978-3.

Rantz, S. E. (1982). Measurement and computation of streamflow (Vol. 2175). US Department of the Interior, Geological Survey.

Rantz, S. E., & Harris, E. E. (1963). Floods of January-February 1963 in California and Nevada. US Geological Survey.

Reddy, T. L., & Thomson, R. J. (2015). Environmental, social and economic sustainability: implications for actuarial science. Actuaries Institute, 23-27.

Replogle, J. A., Myers, L. E., & Brust, K. J. (1966). Flow measurements with fluorescent tracers. Journal of the Hydraulics Division, 92(5), 1-15.

Revilla-Romero, B., Thielen, J., Salamon, P., De Groeve, T., & Brakenridge, G. R. (2014). Evaluation of the satellite-based global flood detection system for measuring river discharge: influence of local factors. Hydrology and Earth System Sciences, 18(11), 4467-4484.

Rickard, C., Day, R., & Purseglove, J. (2003). River Weirs–Good Practice Guide Guide-Section A. Unpublished report for Environment Agency.

Rodriguez-Padilla, I., Castelle, B., Marieu, V., & Morichon, D. (2019). A simple and efficient image stabilization method for coastal monitoring video systems. Remote sensing, 12(1), 70.

Rohwer, C. (1943). Design and operation of small irrigation pumping plants (No. 678). US Department of Agriculture.

Rosten, E., & Drummond, T. (2006, May). Machine learning for high-speed corner detection. In European conference on computer vision (pp. 430-443). Springer, Berlin, Heidelberg.

Roux, H., & Dartus, D. (2006). Use of parameter optimization to estimate a flood wave: Potential applications to remote sensing of rivers. Journal of Hydrology, 328(1-2), 258-266.

Rozos, E., Dimitriadis, P., Mazi, K., Lykoudis, S., & Koussis, A. (2020). On the uncertainty of the image velocimetry method parameters. Hydrology, 7(3), 65.

Ryckborst, H., & Christie, R. O. (1977). FEASIBILITY OF ELECTROMAGNETIC STREAMFLOW MEASUREMENTS USING THE EARTH'S FIELD/La practabilité des mesures électromagnétiques de l'écoulement total en utilisant le champ magnétique de la terre. Hydrological Sciences Journal, 22(2), 241-255.

Sanyal, J., & Lu, X. X. (2004). Application of remote sensing in flood management with special reference to monsoon Asia: a review. Natural Hazards, 33(2), 283-301.

Schumann, G., Matgen, P., Hoffmann, L., Hostache, R., Pappenberger, F., & Pfister, L. (2007). Deriving distributed roughness values from satellite radar data for flood inundation modelling. Journal of Hydrology, 344(1-2), 96-111.

Sciacchitano, A., & Wieneke, B. (2016). PIV uncertainty propagation. Measurement Science and Technology, 27(8), 084006.

Şengörür, B., Dede, C., & Doğan, E. (2014). The examination of the performances of methods used in separating the total stream flow in different rivers. G eofizika, 31(1), 1-12.

Shavit, U., Lowe, R. J., & Steinbuck, J. V. (2007). Intensity capping: a simple method to improve cross-correlation PIV results. Experiments in Fluids, 42(2), 225-240.

SHI, J. T., & Tomasi, C. (1994). C., 1994. Good features to track. IEEE Computer Society.

Shieh, C. L., Jan, C. D., & Tsai, Y. F. (1996). A numerical simulation of debris flow and its application. Natural Hazards, 13(1), 39-54.

Shiklomanov, A. I., Lammers, R. B., & Vörösmarty, C. J. (2002). Widespread decline in hydrological monitoring threatens pan-Arctic research. Eos, Transactions American Geophysical Union, 83(2), 13-17.

Shope, C. L., Bartsch, S., Kim, K., Kim, B., Tenhunen, J., Peiffer, S., ... & Koellner, T. (2013). A weighted, multi-method approach for accurate basin-wide streamflow estimation in an ungauged watershed. Journal of hydrology, 494, 72-82.

Singh, P., Ramasatri, K. S., Kumar, N., & Bhatnagar, N. K. (2003). Suspended sediment transport from the Dokriani Glacier in the Garhwal Himalayas. Hydrology Research, 34(3), 221-244.

Sivapragasam, C., & Muttil, N. (2005). Discharge rating curve extension–a new approach. Water Resources Management, 19(5), 505-520.

Smith, G. W. (1995). A critical review of the aerial and ground surveys of breeding waterfowl in North America.

Smith, L. C. (1997). Satellite remote sensing of river inundation area, stage, and discharge: A review. Hydrological processes, 11(10), 1427-1439.

Smith, L., Isacks, B., Bloom, A. & Murray, A. (1996) Estimation of discharge from three braided rivers using synthetic aperture radar satellite imagery. Water Resour. Res. 32, 2021–2034.

Soupir, M. L., Mostaghimi, S., & Mitchem, Jr, C. E. (2009). A comparative study of stream-gaging techniques for low-flow measurements in two Virginia tributaries 1. JAWRA Journal of the American Water Resources Association, 45(1), 110-122.

Stamhuis, E. J. (2006). Basics and principles of particle image velocimetry (PIV) for mapping biogenic and biologically relevant flows. Aquatic Ecology, 40(4), 463-479.

Stockdale, R. J., McLelland, S. J., Middleton, R., & Coulthard, T. J. (2008). Measuring river velocities using GPS river flow tracers (GRiFTers). Earth Surface Processes and Landforms: The Journal of the British Geomorphological Research Group, 33(8), 1315-1322.

Strelnikova, D., Paulus, G., Käfer, S., Anders, K. H., Mayr, P., Mader, H., ... & Schneeberger, R. (2020). Drone-based optical measurements of heterogeneous surface velocity fields around fish passages at hydropower dams. Remote Sensing, 12(3), 384.

Tang, H. W., Cheng, C. H. E. N., Hong, C. H. E. N., & Huang, J. T. (2008). An improved PTV system for large-scale physical river model. Journal of Hydrodynamics, Ser. B, 20(6), 669-678.

Tang, S., & Tang, X. (2012). Statistical CT noise reduction with multiscale decomposition and penalized weighted least squares in the projection domain. Medical physics, 39(9), 5498-5512.

Tauro, F., & Grimaldi, S. (2017). Ice dices for monitoring stream surface velocity. Journal of Hydro-environment Research, 14, 143-149.

Tauro, F., Grimaldi, S., Petroselli, A., & Porfiri, M. (2012). Fluorescent particle tracers for surface flow measurements: a proof of concept in a natural stream. Water Resources Research, 48(6).

Tauro, F., Olivieri, G., Petroselli, A., Porfiri, M., & Grimaldi, S. (2016). Flow monitoring with a camera: a case study on a flood event in the Tiber river. Environmental Monitoring and Assessment, 188(2), 1-11.

Tauro, F., Piscopia, R., & Grimaldi, S. (2017). Streamflow observations from cameras: Large-scale particle image velocimetry or particle tracking velocimetry?. Water Resources Research, 53(12), 10374-10394.

Tauro, F., Piscopia, R., & Grimaldi, S. (2019). PTV-Stream: A simplified particle tracking velocimetry framework for stream surface flow monitoring. Catena, 172, 378-386.

Tauro, F., Porfiri, M., & Grimaldi, S. (2014). Orienting the camera and firing lasers to enhance large scale particle image velocimetry for streamflow monitoring. Water Resources Research, 50(9), 7470-7483.

Tauro, F., Porfiri, M., & Grimaldi, S. (2016). Surface flow measurements from drones. Journal of Hydrology, 540, 240-245.

Tauro, F., Rapiti, E., Al-Sharab, J. F., Ubertini, L., Grimaldi, S., & Porfiri, M. (2013). Characterization of eco-friendly fluorescent nanoparticle-doped tracers for environmental sensing. Journal of nanoparticle research, 15(9), 1-14.

Tauro, F., Tosi, F., Mattoccia, S., Toth, E., Piscopia, R., & Grimaldi, S. (2018). Optical tracking velocimetry (OTV): leveraging optical flow and trajectory-based filtering for surface streamflow observations. Remote Sensing, 10(12), 2010.

Tensmeyer, C., & Martinez, T. (2020). Historical document image binarization: a review. SN Computer Science, 1(3), 1-26.

Thielicke, W., & Stamhuis, E. (2014). PIVlab–towards user-friendly, affordable and accurate digital particle image velocimetry in MATLAB. Journal of open research software, 2(1).

Thumser, P., Haas, C., Tuhtan, J. A., Fuentes-Pérez, J. F., & Toming, G. (2017). RAPTOR-UAV: Real-time particle tracking in rivers using an unmanned aerial vehicle. Earth Surface Processes and Landforms, 42(14), 2439-2446.

Timmins, B. H., Wilson, B. W., Smith, B. L., & Vlachos, P. P. (2012). A method for automatic estimation of instantaneous local uncertainty in particle image velocimetry measurements. Experiments in fluids, 53(4), 1133-1147.

Tmušić, G., Manfreda, S., Aasen, H., James, M. R., Gonçalves, G., Ben-Dor, E., ... & McCabe, M. F. (2020). Current practices in UAS-based environmental monitoring. Remote Sensing, 12(6), 1001.

Tomasi, C., & Kanade, T. (1991). Detection and tracking of point. Int J Comput Vis, 9, 137-154.

Torgersen, T., & Kennedy, B. M. (1999). Air-Xe enrichments in Elk Hills oil field gases: role of water in migration and storage. Earth and Planetary Science Letters, 167(3-4), 239-253.

Townsend, P. A., & Foster, J. R. (2002). A synthetic aperture radar–based model to assess historical changes in lowland floodplain hydroperiod. Water Resources Research, 38(7), 20-1.

Treitel, S. (1974). The complex Wiener filter. Geophysics, 39(2), 169-173.

Tsubaki, R., Fujita, I., & Tsutsumi, S. (2011). Measurement of the flood discharge of a small-sized river using an existing digital video recording system. Journal of Hydro-environment Research, 5(4), 313-321.

Ufficio Idrografico del Magistrato di Venezia (1914) Norme ed istruzioni per il Servizio di Misura delle Portate, Pubblicazione n. 38, Ristampa (Venezia 1988)

UNESCO IHP (1984) Discharge of selected rivers of the world Vol. I-III. International Hydrology Programme, UNESCO Publication, Paris, France.

Van Leer, B. R. (1924) The California Pipe Method of Water Measurement, Engineering News Record, August 21

Vélez-Nicolás, M., García-López, S., Barbero, L., Ruiz-Ortiz, V., & Sánchez-Bellón, Á. (2021). Applications of unmanned aerial systems (UASs) in hydrology: A review. Remote Sensing, 13(7), 1359.

Visbeck, M. (2002). Deep velocity profiling using lowered acoustic Doppler current profilers: Bottom track and inverse solutions. Journal of atmospheric and oceanic technology, 19(5), 794-807.

Vogel, R. M., Lall, U., Cai, X., Rajagopalan, B., Weiskel, P. K., Hooper, R. P., & Matalas, N. C. (2015). Hydrology: The interdisciplinary science of water. Water Resources Research, 51(6), 4409-4430.

Von Storch, H., & Krauss, W. (2005). Culture contributes to perceptions of climate change. Nieman Reports, 59(4).

Vörösmarty, C. J. (2002). Global water assessment and potential contributions from Earth Systems Science. Aquatic Sciences, 64(4), 328-351.

Vörösmarty, C., Brikett, C., Dingman, S. L., Lettenmaier, D. P., Kim, Y., Plant, R., Rodriguez, E. & Emmitt, G. D. (1999) NASA Post-2002 Land Surface Hydrology Mission Component for Surface Water Monitoring: HYDRA-SAT (HYDRological Altimetry SATellite. Technical report, NASA, USA.

Vörösmarty, C., Fakers, B. & Tucker, B. (1996a) River Discharge Database, Version 1.0 (RivDIS vLO), Volumes 0 through 6. A contribution to IHP-V Theme 1. Technical Documents Series. Technical report, UNESCO, Paris, France.

Waldon, M. G. (2004). Estimation of average stream velocity. Journal of Hydraulic Engineering, 130(11), 1119-1122.

Wang, H., Gao, Q., Feng, L., Wei, R., & Wang, J. (2015). Proper orthogonal decomposition based outlier correction for PIV data. Experiments in fluids, 56(2), 1-15.

Ward, D. P., Hamilton, S. K., Jardine, T. D., Pettit, N. E., Tews, E. K., Olley, J. M., & Bunn, S. E. (2013). Assessing the seasonal dynamics of inundation, turbidity, and aquatic vegetation in the Australian wet–dry tropics using optical remote sensing. Ecohydrology, 6(2), 312-323.

Weight, W. D. (2001). Manual of applied field hydrogeology. McGraw-Hill Education.

Weitsman, Y. J., & Elahi, M. (2000). Effects of fluids on the deformation, strength and durability of polymeric composites–an overview. Mechanics of time-dependent materials, 4(2), 107-126.

Westerberg, I. K., Guerrero, J. L., Younger, P. M., Beven, K. J., Seibert, J., Halldin, S., ... & Xu, C. Y. (2011). Calibration of hydrological models using flow-duration curves. Hydrology and Earth System Sciences, 15(7), 2205-2227.

Westerweel, J. (1993, December). Analysis of PIV interrogation with low-pixel resolution. In Optical diagnostics in fluid and thermal flow (Vol. 2005, pp. 624-635). SPIE.

Westerweel, J. (1994). Efficient detection of spurious vectors in particle image velocimetry data. Experiments in fluids, 16(3), 236-247.

Westerweel, J. (1997). Fundamentals of digital particle image velocimetry. Measurement science and technology, 8(12), 1379.

Westerweel, J., & Scarano, F. (2005). Universal outlier detection for PIV data. Experiments in fluids, 39(6), 1096-1100.

Whalley, N., Iredale, R. S., & Clare, A. F. (2001). Reliability and uncertainty in flow measurement techniques-some current thinking. Physics and Chemistry of the Earth, Part C: Solar, Terrestrial & Planetary Science, 26(10-12), 743-749.

Wieneke, B. (2015). PIV uncertainty quantification from correlation statistics. Measurement Science and Technology, 26(7), 074002.

Wienhöfer, J., Germer, K., Lindenmaier, F., Färber, A., & Zehe, E. (2009). Applied tracers for the observation of subsurface stormflow at the hillslope scale. Hydrology and Earth System Sciences, 13(7), 1145-1161.

Willert, C. E., & Gharib, M. (1991). Digital particle image velocimetry. Experiments in fluids, 10(4), 181-193.

Willert, C., Raffel, M., Kompenhans, J., Stasicki, B., & Kähler, C. (1996). Recent applications of particle image velocimetry in aerodynamic research. Flow Measurement and Instrumentation, 7(3-4), 247-256.

Xu, K., Zhang, J., Watanabe, M., & Sun, C. (2004). Estimating river discharge from very high-resolution satellite data: a case study in the Yangtze River, China. Hydrological Processes, 18(10), 1927-1939.

Xue, Z., Charonko, J. J., & Vlachos, P. P. (2015). Particle image pattern mutual information and uncertainty estimation for particle image velocimetry. Measurement Science and Technology, 26(7), 074001.

Yan, Y. (1996). Mass flow measurement of bulk solids in pneumatic pipelines. Measurement Science and Technology, 7(12), 1687.

Zhang, J., Tao, B., & Katz, J. (1997). Turbulent flow measurement in a square duct with hybrid holographic PIV. Experiments in fluids, 23(5), 373-381.

Zhang, Z., Wang, X., Fan, T., & Xu, L. (2013). River surface target enhancement and background suppression for unseeded LSPIV. Flow Measurement and Instrumentation, 30, 99-111.